TIME-VARYING SOURCES AND VASCULAR CONTRIBUTIONS TO AGE-ACCOMPANIED FUNCTIONAL BRAIN NETWORK RE-ORGANIZATION

by

Liang Han

APPROVED BY SUPERVISORY COMMITTEE:

Gagan Wig, Chair

Yulia Gel

Michael D. Rugg

Bart Rypma

TIME-VARYING SOURCES AND VASCULAR CONTRIBUTIONS TO AGE-ACCOMPANIED FUNCTIONAL BRAIN NETWORK RE-ORGANIZATION

by

LIANG HAN, MA

DISSERTATION

Presented to the Faculty of

The University of Texas at Dallas

in Partial Fulfillment

of the Requirements

for the Degree of

DOCTOR OF PHILOSOPHY IN

COGNITION AND NEUROSCIENCE

THE UNIVERSITY OF TEXAS AT DALLAS

December 2022

ACKNOWLEDGMENTS

Seven years ago, I applied for a PhD program under the supervision of Dr. Wig at The University of Texas at Dallas. I didn't realize this decision could change my career and life in such a profound way at that time. During seven years of graduate studies, I've gained so much support from professors and colleagues at Wig Neuroimaging Lab and School of Behavioral and Brain Sciences at UT Dallas.

First, I want to thank Dr. Wig. As my academic supervisor, Dr. Wig has not only taught me to conduct rigorous studies in the exciting area of functional brain networks, but also helped me develop better capability of scientific thinking in more general domains. It has been a fantastic journey to study time and space in the brain with Dr. Wig. Beyond academic research, Dr. Wig provided great help to me in my life, especially when my family was having a difficult time. My academic advancement and personal development wouldn't be possible without his mentorship, support and encouragement.

I want to thank my dissertation committee members. Dr. Rugg, Dr. Rypma and Dr. Gel have provided insightful comments and suggestions throughout my dissertation, which laid the foundation for this work. I also want to thank Dr. Stillman for being the outside chair of my defense committee, which makes my dissertation defense and timely graduation possible.

I would like to express my gratitude to my colleagues at Wig Neuroimaging Lab – Dr. Micaela Chan, Neil Savalia, Dr. Phillip Agres, Ziwei Zhang, Ezra Winter-Nelson, Linh Nguyen, Anu Nair – for countless help and support both in my academic research and daily life. Working with my brilliant colleagues is one of best memories in my lifetime.

I want to thank my family and friends for supporting me throughout my graduate life. During these 7 years, my wife has taken most of the responsibility to take care the entire family, which allows me to concentrate on my research. My kids have shown their love and great patience to me, even when I'm constantly unavailable from their life. Because of the pandemic, I have not been able to visit my parents in the last 3 years. They keep telling me not to worry about them, but to focus on my research and do my best in my graduate studies. I'm truly lucky to have so much support, love and encouragement from my family; these are all priceless to me. I would also like to thank Uncle Chang for taking care of me, especially before my family moved here. Without all this support, I wouldn't be able to make it through my graduate studies and finish this dissertation.

October 2022

TIME-VARYING SOURCES AND VASCULAR CONTRIBUTIONS TO

AGE-ACCOMPANIED FUNCTIONAL BRAIN NETWORK RE-ORGANIZATION

Liang Han, PhD
The University of Texas at Dallas, 2022

Supervising Professor: Gagan Wig, Chair

The brain is a complex network of interacting brain areas that can be further divided into segregated functional systems. Resting-state system segregation is a feature of brain network organization that has relevance to brain function in both health and disease across adult lifespan. It is unclear what gives rise to system segregation and the individual differences in this brain network measure. In this dissertation, two aspects of this important question are investigated: (1) Do vascular factors contribute to relationships between age and system segregation across the adult lifespan? and (2) Can sources of time-varying information help account for relationships between aging and system segregation? The interplay between these questions reveals how the temporal evolution of system re-configuration at a short time scale impacts more stable individual features of large-scale network organization, in the context of differences in vascular health of adult individuals. This dissertation was accomplished by incorporating data from a total of 894 unique participants, over 3 independent studies (age range: 20 – 100 years) and including multiple neuroimaging modalities and measures of participant health and demographics.

The contribution of vascular factors towards relationships between age and resting-state system segregation is first investigated. There exist relationships between age and vascular measures, including cardiovascular health (CVH) and cerebrovascular reactivity (CVR). Age-related decreases of system segregation persist after controlling for vascular-related variance. This is demonstrated by (i) computing system segregation regional CVR-corrected signals within each participant, and (ii) including CVH as a participant-level covariate in the models. These results demonstrate that age-related differences in system segregation cannot be fully attributed to differences in cerebrovascular and cardiovascular factors.

To examine the contribution of time-varying information to system segregation, I examine the relationship between resting-state BOLD signal variability and system segregation. After controlling for vascular confounds by (i) estimating BOLD variability using CVR-corrected signals, (ii) including CVH as a covariate in the model, there is an absence of a relationship between age and BOLD variability, revealing that vascular factors serve as a major source of variance explaining previously reported relationships between age and resting-state BOLD signal variability. Further, with correction of vascular factors, BOLD variability does not relate to system segregation.

An additional source of time-varying information is evaluated in relation to system segregation, focused on co-fluctuation amplitude of the resting-state time-series. Moments of greater co-fluctuation pattern across edges are identified (events), during which functional brain networks are highly modular relative to non-event moments. I demonstrate that the number of events that are present in an individual's resting-state time-series is related to their system segregation. However, I next demonstrate that age-accompanied decreases of system segregation are evident

across all the moments, irrespective of co-fluctuation amplitude of edges. Collectively, these findings reveal that while high co-fluctuation moments (events) may contribute towards establishing an individual's system segregation, brain network re-organization exists across all time points of a resting-state scan.

In sum, this dissertation provides important support that resting-state system segregation measures brain network re-organization across the adult lifespan. This measure is independent from vascular differences within individuals, and provides critical evidence of brain aging that is consistently evident across periods of rest. Serving as a biomarker of functional brain network integrity, system segregation further supports the application of this approach towards measuring individual brain health across the lifespan.

TABLE OF CONTENTS

ACKNOWLEDGMENTS iv
ABSTRACT vi
LIST OF FIGURES xi
LIST OF TABLES xvii
CHAPTER 1 INTRODUCTION AND BACKGROUND 1
CHAPTER 2 DO VASCULAR FACTORS CONTRIBUTE TO RELATIONSHIPS BETWEEN AGE AND BRAIN SYSTEM SEGREGATION ACROSS THE ADULT LIFESPAN? 11
2.1. Introduction 11
2.2. Methods 15
2.3. Results 23
2.3.1. Measures of cardiovascular health exhibit a strong age effect during adulthood 23
2.3.2. Cerebrovascular reactivity decreases with age across healthy adult lifespan 26
2.3.3. System segregation decreases with age across healthy adult lifespan, independent of vascular measures 27
2.4. Discussion 34
CHAPTER 3 CAN SOURCES OF TIME-VARYING INFORMATION HELP ACCOUNT FOR RELATIONSHIPS BETWEEN AGING AND BRAIN SYSTEM SEGREGATION? 37
3.1. Does resting-state BOLD signal variability relate to the measure of brain system segregation? 37
3.1.1. Introduction 37
3.1.2. Methods 38
3.1.3. Results 39
3.1.3.1. Resting-state BOLD signal variability does not exhibit age-related differences after taking vascular factors into consideration 39
3.1.3.2. Resting-state BOLD signal variability does not relate to system segregation when vascular factors are taken into consideration 43
3.1.4. Discussion 47
3.2. Do individual differences in moments of high pairwise-covariance (i.e., highly modular ‘events’) help explain relationships between age and resting-state brain system segregation? ... 52
3.2.1. Introduction 52

3.2.2. Methods 55
3.2.3. Results 61
3.2.3.1. Events are moments exhibiting a more modular organization and higher resting-state system segregation 61
3.2.3.2. Mathematical proof that CVR-correction does not alter the estimation of RMS and identification of events 66
3.2.3.3. The number of events declines with increasing age 68
3.2.3.4. Participants with a greater number of events in their resting-state BOLD timeseries exhibit higher system segregation 71
3.2.3.5. The relationship between age and resting-state system segregation is not limited to event moments 73
3.2.4. Discussion 77
CHAPTER 4 CONCLUSION 81
REFERENCES 86
BIOGRAPHICAL SKETCH 93
CURRICULUM VITAE 94

LIST OF FIGURES

Figure 1.1. Aging-related decrease of system segregation at rest prevails in distinct types of functional systems. (A) Functional networks across healthy adult lifespan were revealed using age-specific parcels as node set. The topographical organization of the brain networks are highly similar across age. However, the degree to which the systems are segregated from one another (related to their network topology) exhibits an age-related decrease; this trend is consistent for all systems (B), association systems (C), sensory-motor systems (D) and association to sensory-motor systems (E), despite different trajectories of decline. These observations suggest that system segregation could serve as a sensitive network measure capable of revealing altered topological organization of the brain networks across age. Figures adapted from Han et al. (2018). 2

Figure 2.1. Cardiovascular health varies with increasing age. Cardiovascular health (CVH) scores were estimated from 3 separate measures related to cardiovascular health and function (systolic blood pressure, diastolic blood pressure and body mass index [BMI]). Using DLBS dataset 1, age-related increase has been revealed in (A) systolic blood pressure ($r = 0.469$, $p < 0.001$), but not (B) diastolic blood pressure ($r = 0.146$, $p = 0.104$) and (C) BMI ($r = 0.148$, $p = 0.097$). To derive a summary score quantifying CVH, first principal component scores were extracted from these 3 measures, rescaled to the range between 0 and 1, and subtracted by 1 to reverse the trend. A greater score suggests better cardiovascular health of this participant (for detailed computation see Methods). (D) CVH scores exhibits age-related decreases across the healthy adult lifespan in the DLBS dataset 1 ($r = -0.408$, $p < 0.001$). This demonstrates that older adults have less cardiovascular health relative to younger adults. Note that area between doted lines represents 95% confidence interval. 25

Figure 2.2. Cerebrovascular reactivity decreases with age. (A) A mean cerebrovascular reactivity (CVR) score was computed for each participant by averaging CVR maps across all vertices. There is an age-related decline of CVR scores, indicating less flexibility of blood vessel dilation in older adults ($r = -0.576$, $p < 0.001$). (B) Relationship between participant age and vertex-wise CVR values reveal distinct regions that are particularly prone to age-related differences in CVR. Each value on the surface represents the correlation coefficient between CVR values at this vertex and age across all the participants. Correlation coefficient values were FDR-corrected at the significance level of $p = 0.05$. All the survived correlation coefficients are negative, indicating strong aging-related decrease evident at distributed cortical locations, which include insular cortex, dorsal medial prefrontal cortex (dmPFC) and ventral anterior cingulate cortex (vaCing). Lat: lateral view, Med: medial view. 27

Figure 2.3. Brain system segregation decreases with age. Brain system segregation exhibits amount of partitioning between distinct functional systems of the brain. The result shows there is

an aging-related decrease in system segregation ($r = -0.4$, $p < 0.001$), indicating less segregated functional systems in older adults. 28

Figure 2.4. Aging-accompanied decrease of system segregation is independent of cardiovascular influence. To rule out the contribution of cardiovascular factors, CVH variance was regressed out from segregation. Note that residuals were used to visualize relationships after removing confounding variance. In the main analysis I included covariates in the model to control for the confounds. The result shows that residuals of segregation values are negatively correlated to age ($r = -0.265$, $p = 0.008$), indicating robust aging effect of segregation independent of cardiovascular influence. 29

Figure 2.5. Brain system segregation was calculated after vertex (spatially) specific CVR correction of BOLD signals. Brain system segregation declines with increasing adult age. Segregation values were computed using resting-state BOLD time series corrected by each participant's unique CVR map. This provides a more precise correction of BOLD signals by incorporating distinct CVR information at different brain locations. This step results in CVR-corrected segregation that is correlated with the values using original signals (without CVR correction) (A). CVR-corrected segregation exhibits negative relationship with age ($r = -0.362$, $p < 0.001$), which suggests a robust relationship between age and resting-state brain system segregation, even after a stringent correction using cerebrovascular reactivity maps (B). 31

Figure 2.6. System segregation decreases with age, after stringently removing distinct sources of vascular confounds. To rule out different sources of vascular factors, both CVR and CVH were considered in the final analysis. BOLD signals were corrected using fine-grained spatial CVR maps, and used to compute resting-state brain system segregation. Participant's CVH score was regressed out from CVR-corrected segregation. Note that residuals were used to visualize relationships after removing confounding variance. In the main analysis I included covariates in the model to control for the confounds. The result shows that residuals of segregation were negatively correlated with age ($r = -0.234$, $p = 0.02$). These results suggest that brain system segregation is robustly related to participant age during adulthood, after minimizing potentially confounding effects from distinct vascular factors. 33

Figure 3.1. Resting-state BOLD signal variability decreases with increasing age across adult lifespan. BOLD variability was quantified by temporal standard deviation of BOLD signals. Using DLBS dataset, there exists an age-accompanied decrease in BOLD signal variability ($r = -0.391$, $p < 0.001$). These results suggest that BOLD signals may be less temporally variable in older adult individuals..... 40

Figure 3.2. Aging-related decrease of BOLD variability persists after controlling for cardiovascular health (CVH) factors. One possible source contributing to the estimate of BOLD variability is cardiovascular health. To rule out the related confounds, CVH scores were

regressed out from resting-state BOLD variability. Note that residuals were used to visualize relationships after removing confounding variance. In the main analysis I included covariates in the model to control for the confounds. There still exists a relationship between age and residuals of BOLD variability ($r = -0.302$, $p = 0.002$) using DLBS dataset. Note that the correlation coefficients are weaker relative to results using original BOLD variability without controlling for CVH. These results suggest that while BOLD variability may be partly explained by CVH, its relationship with age is robust after controlling for CVH confounds. 41

Figure 3.3. CVR-correction to BOLD signals alters the relation between age and BOLD variability. Another important source of confounds is individual difference of cerebrovascular reactivity. To control for this possible source of variance, BOLD signals were corrected using CVR maps at each brain network node, and were then used to compute BOLD variability. Using DLBS dataset, BOLD variability from CVR-corrected signals was marginally related to age ($r = 0.19$, $p = 0.058$). 42

Figure 3.4. BOLD variability does not relate to age, after controlling for both vascular measures. To provide stringent control for vascular factors, BOLD variability was estimated using BOLD signals corrected using CVR maps, after which CVH variance was removed from CVR-corrected BOLD variability. Note that residuals were used to visualize relationships after removing confounding variance. In the main analysis, I included covariates in the model to control for the confounds. Using DLBS dataset, residual of CVR-corrected BOLD variability is not related to age ($r = 0.09$, $p = 0.38$). 43

Figure 3.5. Relationship between BOLD variability and system segregation. (A) Using DLBS dataset, BOLD variability is positively correlated with system segregation ($r = 0.347$, $p < 0.001$). (B) After controlling for age, this relation is still significant ($r = 0.232$, $p = 0.019$). 44

Figure 3.6. System segregation is not associated with CVR-corrected BOLD variability. To control for the confounding effects, each brain network node's BOLD time series were corrected using CVR maps, based on which CVR-corrected BOLD signal variability was derived. Using DLBS dataset, there is no significant correlation between system segregation and BOLD variability estimated from CVR-corrected time series ($r = -0.177$, $p = 0.085$). 45

Figure 3.7. CVR-correction greatly attenuates the observed regional relationships between age and BOLD variability across most cortical locations. To estimate the aging effect of BOLD variability on the brain, BOLD variability values at each vertex were correlated with age across participants, with the resultant correlation coefficient indicating the aging effect of BOLD variability at this brain location. The correlation coefficients were corrected using FDR at the significance level of $p = 0.05$. (A) Using DLBS dataset, extensive brain regions exhibit an age-related decrease of BOLD variability. These regions include posterior parietal cortex (pPC) and cuneus cortex. (B) However, the prominent regional age-related decline of BOLD variability is

no longer evident at these brain regions when BOLD signals were corrected using CVR maps at each vertex; in fact, the few regions that remain significant are largely exhibiting an opposing pattern (positive relationships). These results collectively suggest that CVR maps provide fine-grained spatial features of vascular factors that largely account for the relationship between age and BOLD signal variability. 47

Figure 3.8. Moments with relatively greater amplitude of co-fluctuation between resting-state BOLD signals exhibit prominent modular structures of brain networks. (A) RSFC was estimated from Pearson correlation that could be temporally unwrapped to generate co-fluctuation timeseries for every pair of brain regions (edges). Co-fluctuation timeseries is the element-wise product of z-scored BOLD time series between node pairs. Conversely, co-fluctuation timeseries can be averaged across time, resulting in the vectorized RSFC matrix. (B) There are moments when co-fluctuation timeseries co-fluctuate collectively across the entire brain. These moments can be identified by estimating spatial variance across all co-fluctuation timeseries at each time point (quantified by root sum square [RSS]). The RSFC matrix from all time points (A) are more similar to the matrix using events' frames (top 5% of RSS) relative to the matrix from frames of non-events (bottom 5%) (C, D). (E) Network modularity is higher during events' frames, relative to non-event frames; also evident in the left half of (C). Figures adapted from Zamani Esfahlani et al. (2020). 53

Figure 3.9. Identification of events using an exemplar participant's data. (A) is an edge matrix, where each row is the element-wise product between every node pair's time series. This reflects the co-fluctuation pattern between each node pair; a positive value means signals of the two nodes fluctuate in the same direction whereas a negative value denotes opposite fluctuation. (B) There are moments exhibiting collective co-fluctuation between edges across the entire brain. These moments can be identified by estimating spatial variability across all co-fluctuation timeseries at each time point (quantified by root mean square [RMS]). These moments are captured by identifying peaks of top RMS (e.g., top 5% [Zamani Esfahlani et al., 2020]), marked by red circles. 61

Figure 3.10. Two independent adult lifespan datasets were used in this chapter: DLBS and HCP Aging datasets. Both datasets exhibit consistent distributions of RMS values. Despite the differences across datasets (e.g., participants, data acquisition parameters), they exhibit consistent right-skewed distributions of RMS, with relatively comparable cutoff values to identify the top 5% of RMS values, which correspond to 'events' (DLBS dataset: $RMS_{top5\%}$ = 1.78; HCP Aging: $RMS_{top5\%}$ = 1.85)..... 62

Figure 3.11. Correlation matrix from events exhibits stronger modular structure of brain networks. To compare network organization during events vs non-events frames, the node-to-node correlations were computed using frames from events (top 5% RMS) or non-events (bottom 5% RMS) in each participant. The matrices were then averaged across all participants in each

dataset. In this figure, the right triangle of each correlation matrix was computed using event frames while left triangle of each matrix was from frames of non-events. The nodes of the correlation matrices are ordered and labelled according to a pre-defined atlas of brain systems (Gordon et al., 2016), to facilitate viewing of the modular pattern. Both DLBS dataset (A) and HCP Aging (B) showed sharp contrast between left and right triangles of correlation matrices, whereby a modular structure is evident in the right triangle (i.e., high within system correlations along the diagonal blocks, lower between system correlations in the off-diagonal blocks), suggesting much stronger modular structure of brain networks during events relative to non-events. 64

Figure 3.12. Moments with greater pairwise-covariance (i.e., events) exhibit higher system segregation relative to moments with low pairwise-covariance. Events are moments that exhibit much stronger co-fluctuation amplitude across a variety of node pairs. These moments can be identified by isolating frames with higher root mean square (RMS) across all edges (e.g., top 5% RMS). To quantify functional network organization during events, system segregation was computed using data from events (top 5% RMS), and compared to system segregation values from non-events (bottom 5% RMS). (A) shows greater system segregation during events relative to non-events using DLBS dataset (paired-samples t-test: $t(216) = 17.823$, $p < 0.001$) and (B) depicts a similar distinction using the HCP Aging dataset (paired-samples t-test: $t(368) = 13.972$, $p < 0.001$, demonstrating that resting-state functional brain networks are more segregated during event time points. In each raincloud plot, individual dots represent participants. Box and whisker plots summarize the distribution of segregation values (upper and lower bound of each box denote 25^{th} and 75^{th} percentiles). Histograms to the left depict kernel density estimate of data distribution. 65

Figure 3.13. Relationship between number of events and age of participant. (A) In the DLBS dataset, events were identified using the top 5% RMS. The number of events is not correlated with age ($r = -0.034$, $p = 0.608$). (C) Using a different threshold (top 10% RMS) does not alter the non-significant result ($r = 0.038$, $p = 0.566$). (B) In contrast, in the HCP Aging dataset there exists a significant relationship between participant's age and the number of events identified in their resting-state time-series, both when calculated using the top 5% RMS ($r = -0.289$, $p < 0.001$), and (D) top 10% RMS ($r = -0.313$, $p < 0.001$). 70

Figure 3.14. Resting-state system segregation is positively related to number of events that are evident in a participant's resting-state time-series. System segregation reflects the level of partitioning between distinct functional brain systems, calculated based on the correlation matrix from the entire BOLD time-series. This measure is correlated with number of events (top 5% of RMS; corresponding to moments exhibiting heightened modular structures of brain networks) using DLBS data (A). This relation persists after controlling for age (C). Using an independent dataset (HCP Aging), a similar relationship is evident (B) and remained significant after controlling age-related variance (D). Each in plot, dots represent individual participants..... 72

Figure 3.15. Estimating system segregation from data frames of differing RMS strength. To assess whether the relationship between a participant's age and their resting-state system segregation is limited to high co-fluctuation moments of the resting-state time-series, the following steps were taken to sample data and evaluate system segregation at distinct moments for each participant. (A) RMS was computed to reflect the degree to which edges collectively co-fluctuate at different moments. (B) The distribution of RMS was derived, based on which 10 bins were created to categorize moments of different RMS amplitude (i.e., 0% - 10%, 10% - 20%, …, 90% - 100%). (C) For each RMS bin (e.g., 90% - 100%), functional time series (frames) were sampled from only those moments, based on which a correlation matrix was computed for each participant. This correlation matrix reflected the participant's functional network at the corresponding moments with specific RMS strength. (D) The participant's resting-state system segregation was computed based on this correlation matrix for each RMS bin. As such, system segregation reflects organization of functional networks at the moments when levels of co-fluctuation across edges are similar. By comparing relationships between age and system segregation from distinct RMS bins allows testing of whether age-associated differences in brain network organization are specific to certain moments with strong RMS amplitude or across all resting-state time points irrespective of RMS strength..... 74

Figure 3.16. The relationship between an individual's age and the magnitude of their resting-state system segregation is evident in moments of higher RMS (e.g., events) and low RMS (non-events). Data frames were sampled into high RMS (top 10%) and low RMS (bottom 10%) bins. For each RMS bin, system segregation was computed using all frames in the corresponding bin for each participant, and then correlated with age across participants. There is an age-related decrease of system segregation using data sampled from the highest RMS frames (i.e., top 10% RMS frames) using DLBS data (A). However, this aging-related decrease of segregation is also evident using the lowest RMS frames (C). Similar relationships were revealed in an independent dataset (HCP Aging, B and D)..... 75

LIST OF TABLES

Table 3.1. The relationship between an individual's age and the magnitude of their resting-state system segregation is evident across the resting-state time-series and is not limited to moments of higher RMS (e.g., events). Data frames were sampled into 10 bins based on RMS magnitude with 10% increments (i.e., 0% - 10%, 10% - 20%, …, 90% - 100%). For each RMS bin, system segregation was computed using all frames in the corresponding bin for each participant, and then correlated with age across participants. Significant correlations between age and segregation were evident across all RMS bins using DLBS (A) and HCP Aging (B) datasets. These results demonstrate that relationship between an individual's age and their resting-state system segregation is evident across the resting-state time-series and is not limited to moments of higher RMS (e.g., events). 76

CHAPTER 1

INTRODUCTION AND BACKGROUND

The brain is a complex network of interacting brain areas that can be further divided into multiple sub-networks (i.e., functional systems [for review see Bullmore and Sporns, 2009; Wig et al., 2011]). Each of the systems is dedicated to sets of functionally dissociable cognitive processes (e.g., a visual system is involved in processing sensory information primarily from the visual modality; for review see Mesulam, 1990). Effective functioning of the brain networks requires this modular organization, wherein the systems remain segregated to maintain relative functional independence, while also allowing for necessary communications between distinct systems (Sporns and Betzel, 2016; Wig, 2017).

Resting-state system segregation varies across individuals in both health and disease

The segregation of the brain's functional systems is evident even while participants are lying in resting wakefulness, and has been shown to be an important feature of the brain network function and organization in both healthy adults along the lifespan and the diseased populations (for review see Wig, 2017). Three lines of evidence are highlighted here to show the significance of system segregation in relation to the brain network organization and behavioral outcomes. First, studies using resting-state fMRI have revealed that a greater level of segregation between functional systems at rest is positively correlated with cognitive performance, such as working memory capacity (Stevens et al., 2012), visual attention (Yue et al., 2017), processing speed (Chan et al., 2014; Wang et al., 2021), and episodic memory (Chan et al., 2014). These observations suggest that functional systems with greater segregation may reflect an optimal organization of the brain networks, enabling superior behavioral performance across a variety of

cognitive domains. Second, older healthy adults have lower system segregation for both association systems (systems responsible for information integration at a higher level) and sensory-motor systems (systems dedicated to processing incoming and outgoing sensory/motor information), indicating an aging-related decrease of segregation across multiple functional systems (**Figure 1.1**; Chan et al., 2014; Han et al., 2018).

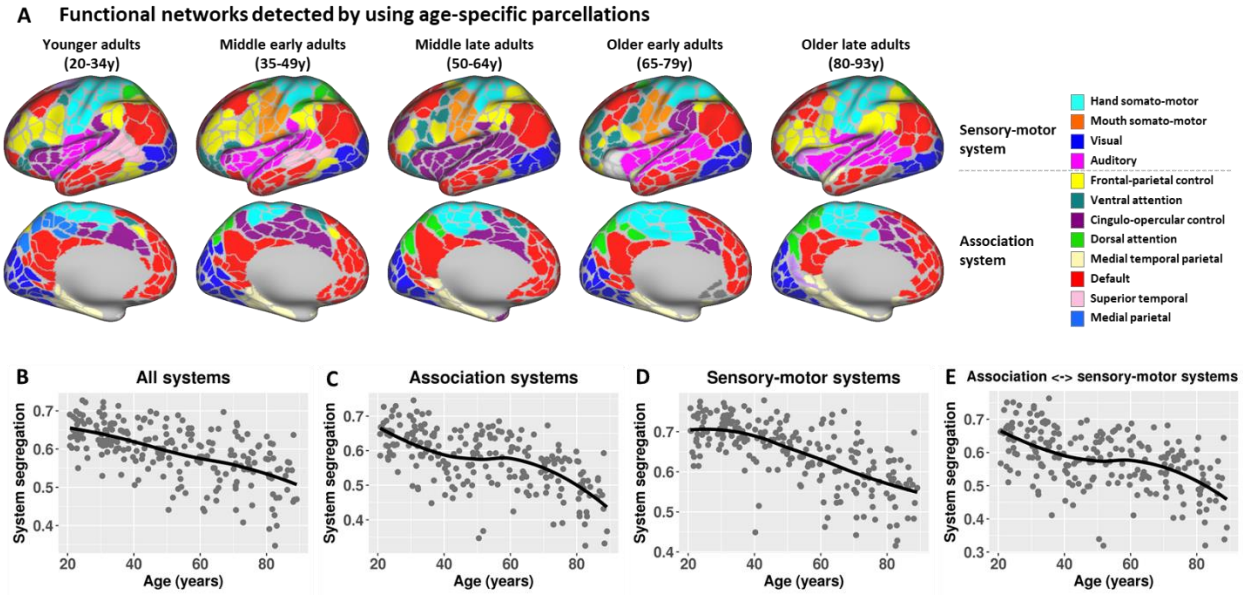

Figure 1.1. Aging-related decrease of system segregation at rest prevails in distinct types of functional systems. (**A**) Functional networks across healthy adult lifespan were revealed using age-specific parcels as node set. The topographical organization of the brain networks are highly similar across age. However, the degree to which the systems are segregated from one another (related to their network topology) exhibits an age-related decrease; this trend is consistent for all systems (**B**), association systems (**C**), sensory-motor systems (**D**) and association to sensory-motor systems (**E**), despite different trajectories of decline. These observations suggest that system segregation could serve as a sensitive network measure capable of revealing altered topological organization of the brain networks across age. Figures adapted from Han et al. (2018).

Third, functional systems are less segregated in participants suffering from neurological disease (e.g., Alzheimer's disease [Brier et al., 2014] and schizophrenia [Yang et al., 2016]), suggesting

brain dysfunction and behavioral disorders may be associated with altered organization of the brain networks. Finally, declining brain system segregation predicts impending changes in dementia severity (Chan et al., 2021). These observations collectively suggest that resting-state system segregation is a measure that summarizes important features of the brain network organization and predicts behavioral outcomes in both healthy and diseased individuals. Critically, it is not clear what establishes an individual's resting-state system segregation. One way to better understand resting-state system segregation is to better understand the signals that contribute to it, and properties that modify it.

Vascular health is altered in older adults

Aging is accompanied by changes of vascular health, including cardiovascular and cerebrovascular alterations. It has been revealed that vascular dysfunction is associated with structural alterations in the brain, including alterations of white matter (e.g., white matter lesions [Bots et al., 1993; Longstreth et al., 1996; Moroni et al., 2018], presence of white matter hyperintensities [Raz et al., 2007]), gray matter differences (e.g., cortical thickness in the motor cortex [Marshall et al., 2017], volume of the primary visual cortex [Raz et al., 2007]), and subcortical atrophy (e.g., hippocampal shrinkage [Raz et al., 2005; Du et al., 2006; Debette et al., 2011]). Vascular-related changes of brain structures across age are also linked to differences of cognitive performance (for review see Raz and Rodrigue, 2006; Salat, 2011). For instance, a longitudinal study reported that participants of higher vascular risk exhibited greater white matter hyperintensity progression and shrinkage of the fusiform cortex, and that these age-related changes were correlated with declines in working memory (Raz et al., 2007). As such, individual

difference of vascular health gives rise to structural variability of the brain across the adult lifespan, which plays unique roles towards aging-related changes in cognitive performance. Vascular health not only impacts brain structure, but also leads to differences in neural function and behavioral performance (for review see Zimmerman et al., 2021). Vascular impairments lead to cellular dysfunction (e.g., through ischemia that interrupts metabolic functions [Fricker et al., 2018]), and reduced efficiency in neural processing (e.g., impaired timing of signaling in neuronal circuits due to aging-accompanied decline of cerebrovascular reactivity [Hutchison et al., 2013; Toth et al., 2017]). Consequently, the impacts of vascular health on neural function are also linked to age-related cognitive decline (Colcombe et al., 2004; Crichton et al., 2014, Abdelkarim et al., 2019; Hutchison et al., 2013; Tarantini et al., 2015; Toth et al., 2017; Yabluchanskiy et al., 2021).

Aging-accompanied vascular changes can also lead to alterations in regional cerebral blood flow, which poses a challenge for estimating neural activity using functional MRI measures that are sensitive to properties of blood flow. Functional MRI reveals neural activity via BOLD signals that reflect the concentration of oxygenated hemoglobin in blood vessels varying with neural activity. Greater neural activity (e.g., higher neuronal firing rates) increase energy consumption, resulting in changes of the ratio of oxygenated hemoglobin to deoxyhemoglobin and altered cerebral blood flow. Critically, aging-related alteration of regional cerebral blood flow affects properties of BOLD signals (e.g., magnitude of activations), even when neural activity remains comparable (Cohen et al., 2002; Brown et al., 2003; Stefanovic et al., 2005).

Indeed, measuring age-related changes of neural activity in humans has been challenging. One method is to examine the cerebral metabolic rate of oxygen ($CMRO_2$) that measures

consumption of oxygen during neural metabolism. Studies have revealed different results with respect to the age-related differences of resting-state $CMRO_2$ using distinct imaging methods; relatively consistent decreases in $CMRO_2$ with aging in PET-based studies (Aanerud et al., 2012; Eustache et al., 1995; Goyal et al., 2017; Ibaraki et al., 2010; Kuhl et al., 1982; Yamaguchi et al., 1986), but mixed finding using MRI-based methods (age-related increases [Lu et al., 2011; Peng et al., 2014], decreases [De Vis et al., 2015], or no change [Catchlove et al., 2018]). These differences in measured $CMRO_2$ may be attributive to limitations of MRI-based methods that depend on blood flow to indirectly measure neural metabolism. As such, varying blood flow may not necessarily relate to metabolic changes but reflect differences in hematocrit (e.g., Aanerud et al., 2012) or other non-brain effects (e.g., scanning parameters [Liu et al., 2013]).

Age-related differences in neurovascular coupling and neurovascular energetics could also lead to changes of BOLD signal across age. It has been shown that changes in BOLD signal with age is predicted by decreases of neurovascular coupling, and this relationship is independent from changes in metabolism (Fabiani et al., 2014). Changes in BOLD responses in older adults could lead to aging-accompanied differences of BOLD signals, such as signal timing changes (Taoka et al., 1998) and increased noise in image voxels (D'Esposito et al., 1999). More recent studies have been focusing on changes in neurovascular energetics and neurovascular coupling, which may confound interpretations of BOLD signals in older adults (Abdelkarim et al., 2019; Rypma et al., 2021; West et al., 2019; Wright & Wise, 2018; for review and discussion see Zimmerman et al., 2021).

Collectively, these findings demonstrate that vascular factors can relate to altered brain structures and function in older adult individuals. As such, it is possible that there is a link between

vascular alterations and large-scale resting-state functional brain network re-organization observed in aging, especially as this property is based on the BOLD signal. In line with this possibility, Kong et al. (2020) reported that differences of cerebrovascular elasticity are related to differences in resting-state system segregation. The relationship between cerebrovascular elasticity and system segregation was weakened but persists after controlling for age, which suggests that vascular health explains at least some, but not all, of the aging effects on the segregation of resting-state brain networks. Notably, this study used a summary measure of cerebrovascular function. However, cerebrovascular reactivity maps reveal that there exists variation in cerebrovascular function across the cortex (Liu et al., 2013; Meng et al., 2008; McKetton et al., 2018) which might then have different impacts on the resting-state signals of different brain regions, an aspect which will be directly examined in the present dissertation.

Resting-state correlations are dynamic

While measures of brain network organization are typically defined over an extended period of time, corresponding to one or more resting-state scans collected in a given session, closer examination of resting-state signals reveals that functional segregation varies over short timescales during the fMRI scan (Betzel et al., 2016). The temporal variability of system segregation arises from the dynamics of resting-state BOLD signals. System segregation is estimated from resting-state functional connectivity (RSFC) based on the BOLD signals sampled from different brain locations. It has been shown that the resting-state BOLD signals are non-stationary over time (e.g., Chang and Glover, 2010), leading to dynamic fluctuation of RSFC that may reflect moment-to-moment transitions between distinct brain states (Allen et al., 2014; Hutchison and Morton, 2015). These brain states may reflect reconfiguration of the brain

networks that can be associated with varying levels of vigilance, consciousness and executive function (Barttfeld et al., 2015; Nomi et al., 2017; Shine et al., 2016; Wang et al., 2016), as well as psychiatric disorders (Damaraju et al., 2014; Rashid et al., 2014; Su et al., 2016; Du et al., 2016). As such, the non-stationary BOLD signals may reflect ongoing changes in information processing, which give rise to reconfiguration of brain networks as evident by changes of system segregation. However, recent studies have revealed that the non-stationarity of BOLD signals may not reflect ongoing changes of the brain networks. Rather, it may be largely attributed to data sampling error, head motion and fluctuating drowsiness (although the latter would still be considered a 'state' relevant to level of arousal; Laumann et al., 2015; Laumann et al., 2017). Irrespective of the source of dynamics of resting-state correlations, it seems clear that a deeper understanding of the temporal variability might contribute towards our understanding of the genesis of resting-state system segregation and its variability across individuals.

Evidence that BOLD variability may relate to brain network organization and function. An important parallel body of work has provided clues relevant to the discussion above. In contrast to earlier studies that considered the variability of neural signals as a source of noise to nervous system, accumulating research has proposed that such variability could be necessary for optimal brain functioning. In support of this account, the brain has been shown to maintain metastable dynamics via a variable signal that facilitates switching between segregation and integration across brain networks (Tognoli and Kelso, 2014). Systems with adequate levels of variability may exhibit more flexible configurations, as evidenced by somewhat coupled but not completely phase-locked signals that show coexistence and shifting between integrative and segregation tendencies (Kelso, 2008; Kelso et al., 1990; Kelso and Haken, 1995; Kelso and Tognoli, 2007).

Another piece of evidence shows that the variability of neural signals may reflect a dynamic process in the nervous systems that copes with external uncertainty (e.g., Knill and Pouget, 2004; Ma et al., 2006; Beck et al., 2008; Garrett et al., 2013a; Garrett et al., 2013b). As such, greater variability of signal may reflect optimal tuning of functional systems with better adaptability to changes of the external environment. These observations collectively suggest that neural variability over time may facilitate the dynamic reconfiguration of brain networks in response to task-related processing demands which alter the connectivity within/between systems, and thus relate to task-related performance.

Consistent with the above ideas, accumulating observations have revealed that resting-state BOLD variability (and BOLD variability more generally) is related to individual differences in cognitive ability and also varies across age. It has been shown that greater variability of BOLD signals at rest is related to better cognitive performance, such as flanker task performance (Mennes et al., 2011), fluid abilities and episodic memory (Burzynska et al., 2015). In addition, resting-state BOLD variability is positively associated with task-evoked BOLD signal magnitude (Mennes et al., 2011) and variability (Mennes et al., 2013; Grady and Garrett, 2018). When compared to younger adults, older adult's cortical BOLD exhibit less variability during a variety of conditions (eye-fixation to a cross on screen [Garrett et al., 2010], cognitive tasks [Garrett et al., 2011; Grady and Garrett, 2018], and resting-state scans [Kielar et al., 2016; Grady and Garrett, 2018]). There is evidence that the relationship between age and BOLD variability during resting-state persists after controlling for motion and cardiovascular influences (e.g. Millar et al., 2020), although there is also some evidence that it diminishes after controlling for both cardiovascular and cerebrovascular estimates (Tsvetanov et al., 2020).

While the biological significance of BOLD variability has yet been fully understood, accumulating evidence has suggested that the variability of BOLD signals may summarize the moment-to-moment alterations of brain region signal processing relevant for task-related processing demands and that the variability supports behavioral outcomes which covary with age. The observations described also have clear parallels with those noted for resting-state system segregation (e.g., better cognitive performance is associated with greater system segregation and higher BOLD variability), although the two bodies of work have yet to be linked. A natural question is to ask whether there exists a direct relationship between measures of resting-state BOLD variability and summary measures of resting-state system segregation; overall BOLD signal variability may serve as a trait-like feature characterizing ongoing reconfigurations of brain network organization.

Evidence that resting-state brain system segregation may be a product of highly modular 'events' that occur during rest. Evidence for a link between BOLD variability at rest and resting-state system segregation has emerged from recent work (Zamani Esfahlani et al., 2020). Esfahlani and colleagues examined co-fluctuating patterns of BOLD signals between sets of network nodes and identified brief moments that exhibited much stronger co-fluctuation amplitude across a variety of node pairs (termed as 'event') relative to other moments of weaker co-fluctuation ('non-event'). They found that the modular structure of brain networks is much more prominent during events relative to non-events. This interesting observation suggests that neural signals may consist of heterogeneous components (moments) that exhibit different patterns of connectivity. Critically, these events coincide with moments when BOLD signals exhibit greater amplitude across the brain relative to non-events (Zamani Esfahlani et al., 2020). This result further

suggests that the presence of events may directly relate to the temporal variability of BOLD signals for each individual.

Summary

Resting-state system segregation is a feature of brain network organization that has relevance to brain function in both health and disease across adult lifespan. It is unclear what gives rise to brain system segregation and the individual differences in this brain network measure. Here, I will explore two aspects of this important question: (1) Do vascular factors contribute to relationships between age and brain system segregation across the adult lifespan, and (2) Can sources of time-varying information help account for relationships between aging and brain system segregation? The interplay between these questions may further reveal how the temporal evolution of system reconfiguration at a short time scale impacts more stable features of large-scale network organization as a function of cardiovascular health. I will describe my efforts to answer these questions, whereby I have studied multiple large healthy adult lifespan datasets which each contain unique features relevant towards the questions at hand. The investigation in the context of healthy adult lifespan may further provide new perspectives in understanding decreased system segregation and behavioral outcomes in an aging population, and its relevance to brain and cognitive decline in both health and disease.

CHAPTER 2

DO VASCULAR FACTORS CONTRIBUTE TO RELATIONSHIPS BETWEEN AGE AND BRAIN SYSTEM SEGREGATION ACROSS THE ADULT LIFESPAN?

2.1. Introduction

Functional brain network organization can be estimated using BOLD signals detected by fMRI (Power et al., 2011) and has been shown to differ and change with adult age (Chan et al., 2014; Han et al., 2018; for reviews see Wig, 2017, Damasioux, 2017). It is presumed that age-related BOLD differences are due to differences in neuronal activity, however, BOLD signals may vary across age because of aging-accompanied changes in vascular factors. Vascular differences have been linked to brain structure changes in aging, including white matter lesions (Bots et al., 1993; Longstreth et al., 1996; Moroni et al., 2018) and cortical thinning (e.g., Marshall et al., 2017). Importantly, as vascular changes in aging impact dynamics of regional blood flow (Ito et al., 2002), this may lead to alterations of functional brain network organization that are measured using BOLD signals.

Functional MRI has been widely used to reveal neural activity of the brain (Ogawa et al., 1990). This technique measures BOLD signals which reflect the relative concentration of oxygenated to deoxygenated hemoglobin in blood vessels (Ogawa et al., 1990, 1993; Bandettini et al., 1992; Kwong et al., 1992). Greater neural activity (e.g., higher neuronal firing rate) increases energy consumption, resulting in altered cerebral blood flow and disproportional changes of the ratio of oxy- to deoxyhemoglobin (Buxton and Frank, 1997; Buxton et al., 1998). As such, BOLD based fMRI measures are inherently sensitive to both vascular and neuronal factors.

Vascular health decreases with age and impacts multiple levels of brain organization (molecular, cellular and structural [Paneni et al., 2017; Abdelkarim et al., 2019]). A prominent feature of aging is the impaired regulation of blood vessels that leads to global decreases of baseline cerebral blood flow across the brain of older adult individuals (Leenders et al., 1990; Ambarki et al., 2015; Nagata et al., 2016). These aging-related alterations of cerebral blood flow can affect properties of BOLD signals (e.g., magnitude), even when neural activity remains comparable (Cohen et al., 2002; Brown et al., 2003; Stefanovic et al., 2005).

Regulation failure can be a consequence of decreased flexibility of blood vessels to dilate and contract in order to adjust blood flow in response to neuronal activity (O'Rourke and Hashimoto, 2007). This property of vascular health can be measured using cerebrovascular reactivity (CVR). CVR quantifies the response of blood vasculature to changes in cerebral perfusion under the presence of vasodilatory stimuli (e.g., changes in CO_2 concentration via breath-holding or inhalation of CO_2 enriched gases).

There exist multiple methods to quantify CVR. BOLD-based CVR estimation relies on experimentally perturbing physiological states during functional MRI data acquisition, in which changes in BOLD signals are dominated by vascular factors while any apparent changes in neuronal activity are absent (Cohen et al., 2002; Brown et al., 2003; Stefanovic et al., 2005). With this approach, CVR values are derived as the ratio between BOLD signal changes and CO_2 level changes, reflecting local changes of venous functions with varying blood concentrations of CO_2.

CVR can also be estimated with imaging sequences sensitive to cerebral blood flow, such as arterial-spin labelling (ASL, Detre et al., 2009). ASL uses blood water proton as a diffusible

tracer labeled in the magnetic field, and serves as a proxy for quantifying cerebral blood flow at different locations of the brain (for review see Alsop et al., 2014). Similar to BOLD-based CVR, this approach monitors levels of end-tidal CO_2 but quantifies changes of cerebral blood flow (CBF) instead of BOLD signals. Specifically, increased pressure of CO_2 (hypercapnia) results in dilation of vascular smooth muscle and increased regional cerebral blood flow, while decreased CO_2 pressure (hypocapnia) causes vasoconstriction that leads to decreased regional blood flow (Mandell et al., 2008; Bright et al., 2009; Lu et al., 2011).

There exist important distinctions between CBF-based and BOLD-based CVR. As mentioned, CBF-based CVR (e.g., ASL) uses blood water proton as tracers, so it directly measures changes of cerebral blood flow and reflects arterial perfusion (Lee et al., 2001). By contrast, BOLD signal reflects venous activities because the signal is sensitive to changes of deoxyhemoglobin that is primarily in veins (Ogawa et al., 1990, 1993; Lee et al., 2001; Zhou et al., 2015). Arterial blood contains diamagnetic oxyhemoglobin that does not contribute significantly to BOLD signals (Ogawa et al., 1990; Lee et al., 1999). As such, CVR estimated from BOLD signals largely exhibit flexibility of venous systems to dilate/contract and regulate blood flow. Altogether, it is critical to note that while the two have been found to be highly related, CBF-based and BOLD-based CVR may reflect distinct aspects about the relationship between vascular functions and neural activities, and thus provide complementary information of brain activity in health and disease (Kastrup et al., 1999; Williams et al., 1992; Bright et al., 2009; Zhou et al., 2015).

In keeping with the above, both BOLD- and ASL-based CVR measures have been used to correct BOLD signals and minimize vascular confounds. For instance, ASL-based CVR maps can reveal spatial variability of cerebral blood flow. ASL-based CVR decreases with age at

multiple distributed brain locations, including the prefrontal cortex, anterior cingulate cortex, insular cortex, and caudate nucleus (Lu et al., 2011). While the spatial information provided by ASL imaging renders a possible contribution of regional blood flow to correct BOLD signals (e.g., Krishnamurthy et al., 2020), there exist a number of constraints that impede using cerebral blood flow to normalize BOLD signals. One disadvantage is the low spatial resolution of ASL images. ASL imaging requires fast image acquisition to capture signals from magnetically labeled blood water protons before relaxing to equilibrium state. This process leads to lower spatial resolution of ASL data that possibly mix signals from distinct brain tissues, such as gray matter, white matter, and CSF (Asllani et al., 2008). In addition to this technical challenge, cerebral blood flow data from ASL imaging relies on weak signals of perturbed magnetization that are highly susceptible to signal fluctuation from head motion and other spurious sources (Alsop et al., 2014). As such, low spatial resolution, low signal-to-noise ratio and prolonged acquisition time make it less desirable to use ASL data to minimize confounding effects of vascular factors on fMRI signals (for review see Tsvetanov et al., 2020).

In contrast BOLD-based CVR does not rely on tracers of blood water protons; accordingly, the images have been shown to exhibit higher signal-to-noise ratio in comparison to the ASL images (Alsop et al., 2014; Kassner et al., 2010). In addition, BOLD-based CVR is less susceptible to technical challenges in ASL imaging that are associated with shorter TR and lower SNR, rendering a higher spatial resolution of cerebrovascular reactivity images (Kassner et al., 2010; Tsvetanov et al., 2020).

As mentioned earlier BOLD-based CVR provides information of vascular health reflecting dynamic vascular function, especially the integrity of vascular endothelium and smooth muscle

in the vessel wall (Kety and Schmidt, 1948; Kuschinsky, 1996). As such, BOLD-based CVR has been utilized as an important biomarker for brain disorders (e.g., arteriovenous malformation [Fierstra et al., 2011]) and normal aging (Lu et al., 2011). Based on these considerations and availability of BOLD-based CVR maps, this information was used in the present chapter to account for vascular contributions to BOLD signals in this report.

In this chapter, a two-pronged approach was used to account for potential contributions of vascular factors on individual differences in brain system segregation across individuals. First, overall cardiovascular health measures were included as individual participant trait variables to account for individual differences in health conditions of the heart and blood vessels contributing to estimates of system segregation. Second, individual CVR maps were used to specifically correct BOLD signals for differences in functional flexibility of blood vessels at individual cortical surface vertices (analogous to voxels). Finally, the two approaches were combined to determine whether the relationship between adult age and brain system segregation remains after controlling for variation in vascular health and regional cerebrovascular properties. Collectively, these steps provide a stringent means to examine potential vascular confounds in the estimation of aging-related alterations in brain system segregation and its relationship with adult age.

2.2. Methods

Participants

This study included a large dataset consisting of healthy participants sampled from across adult lifespan. This dataset was comprised of data from 205 participants (age range: 24 – 93 years; female = 66.8%) from the Dallas Lifespan Brain Study (DLBS; 2nd timepoint of data

acquisition). Participants were recruited from the Dallas–Fort Worth community and were provided with written consent before participating. Study procedures were reviewed and approved by the Institutional Review Boards at The University of Texas at Dallas and The University of Texas Southwestern Medical Center. All participants were neurologically normal, right-handed, native English speaking healthy adults from DLBS. The exclusion criteria for participation are (i) disorders of the immune system, (ii) major substance abuse, (iii) coronary bypass surgeries, (iv) chemotherapy in the past 5 years, (v) loss of consciousness for more than 10 minutes, and (vi) any MRI safety contraindications. In addition, all participants went through a rigorous screening procedure to ensure cognitive health (Mini-Mental State Examination [MMSE] $\geq$ 26) and physical health (SF-36 Physical Component Score [M = 87.49±16.23]; SF-36 scores ranging from 0 to 100; higher scores indicate better health status, and 50 is a normative score). Participants with at least 150 frames of high-quality resting-state data (see RSFC Preprocessing) and CVR maps were included in the final sample (n = 102; female = 66.7%).

Imaging data acquisition

Brain images were acquired at the University of Texas Southwestern Medical Center, using a Philips 3T Achieva whole-body scanner (Philips Medical Systems, Bothell, WA) and a Philips 8-channel head coil with the Philips SENSE parallel acquisition technique. Each participant underwent 1 session in this dataset.

Anatomical Images. A T1-weighted sagittal magnetization-prepared rapid acquisition gradient echo (MP-RAGE) structural image was obtained (TR = 8.1 ms, TE = 3.7 ms, flip angle = 12°, FOV = 204 × 256 mm2, 160 slices with 1 × 1 × 1 mm^3 voxels).

Functional Images. Functional magnetic resonance imaging (fMRI) used a blood oxygenation level-dependent (BOLD) contrast sensitive gradient echo echo-planar sequence (TR = 2000 ms, TE = 25 ms, flip angle = 80°, FOV = 220 mm, 43 interleaved axial slices per volume, 3.5/0 mm (slice-thickness/gap), in-plane resolution = 3.4 × 3.4 mm^2). Two functional runs were acquired for each participant. In each functional run, the beginning 5 volumes were discarded to allow the MR signals reach a steady-state, and there were totally 180 volumes (acquisitions) left. During data acquisition, each participant was instructed to remain still while fixating on a white crosshair against a black background. Experimenters verified that participants complied with the instructions and did not fall asleep during the functional scan via verbal confirmation.

Processing of anatomical MRI images, cortical surface and subcortical anatomy

Anatomical images in their native space were first processed through FreeSurfer automated processing pipeline. (v5.3; Dale et al., 1999; Fischl et al., 1999; Ségonne et al., 2005). This pipeline includes sequential steps of processing, such as brain extraction, cortical and subcortical segmentation, generation of the gray matter-white matter boundary (white matter surface) and outer cortical surface (pial surface), inflation of the cortical surfaces to a spherical surface, and surface shape-based spherical registration of the participant's native surface to atlas surface (fs-average surface).

Additional measures were adopted to minimize the influence of head motion and other possible age-related confounds. For each participant, FreeSurfer output from its automatic pipeline was were manually inspected and edited as necessary. Results of inspection and manual editing were verified by an independent researcher. Specifically, manual editing included removal of nonbrain

tissue misclassified as part of the cortical surface, and adjusting voxel intensity values of tissue that led to misclassification of gray and white matter (Savalia et al., 2017).

A single deformation map was created for each participant by combining (i) the deformation map from native space to FreeSurfer's fsaverage atlas and (ii) the deformation map from fsaverage-aligned data to a hybrid left-right fsaverage surface (fs_LR; Van Essen et al., 2012). Each individual's surface in native space were then registered to the 164k fs_LR atlas using this single deformation map in a one-step resampling procedure and down-sampled to 32k standard mesh (Van Essen et al., 2012).

Due to age-related volume shrinkage of subcortical gray matter (Pfefferbaum et al., 1994; Good et al., 2001; Fox and Schott, 2004) and individual variability in change across age (Raz et al., 2005), the subcortical structures and cerebellum were aligned across participants to enable more precise comparison of anatomical features between participants and to better align functional data. The volumetric subcortical structures and cerebellum labeled by FreeSurfer in native space were registered to the DLBS adult-lifespan atlas (Chan et al., 2014). Atlas transformation was computed for each participant using the atlas-registered anatomical image.

Basic fMRI preprocessing

To reduce artifacts in functional images, measures were adopted to (i) correct intensity differences between odd and even slices attributable to interleaved acquisition without gaps, (ii) correct head movement within runs, and (iii) normalize image intensity to a whole brain mode value of 1000 (Miezin et al., 2000).

RSFC preprocessing

Functional volumes have been gone through additional preprocessing steps to reduce spurious variance unlikely to reflect neuronal activity in RSFC data (Power et al., 2014). These steps include (i) demeaning and detrending, (ii) multiple regression of the functional data to remove variance related to the whole brain gray matter signal (defined by each participant's own anatomy), ventricular signal, white matter signal, six detrended head realignment parameters obtained by rigid-body head motion correction, and the first-order derivative terms for all aforementioned nuisance variables. Despite of different opinions toward global signal regression in RSFC data processing, it has been shown that this method is effective to minimize motion-related artifacts (Satterthwaite et al., 2013; Power et al., 2017) and respiration-related artifacts when direct estimates of respiration are unavailable (Power et al., 2018). Because older adults are more prone to head movement [Van Dijk et al., 2012; Savalia et al., 2017] that leads to altered RSFC profiles [Satterthwaite et al., 2013; Power et al., 2014], it is critical to minimize the source of bias that may contribute to erroneous estimation of RSFC for the participants in this dataset. (iii) To reduce the effect of motion artifact, functional data were processed following a "scrubbing" procedure (Power et al., 2014). Motion-contaminated volumes were identified by frame-by-frame displacement (FD) that was calculated as the sum of absolute values of the differentials of the 3 translational motion parameters and 3 rotational motion parameters (Power et al., 2014). Volumes with excessive head motion (i.e., FD > 0.3 mm) were flagged. In addition, data between two motion-contaminated frames that were less than 5 frames were also flagged. These flagged motion-contaminated frames were removed and interpolated for the subsequent processing. (iv) Band-pass filtering ($0.009Hz < f < 0.08Hz$). (v) Removing the interpolated

frames that were used to preserve the time series during regression and bandpass filtering. Following RSFC preprocessing, 102 participants remained with 150 frames of clean data (female = 66.7%) for subsequent analyses.

Mapping functional data to surfaces

Connectivity Informatics Technology Initiative (CIFTI; Glasser et al., 2013) data files were created to integrate functional data from all possible locations of gray matter (such as the cerebral cortex, subcortical structures, and the cerebellum). Specifically, functional data of cortical surface were obtained by resampling functional volumes in "native" space to a 32k mesh surface using single deformation maps derived from surface data processing and smoothed on the surface with a Gaussian kernel (6 mm full width-half maximum [FWHM]). Functional data of each participant's subcortical structures and cerebellum were resampled from native volumes to an isotropic 3 mm atlas volumetric space, combining movement correction and atlas transformation in a single cubic spline interpolation (Lancaster et al., 1995; Snyder, 1996). This single interpolation procedure eliminates blurring that would be introduced by multiple interpolations. Subcortical data were smoothed in volumetric space with a Gaussian kernel (6 mm FWHM). Finally, functional data of the cortical surface, as well as volumetric time series of subcortical structures and the cerebellum (labeled by FreeSurfer pipeline) were combined to create the CIFTI files.

Regional cerebrovascular reactivity data (CVR)

Data were collected on a 3T MR system (Philips Healthcare, Best, The Netherlands). CVR was measured using a previously established hypercapnia paradigm (Liu et al., 2014; Lu et al., 2011; Marshall et al., 2014; Yezhuvath et al., 2009). For each participant, a plastic bag with a valve

was used to switch between room air and hypercapnic gas (5% CO_2 mixed with 21% O_2 and 74% N_2). The participant inspired room air and the hypercapnic gas in an interleaved manner (1-minute room air inhalation, followed by1-minute hypercapnic gas inhalation, which were repeated three times with additional 1-minute room air inhalation at the end). The duration of this this experiment was 7 minutes. BOLD MR images were acquired during the experiment (field of view [FOV] = 220×220 mm^2, matrix size = 64×64, 43 axial slices, thickness = 3.5 mm, no gap, TR = 200ms, TE = 25ms, flip angle = 80°, and single-shot EPI). Each participant's physiologic data (end-tidal CO_2, breathing rate, heart rate, and arterial oxygenation) were also recorded during this period (MEDRAD; Novametrix Medical Systems).

A volumetric CVR map was derived for each participant (N = 131 [female = 65.9%]; provided by Dr. Hanzhang Lu [Lu et al., 2011; Liu et al., 2013; Peng et al., 2018]). Briefly, this map was estimated by a general linear model (SPM, University College London, UK) with dependent variable of BOLD time series and independent variable of $EtCO_2$ measures, in which each resultant value represents %BOLD signal change per mm Hg of CO_2 change (%BOLD/mm Hg CO_2). For each participant, the CVR volumetric map was smoothed using a Gaussian filter with FWHM of 8 mm, and subsequently sampled to their 32k fs_LR surface (for additional details of generating these images, see Liu et al., 2013).

Correction of resting-state fMRI BOLD time-series using regional measure of CVR

Each participant's resting-state BOLD data were corrected to account for their measure of CVR, at a vertex-wise level. To do so, the resting-state fMRI BOLD time-series for each vertex was divided by the smoothed CVR value at the same vertex location, resulting in a CVR-corrected resting-state BOLD time-series.

Cardiovascular health (CVH) scores

For each participant, three measures were used to derive their cardiovascular health (CVH) scores: systolic blood pressure, diastolic blood pressure and body mass index (BMI). Each type of blood pressure was measured during participant's cognitive session and MRI session, then averaged across the 2 sessions. BMI was measured during MRI session, calculated using the following formula:

$$BMI = \frac{W}{H^2}$$

where W is the body weight and H is the height of each participant.

Cardiovascular health scores were calculated with these steps; (i) extracting the first principal component scores of the 3 variables, (ii) rescaling the scores to [0 1], (iii) subtracting scores by 1 such that a higher CVH value indicates better cardiovascular health condition of a participant.

Data analyses

System segregation

Using a published node set (333 nodes located on the cortical surface [Gordon et al., 2016]), a measure of brain system segregation will be computed to summarize values of within-system correlations in relation to between-system correlations (Chan et al., 2018; Chan et al., 2014). Without thresholding the correlation coefficients, this measure takes the differences in mean within-system and mean between-system correlation as the proportion of mean within-system correlation, as noted in the following formula (Chan et al., 2021):

$$System\ segregation = \frac{\frac{\sum_w^W Z_w}{W} - \frac{\sum_b^B Z_b}{B}}{\frac{\sum_w^W Z_w}{W}}$$

where Z_w represents connections (Fisher z-transformed correlation coefficients) within the same system, Z_b denotes connections between nodes of one system and nodes of other systems, W is the total number of within-system connections across all functional systems, and B is the total number of between-system connections. In previous work from our lab (Chan et al., 2014), calculation of system segregation was reported using the following formula:

$$System\ Segregation = \frac{\overline{Z_w} - \overline{Z_b}}{\overline{Z_w}}$$

where $\overline{Z_w}$ represents mean connectivity (Fisher *z*-transformed correlation coefficients) within the same system and $\overline{Z_b}$ denotes mean connectivity between nodes of one system and nodes of other systems. For overall system segregation, Z_w is the mean within-system connectivity of each system and Z_b is the mean between-system connectivity of each system to all other systems regardless of system types. A comparison between the 2 equations revealed that the updated formula more accurately specifies the exact computation of the measure and minimizes ambiguity (Chan et al., 2021).

2.3. Results

2.3.1. Measures of cardiovascular health exhibit a strong age effect during adulthood

To understand the relationship between vascular factors and brain system segregation, multiple measures of cardiovascular health (CVH) were investigated in this current report. Three related but independent variables were considered: systolic blood pressure, diastolic blood pressure and body mass index [BMI]. Systolic blood pressure exhibits an age-related increase ($r = 0.47$, $p < 0.001$), while no aging effect was found for diastolic pressure ($r = 0.146$, $p = 0.104$) or BMI ($r =$

0.148, p = 0.097). (**Figure 2.1 A – B**). Importantly, additional covariates were considered, including sex and education that are important participant-level measures contributing to aging brain (e.g., Chan et al., 2021). Controlling for sex and educational years did not alter these overall relationships (systolic pressure: $r = 0.483$, $p < 0.001$; diastolic pressure: $r = 0.138$, $p = 0.125$; BMI: $r = 0.151$, $p = 0.092$).

Given the similar but potentially unique sources of variance across the variables of CVH, the three measures were combined to derive a composite cardiovascular health score for each individual (see Methods of this chapter). A higher CVH score suggests better cardiovascular health in a participant. As expected, CVH scores exhibit a strong relationship with participant's age. CVH scores decrease with increasing age ($r = -0.408$, $p < 0.001$), indicating that cardiovascular health conditions are lower in older relative to younger adults (**Figure 2.1 D**). This relationship remains significant after controlling for sex and education ($r = -0.418$, $p < 0.001$).

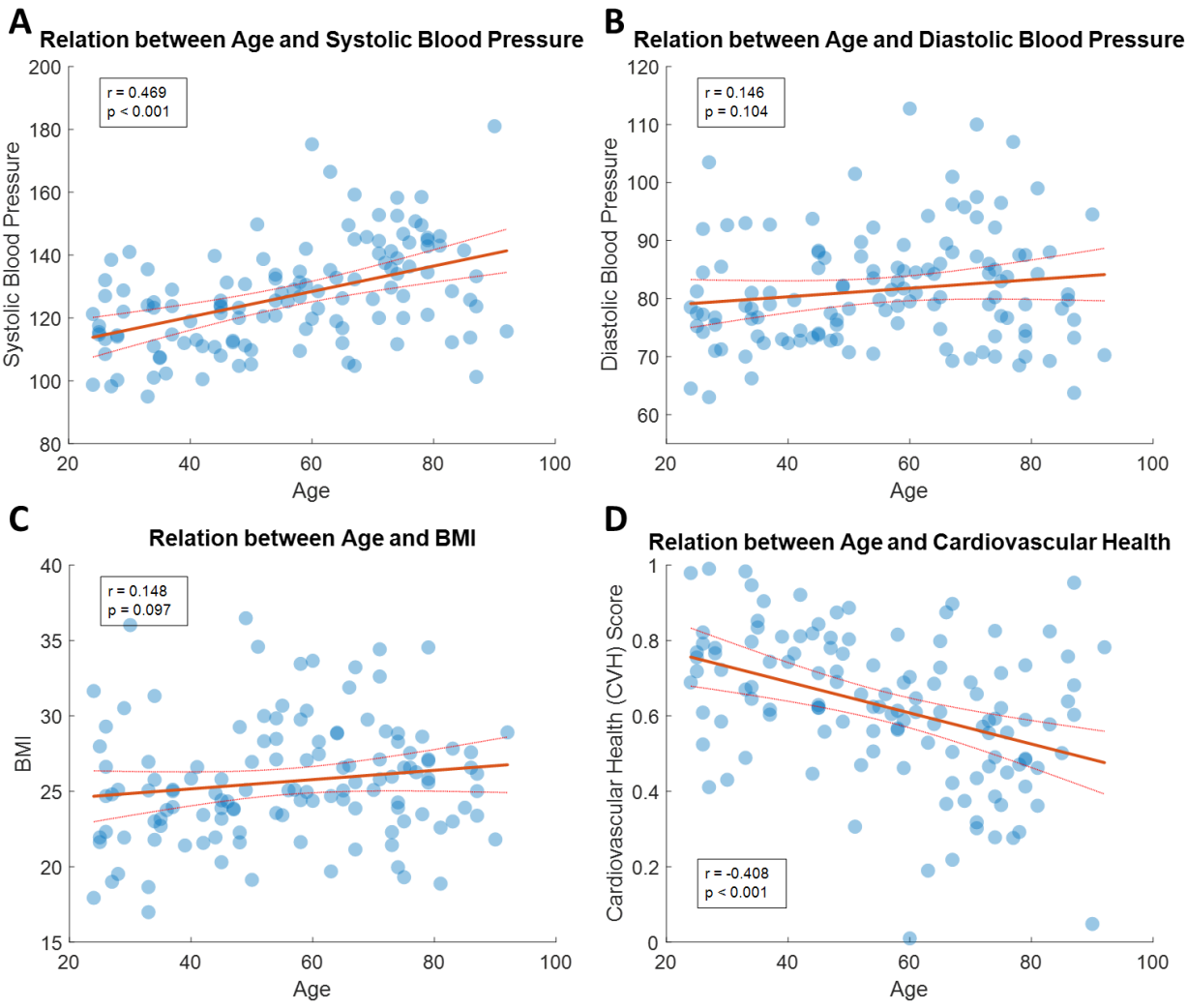

Figure 2.1. Cardiovascular health varies with increasing age. Cardiovascular health (CVH) scores were estimated from 3 separate measures related to cardiovascular health and function (systolic blood pressure, diastolic blood pressure and body mass index [BMI]). Using DLBS dataset 1, age-related increase has been revealed in (**A**) systolic blood pressure ($r = 0.469$, $p < 0.001$), but not (**B**) diastolic blood pressure ($r = 0.146$, $p = 0.104$) and (**C**) BMI ($r = 0.148$, $p = 0.097$). To derive a summary score quantifying CVH, first principal component scores were extracted from these 3 measures, rescaled to the range between 0 and 1, and subtracted by 1 to reverse the trend. A greater score suggests better cardiovascular health of this participant (for detailed computation see Methods). (**D**) CVH scores exhibits age-related decreases across the healthy adult lifespan in the DLBS dataset 1 ($r = -0.408$, $p < 0.001$). This demonstrates that older adults have less cardiovascular health relative to younger adults. Note that area between doted lines represents 95% confidence interval.

2.3.2. Cerebrovascular reactivity decreases with age across healthy adult lifespan

Another important vascular factor is cerebrovascular reactivity (CVR) that reflects the flexibility of blood vessels to dilate/contract. To summarize CVR information for each participant, mean cortical CVR was first calculated by averaging across all the vertices of each participant's CVR map. Mean CVR is negatively correlated with age ($r = -0.576$, $p < 0.001$), indicating that older participants have lower mean cortical CVR (**Figure 2.2 A**). This negative relationship remains after controlling for sex and education ($r = -0.587$, $p < 0.001$).

While mean CVR declines with increasing age, the relationship between age and CVR exhibits distinct spatial patterns across cortical brain locations. The CVR value at each vertex was correlated with age across all the participants. This calculation resulted in a 64k × 1 vector, in which each value represents the correlation coefficient between age and CVR at a given vertex on the brain surface. These correlation coefficient values were thresholded using false discovery rate (FDR) correction at the significance level of $p = 0.05$. The resultant correlation maps suggest that age-associated decreases in CVR are evident across many locations in the brain and are particularly prominent at specific brain regions which include insular cortex, dorsal medial prefrontal cortex and anterior cingulate cortex (**Figure 2.2 B**).

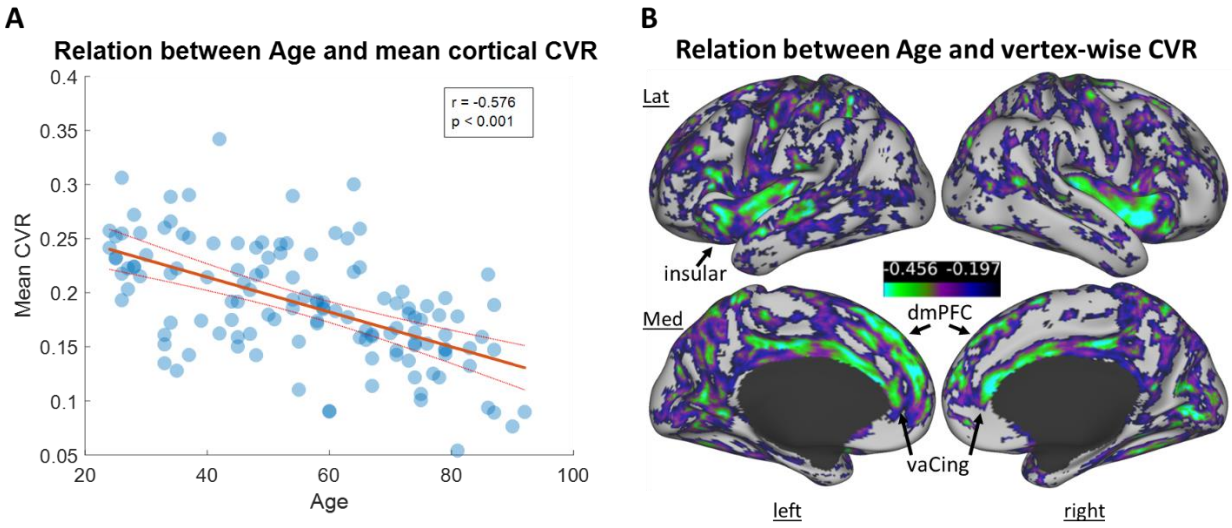

Figure 2.2. Cerebrovascular reactivity decreases with age. (**A**) A mean cerebrovascular reactivity (CVR) score was computed for each participant by averaging CVR maps across all vertices. There is an age-related decline of CVR scores, indicating less flexibility of blood vessel dilation in older adults ($r = -0.576$, $p < 0.001$). (**B**) Relationship between participant age and vertex-wise CVR values reveal distinct regions that are particularly prone to age-related differences in CVR. Each value on the surface represents the correlation coefficient between CVR values at this vertex and age across all the participants. Correlation coefficient values were FDR-corrected at the significance level of $p = 0.05$. All the survived correlation coefficients are negative, indicating strong aging-related decrease evident at distributed cortical locations, which include insular cortex, dorsal medial prefrontal cortex (dmPFC) and ventral anterior cingulate cortex (vaCing). Lat: lateral view, Med: medial view.

2.3.3. System segregation decreases with age across healthy adult lifespan, independent of vascular measures

Resting-state brain system segregation quantifies the amount of partitioning between distinct communities (i.e., functional systems) of a network, and has been shown to exhibit aging-related decreases across the healthy adult lifespan (e.g., Chan et al., 2014, 2021; Han et al., 2018; for review see Wig, 2017). In line with these observations, consistent aging effects were observed in

the present project (r = -0.4, p < 0.001; **Figure 2.3**). This aging-accompanied relationship persists after controlling for sex and education (r = -0.392, p < 0.001).

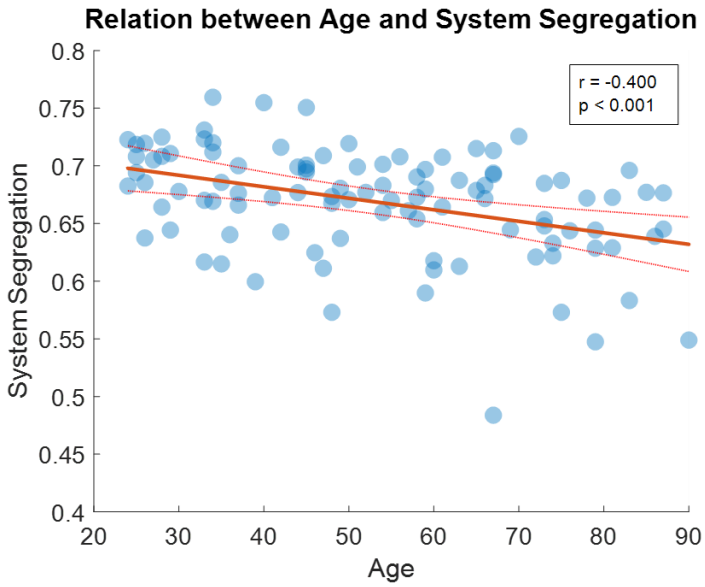

Figure 2.3. Brain system segregation decreases with age. Brain system segregation exhibits amount of partitioning between distinct functional systems of the brain. The result shows there is an aging-related decrease in system segregation (r = -0.4, p < 0.001), indicating less segregated functional systems in older adults.

A primary goal of the present research aim is to determine whether the relationship between age and brain system segregation persists despite the age-accompanied differences in vascular health and vascular measures reported in the previous section. This hypothesis was tested by first including the participant-level measures of CVH into calculations of the relationship between age and brain system segregation.

Controlling for CVH scores, relationship between age and resting-state brain system segregation is still significant (r = -0.265, p = 0.008; **Figure 2.4**). A comparison revealed that models before and after controlling CVH did not differ in ΔR^2 (F(96) = 3.561, p = 0.062). Critically, the age-

relationship with system segregation persists after further controlling for sex and education in the model (r = -0.271, p = 0.007). After all variables were included (age, sex, education), models before and after controlling CVH were not different (F(94) = 1.928, p = 0.168).

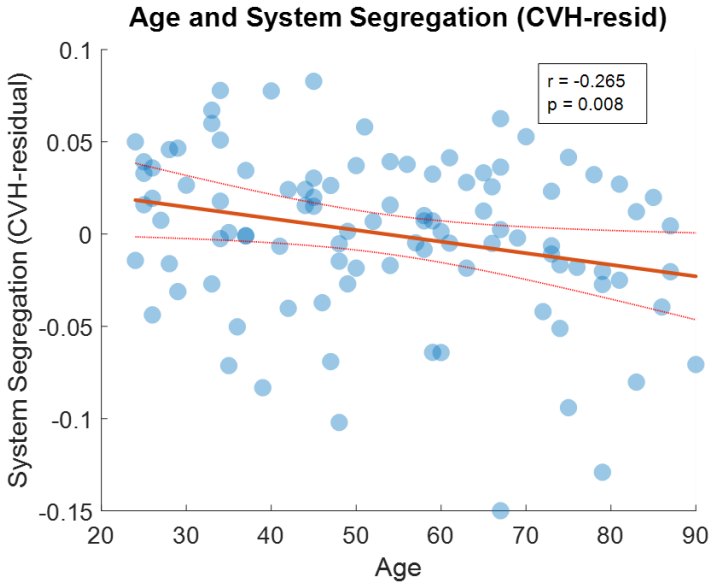

Figure 2.4. Aging-accompanied decrease of system segregation is independent of cardiovascular influence. To rule out the contribution of cardiovascular factors, CVH variance was regressed out from segregation. Note that residuals were used to visualize relationships after removing confounding variance. In the main analysis I included covariates in the model to control for the confounds. The result shows that residuals of segregation values are negatively correlated to age (r = -0.265, p = 0.008), indicating robust aging effect of segregation independent of cardiovascular influence.

To further understand sources of variance contributing to individual differences of segregation, a multiple regression was performed to predict system segregation using independent variables of age, CVH scores, sex and education. Using DLBS dataset revealed a significant contribution of age (t(94) = -3.203, p = 0.002) to the prediction of segregation, while no effect was observed for other variables (CVH: t(94) = 1.388, p = 0.168; sex: t(94) = -1.231, p = 0.221; education: t(94) = 0.462, p = 0.645). Including an age × CVH interaction in a second model along with the previous

variables (age, CVH scores, sex and education) also revealed a weak but significant interaction of the two on system segregation ($t(93) = 2.22$, $p = 0.029$) whereby older participants who had less cardiovascular health (lower CVH) exhibited lower system segregation than younger participants with similar level of cardiovascular health. These results indicated that CVH may contribute limited variance towards system segregation, some of which is related to participant's age. Consistent with the observations above, a formal mediation analysis where the IV was age, DV was system segregation and the mediator being CVH did not reveal that participant's CVH fully or partially mediated the relationship between age and system segregation. Specifically, the average causal mediation effects (ACME) was -0.0003, $p = 0.306$ ($CI_{95\%}$: -0.001, 0.000) (mediation effect confidence interval were estimated using 1000 bootstrap).

To investigate whether beta of age attenuates after including CVH in the model, beta of age from 2 models predicting system segregation were compared. The first model included age, sex, and education as independent variables; the second model included CVH in addition to age, sex, and education as independent variables. Beta of age of the first model was compared to beta of age from the second model using a bootstrap method. For each model, participants were bootstrapped 1000 times to create 1000 samples. The linear model was estimated for each sample, resulting in totally 1000 beta values of age. The distribution of beta values of age from model 1 (without CVH) was then compared to the distribution of beta values of age from model 2 (with CVH) using a two-sample t-test. The result demonstrated that beta from model 1 is statistically stronger than the beta from model 2 (β_{age_model1} = -0.001±0.0002; β_{age_model2}= -0.0008±0.0003; t = -12.595, $p < 0.001$).

Given the varying spatial distribution of age-related differences in cortical CVR, I incorporated this fine-grained spatial information about flexibility of blood vessel dilation at different brain locations. Specifically, to control for regionally specific cerebrovascular confounds, each participant's unique CVR map was used to correct BOLD signals at every vertex on the brain and then calculate system segregation using CVR-corrected signals (see **Methods** for details). Segregation values from CVR-corrected BOLD time series are positively correlated with segregation estimates from the original signals (without correction) ($r = 0.838$, $p < 0.001$; **Figure 2.5 A**). In keeping with this, the CVR-corrected segregation values continue to exhibit a significant decrease with increasing age ($r = -0.362$, $p < 0.001$; **Figure 2.5 B**), even after controlling for sex and education ($r = -0.356$, $p < 0.001$).

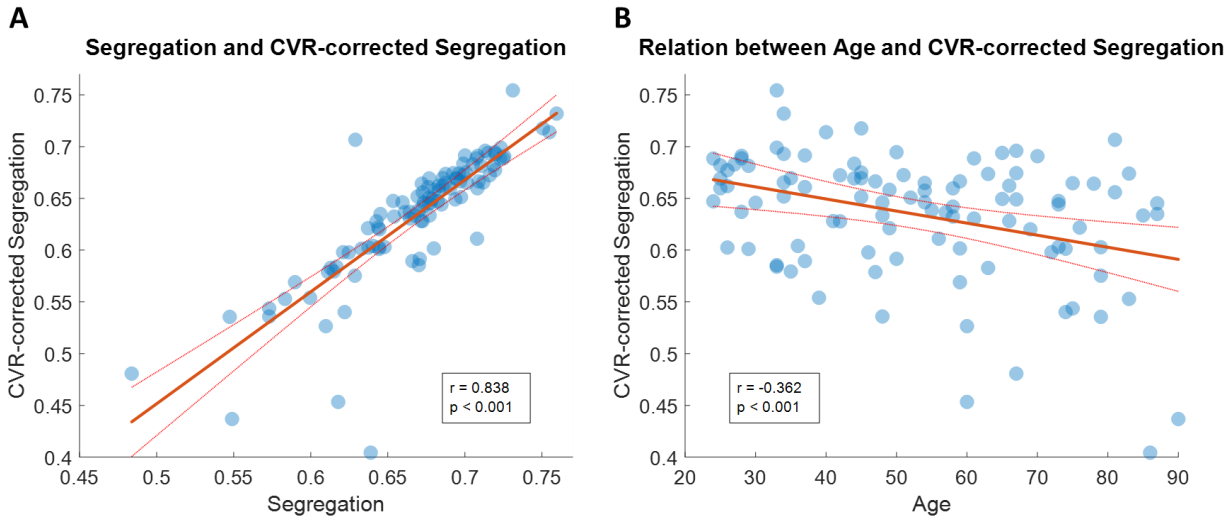

Figure 2.5. Brain system segregation was calculated after vertex (spatially) specific CVR correction of BOLD signals. Brain system segregation declines with increasing adult age. Segregation values were computed using resting-state BOLD time series corrected by each participant's unique CVR map. This provides a more precise correction of BOLD signals by incorporating distinct CVR information at different brain locations. This step results in CVR-corrected segregation that is correlated with the values using original signals (without CVR correction) (**A**). CVR-corrected segregation exhibits negative relationship with age ($r = -0.362$, p

< 0.001), which suggests a robust relationship between age and resting-state brain system segregation, even after a stringent correction using cerebrovascular reactivity maps (**B**).

Next, both CVH and CVR information were included in the analysis to minimize confounding effects of all available vascular factors on the relationship between age and brain system segregation. Specifically, system segregation using CVR-corrected signals was correlated to age, while including CVH as a covariate in the model. Using this stringent method, aging-accompanied decrease of system segregation persist in both datasets (r = -0.265, p = 0.008; **Figure 2.6**). Further including sex and education as covariates revealed consistent relationships (DLBS dataset 2: r = -0.271, p = 0.008).

To investigate whether including CVH and CVR leads to attenuated variance of age to system segregation, a bootstrap analysis was performed as described earlier. Specifically, 2 models were estimated; The first model included age, sex, and education as independent variables and system segregation from original signals (without CVR-correction) as dependent variable, while the second model included age, sex, education, CVH as independent variables and system segregation from CVR-corrected signals as dependent variable. The beta of age from model 1 was compared to beta of age from model 2, using the bootstrap method as described above. Briefly, participants were bootstrapped 1000 times to create 1000 samples. A linear model was estimated for each sample, resulting in totally 1000 beta values of age. The beta value distribution of age from model 1 was found to be not statistically different than beta values from model 2 (β_{age_model1} = -0.001±0.0002; β_{age_model2}= -0.001±0.0004; t = -1.136, p = 0.256). After accounting for the vascular variance based on multiple measures (CVH and CVR

correction), age-accompanied relationships with system segregation are not found to be generally attenuated.

Altogether, these collective results indicate that system segregation is a robust biomarker of aging brain networks, independent of regional differences in cerebrovascular properties and after accounting for individual variability in cardiovascular health.

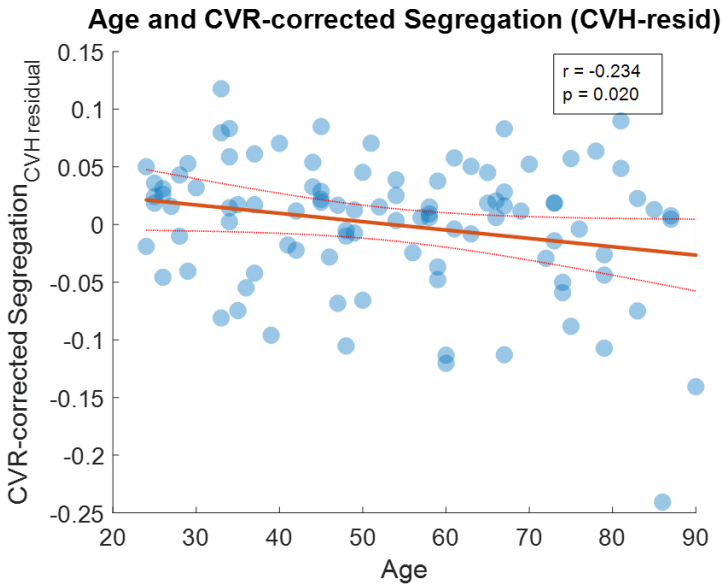

Figure 2.6. System segregation decreases with age, after stringently removing distinct sources of vascular confounds. To rule out different sources of vascular factors, both CVR and CVH were considered in the final analysis. BOLD signals were corrected using fine-grained spatial CVR maps, and used to compute resting-state brain system segregation. Participant's CVH score was regressed out from CVR-corrected segregation. Note that residuals were used to visualize relationships after removing confounding variance. In the main analysis I included covariates in the model to control for the confounds. The result shows that residuals of segregation were negatively correlated with age ($r = -0.234$, $p = 0.02$). These results suggest that brain system segregation is robustly related to participant age during adulthood, after minimizing potentially confounding effects from distinct vascular factors.

2.4. Discussion

In this chapter, using a large dataset that includes participants across the adult lifespan, I have demonstrated that aging is accompanied by altered vascular measures, including cardiovascular health (CVH) and cerebrovascular reactivity (CVR). These relationships were robust after controlling for individual differences in sex and education. Compared to summarized CVH scores which are a participant-level trait measure of overall health conditions of the heart and blood vessels, CVR provided fine-grained spatial information that exhibits aging effect at different brain locations, including insular cortex, dorsal medial prefrontal cortex and anterior cingulate cortex. I next investigated the impact of vascular factors on the well-established relationship between age and resting-state brain system segregation during adulthood. The relationship remains after controlling for each type of vascular factor. Finally, a stringent applied wherein both sources of vascular information were incorporated simultaneously: i) BOLD signals were corrected using CVR maps at each vertex and used to compute system segregation, ii) CVH scores were included as a covariate in the model. The age-related decrease of brain system segregation persists, even after further controlling for other confounds including sex and education. These results collectively demonstrate that resting-state brain system segregation serves as a robust biomarker reflecting brain re-organization across adult lifespan.

Consistent with prior reports (D'Esposito et al., 2003; Lu et al., 2010), my analysis revealed that an age-related decline of vascular measures, including cardiovascular health and cerebrovascular reactivity. Both of the two measures were summarized for each individual participant, demonstrating an overall aging effect on vascular factors (e.g., Tsvetanov et al., 2021). On the other hand, cerebrovascular reactivity maps provided fine-grained spatial information, and

revealed that aging-related decreases in CVR are evident across many locations in the brain, and are particularly prominent at specific brain regions which include insular cortex, dorsal medial prefrontal cortex and anterior cingulate cortex. These results are also consistent with previous findings (e.g., Lu et al., 2010), suggesting the importance of including vascular factors in understanding age-related alterations of neural activity across multiple brain regions.

One important caveat of this research is that BOLD-based CVR has been used to quantify cerebrovascular functions across adult lifespan. This method primarily reflects venous responses at the presence of vasodilatory stimulus, because BOLD signals are sensitive to deoxyhemoglobin that exists in veins (Ogawa et al., 1990, 1993; Lee et al., 2001; Zhou et al., 2015). By contrast, arterial responses would be better captured by alternate imaging methods (e.g., ASL; Detre et al., 2009). This distinction requires caution in the interpretation of CVR-related findings of this report.

Age-accompanied vascular changes relate to differences in brain structures (e.g., white matter lesions and cortical thinning), and dynamics of regional blood flow, even when neural activity remains comparable (Cohen et al., 2002; Brown et al., 2003; Stefanovic et al., 2005). These aspects pose critical challenges for estimating neural activity via BOLD signals. Accumulating evidence has shown that resting-state brain system segregation decreases with age across adult lifespan (Chan et al., 2014; Han et al., 2018; for review see Wig, 2017). Estimation of segregation is based on correlation patterns of BOLD signals sampled across the brain. As such, it is critical to evaluate whether the relationship between age and brain segregation is independent from vascular alterations. This report directly addresses this question by adopting a stringent procedure to control for vascular factors, and reveals that decreased system segregation

with age is not fully explained by non-neural vascular contributions (in fact, CVH was shown to not relate to brain system segregation when included in a larger model which also incorporated age, education, and sex as measures of interest), and strengthening the proposal that it serves as a measures of brain network re-organization which varies with age.

CHAPTER 3

CAN SOURCES OF TIME-VARYING INFORMATION HELP ACCOUNT FOR RELATIONSHIPS BETWEEN AGING AND BRAIN SYSTEM SEGREGATION?

3.1. Does resting-state BOLD signal variability relate to the measure of brain system segregation?

3.1.1. Introduction

Accumulating observations have revealed relationships between resting-state BOLD variability and individual differences in cognition and brain function across age. It has been shown that BOLD signals in the cortical regions exhibit less variability in older adults during a variety of conditions (including eye-fixation to a cross on the screen [Garrett et al., 2010], cognitive tasks [Garrett et al., 2011; Grady and Garrett, 2018], and resting-state scans [Kielar et al., 2016; Grady and Garrett, 2018]). A study of pharmacological intervention found that older participants receiving a GABA agonist experienced increases of BOLD signal variability and improved cognitive performance (Lalwani et al., 2021). Given that brain system segregation and BOLD variability are calculated from common measures, individual differences in BOLD variability may help explain some of the individual differences of resting-state brain system segregation across the adult lifespan, and contribute to our understanding of the mechanisms that establish brain system segregation more broadly.

As revealed in the previous chapter, vascular factors serve as a major source of confounds in BOLD signals. While it has been reported that the relationship between age and BOLD variability during resting-state persists after controlling for motion and cardiovascular influences

(e.g. Millar et al., 2020), there is also evidence that the relationship significantly diminishes after controlling for both cardiovascular and cerebrovascular estimates (Tsvetanov et al., 2020). These findings suggested that resting-state BOLD variability in older adults may need a more comprehensive evaluation by including non-neural factors that covary with age.

In this chapter, resting-state BOLD variability was directly compared to resting-state brain system segregation across individuals using DLBS dataset. Before doing so, I first evaluated the basic relationship between age and BOLD variability while controlling for vascular factors, in a manner consistent with the previous chapter. Specifically, I first investigated the relationship between BOLD signal variability and age while controlling for CVH, next I assessed this age-relationship with BOLD variability by initially correcting the variability measure using CVR maps at each vertex on the brain surface, and finally I combined both approaches to assess the robustness of the age versus BOLD signal variability relationship. In the second section of this chapter, I examined the relationship between resting-state BOLD signal variability and brain system segregation, including vascular controls throughout the comparisons.

3.1.2. Methods

Participants

DLBS data was used in this section. For detailed information about participant demographics and inclusion criteria see Methods of Chapter 2.

Data analyses

Variability of BOLD signals

BOLD signal variability was estimated using the standard deviation (SD) of the signals across time (e.g., Millar et al., 2020). To allow direct comparison between measures of BOLD signal

variability, regional CVR, and brain system segregation, variability was computed on brain network nodes (see Methods of Chapter 2 for description of nodes). Specifically, for each node of a given participant, the time series of all vertices within the node (n×t matrix, where n is the number of vertices and t is the time points) were first averaged (1×t vector). The temporal SD was calculated on this vector (resulting in a single SD value for each node). Finally, the SDs were averaged across all brain network nodes as a general estimate of BOLD variability for each participant (e.g., Millar et al., 2020).

To control for regionally specific cerebrovascular confounds, each participant's unique CVR map was used to correct BOLD signals at every vertex on the brain. CVR-corrected BOLD signals were averaged across all the vertices within each brain network node, and BOLD variability (SD) was computed on this CVR-corrected time-series. SD values of all nodes were finally averaged to derive an overall estimate of BOLD signal variability for each participant. To minimize biases from outliers, CVR-corrected BOLD variability values greater than 2.5 SD were excluded.

3.1.3. Results

3.1.3.1. Resting-state BOLD signal variability does not exhibit age-related differences after taking vascular factors into consideration

Each individual participant's overall resting-state BOLD variability was estimated using the temporal standard deviation of signals for each node, and then averaging across all nodes for that participant. Consistent with previous reports (e.g., Kielar et al., 2016; Grady and Garrett, 2018; Millar et al., 2020), there existed a significant relationship between participants age and BOLD signal variability whereby BOLD variability decreased with increasing age ($r = -0.391$, $p <$

0.001; **Figure 3.1**) using the DLBS dataset. This negative relationship remained after controlling for sex and education ($r = -0.416$, $p < 0.001$).

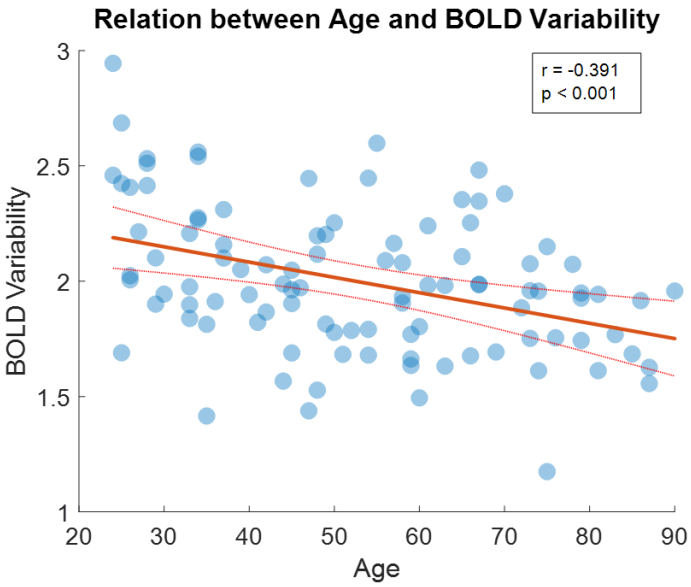

Figure 3.1. Resting-state BOLD signal variability decreases with increasing age across adult lifespan. BOLD variability was quantified by temporal standard deviation of BOLD signals. Using DLBS dataset, there exists an age-accompanied decrease in BOLD signal variability ($r = -0.391$, $p < 0.001$). These results suggest that BOLD signals may be less temporally variable in older adult individuals.

I next examined whether the relationship between age and BOLD variability persists despite the age-accompanied differences in vascular health and measures described in Chapter 2 of the present dissertation. After controlling for CVH scores, there still existed an age-related decrease of BOLD variability ($r = -0.342$, $p < 0.001$) using DLBS dataset (**Figure 3.2**). This relationship persisted after further controlling for sex and education ($r = -0.335$, $p < 0.001$).

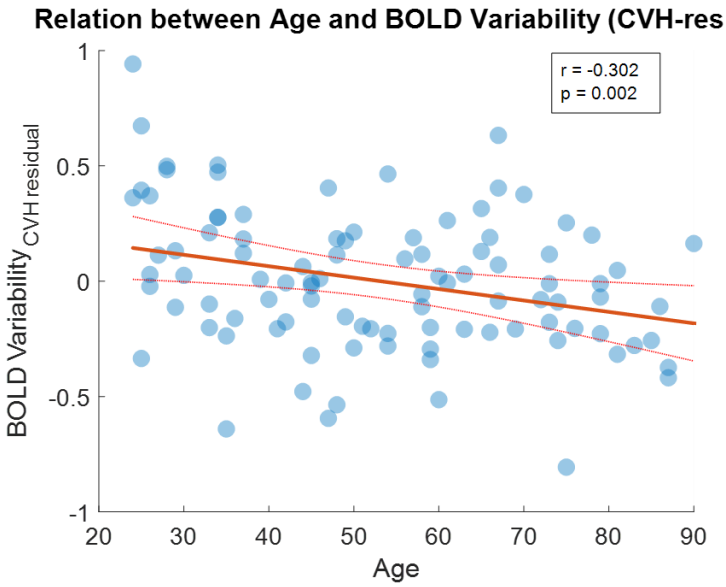

Figure 3.2. Aging-related decrease of BOLD variability persists after controlling for cardiovascular health (CVH) factors. One possible source contributing to the estimate of BOLD variability is cardiovascular health. To rule out the related confounds, CVH scores were regressed out from resting-state BOLD variability. Note that residuals were used to visualize relationships after removing confounding variance. In the main analysis I included covariates in the model to control for the confounds. There still exists a relationship between age and residuals of BOLD variability (r = -0.302, p = 0.002) using DLBS dataset. Note that the correlation coefficients are weaker relative to results using original BOLD variability without controlling for CVH. These results suggest that while BOLD variability may be partly explained by CVH, its relationship with age is robust after controlling for CVH confounds.

Next, cerebrovascular factors were taken consideration. Specifically, to control for regionally specific cerebrovascular confounds, each participant's unique CVR map was used to correct BOLD signals at every brain network node and then calculate BOLD variability using CVR-corrected signals (see **Methods** for details). To minimize biases from outliers, CVR-corrected BOLD variability values greater than 2.5 SD were excluded. The CVR-corrected BOLD variability was no longer related to age using DLBS dataset (r = 0.19, p = 0.058; **Figure 3.3**). Including sex and education did not alter the results (r = 0.194, p = 0.056).

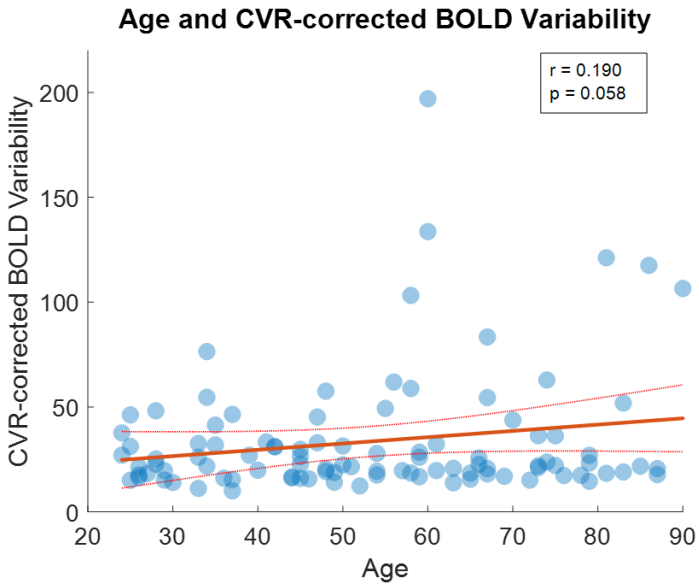

Figure 3.3. CVR-correction to BOLD signals alters the relation between age and BOLD variability. Another important source of confounds is individual difference of cerebrovascular reactivity. To control for this possible source of variance, BOLD signals were corrected using CVR maps at each brain network node, and were then used to compute BOLD variability. Using DLBS dataset, BOLD variability from CVR-corrected signals was marginally related to age (r = 0.19, p = 0.058).

As a final analysis, both CVH and CVR factors were included to stringently control for distinct sources of vascular confounds. Specifically, BOLD variability estimated using CVR-corrected signals was correlated to age, while CVH was included as a covariate in the model. With this stringent method, age was no longer related to BOLD variability (r = 0.102, p = 0.325; **Figure 3.4**). Further including sex and education as covariates in the model did not alter the results (r = 0.094, p = 0.37). Taken together, the relationship between age and BOLD variability seems to be largely explained by contributions from both cardiovascular health and cerebrovascular factors.

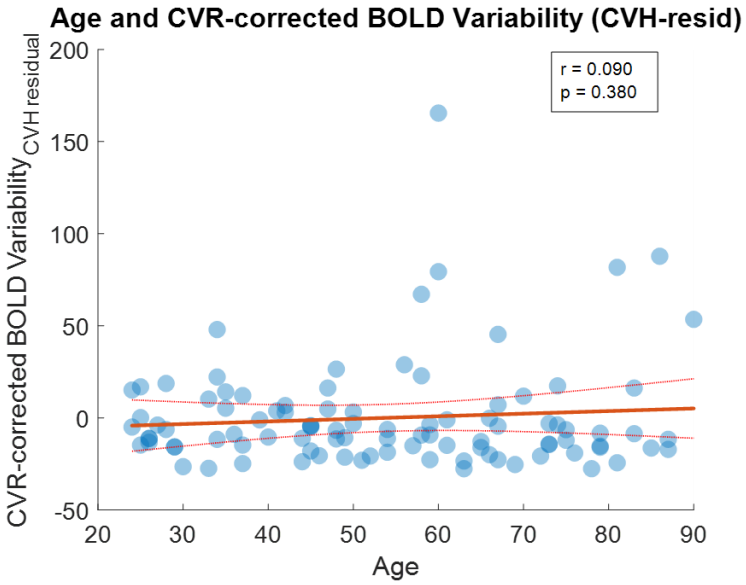

Figure 3.4. BOLD variability does not relate to age, after controlling for both vascular measures. To provide stringent control for vascular factors, BOLD variability was estimated using BOLD signals corrected using CVR maps, after which CVH variance was removed from CVR-corrected BOLD variability. Note that residuals were used to visualize relationships after removing confounding variance. In the main analysis, I included covariates in the model to control for the confounds. Using DLBS dataset, residual of CVR-corrected BOLD variability is not related to age (r = 0.09, p = 0.38).

3.1.3.2. Resting-state BOLD signal variability does not relate to system segregation when vascular factors are taken into consideration

The relationship between BOLD variability and system segregation was first examined directly. Mean BOLD variability was positively correlated to system segregation (r = 0.347, p < 0.001; **Figure 3.5 A**). The previous findings in this project revealed an association between age and each of the variables. To control for the confounding effect, age was included as a covariate in the model correlating segregation to BOLD variability, revealing a significantly positive relation between the two variables (r = 0.232, p = 0.019; **Figure 3.5 B**). After additionally controlling for

sex and education, the relation between segregation and BOLD variability was still significant (r = 0.256, p = 0.011).

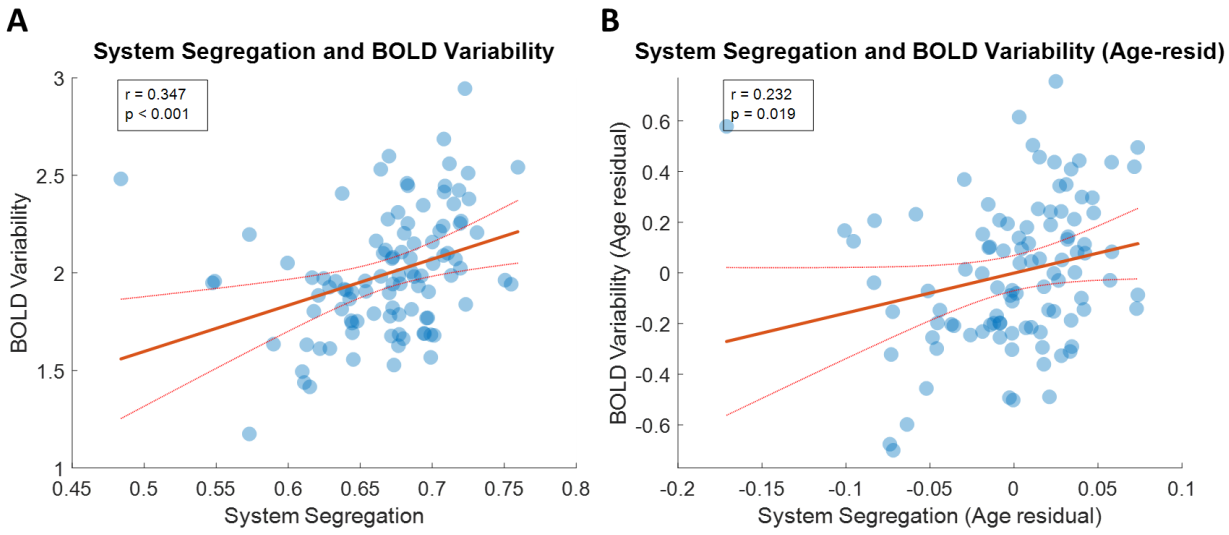

Figure 3.5. Relationship between BOLD variability and system segregation. (**A**) Using DLBS dataset, BOLD variability is positively correlated with system segregation (r = 0.347, p < 0.001). (**B**) After controlling for age, this relation is still significant (r = 0.232, p = 0.019).

Based on the above, it appears that resting-state BOLD signal variability directly relates to system segregation. However, the primary relationship between age and BOLD signal variability was found to not be significant after controlling for vascular factors. As such, it is important to control for this source of variance when examining the relationship between system segregation and BOLD signal variability.

BOLD variability was estimated using CVR-corrected BOLD time series. To minimize biases from outliers, BOLD variability values greater than 2.5 SD were excluded. Earlier findings in Chapter 2 revealed that the relationship between age and system segregation remains after CVR-correction. Consistent with this, system segregation values before and after CVR-correction were

highly correlated (r = 0.838, p < 0.001). Based on these observations, I included the original values of system segregation. The result showed that system segregation was no longer related to BOLD variability using node-wise CVR-corrected BOLD signals (r = -0.177, p = 0.085; **Figure 3.6**). After controlling for age, the relationship between system segregation and CVR-corrected BOLD variability was also not significant (r = -0.153, p = 0.139). Further including sex and education in the model did not alter the insignificant relationship (r = -0.141, p = 0.177). These results suggest that BOLD variability does not explain age-relationships with segregation.

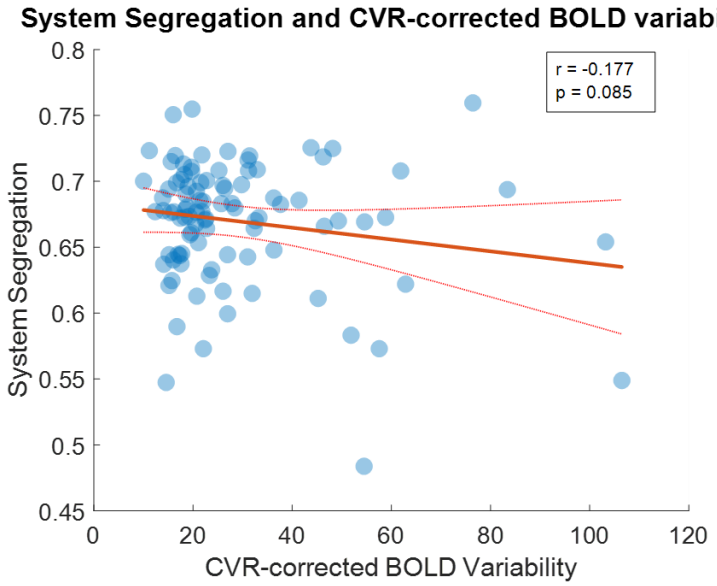

Figure 3.6. System segregation is not associated with CVR-corrected BOLD variability. To control for the confounding effects, each brain network node's BOLD time series were corrected using CVR maps, based on which CVR-corrected BOLD signal variability was derived. Using DLBS dataset, there is no significant correlation between system segregation and BOLD variability estimated from CVR-corrected time series (r = -0.177, p = 0.085).

3.1.3.3. Regionally specific considerations

While BOLD signal variability was calculated at the brain network node level and then averaged for the primary comparisons reported here, the relationship between age and BOLD signal

variability can also be investigated at different brain locations. As a supplemental analysis, I included this here information for completeness. For each vertex, BOLD variability was estimated from standard deviation of BOLD time series at this vertex. To estimate the relationship between age and BOLD variability on the brain, BOLD variability values at each vertex were correlated with age. The correlation coefficients were corrected using FDR at the significance level of $p = 0.05$. Using DLBS dataset (**Figure 3.7 A**), there existed spatially distributed brain regions in terms of the relationship between age and BOLD signal variability (e.g., posterior parietal cortex, cuneus cortex).

To derived CVR-corrected BOLD variability, BOLD signals at each vertex were corrected using the CVR value at the same vertex. CVR-corrected BOLD variability was estimated by deriving standard deviation of the CVR-corrected BOLD signals. However, consistent with observations on mean BOLD signal variability reported earlier, CVR-correction greatly attenuated the observed regional relationships between age and BOLD signal variability (**Figure 3.7 B**). The age-related decreases of BOLD variability were greatly diminished across the cortical surface, with few scattered locations exhibiting a positive relationship between age and BOLD variability (e.g., anterior cingulate cortex, insular cortex).

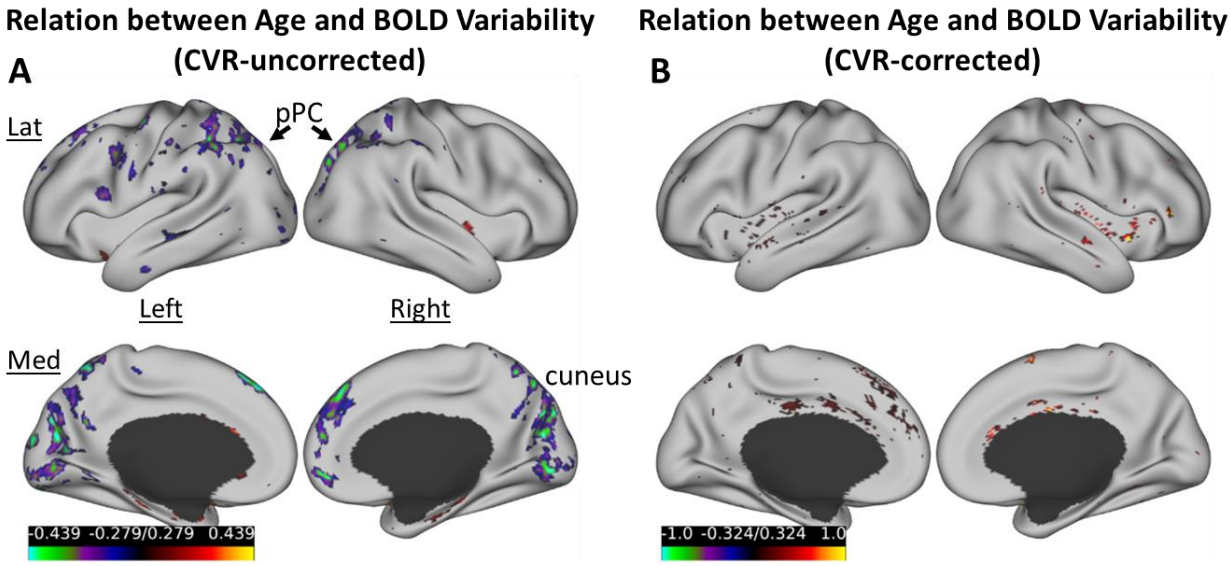

Figure 3.7. CVR-correction greatly attenuates the observed regional relationships between age and BOLD variability across most cortical locations. To estimate the aging effect of BOLD variability on the brain, BOLD variability values at each vertex were correlated with age across participants, with the resultant correlation coefficient indicating the aging effect of BOLD variability at this brain location. The correlation coefficients were corrected using FDR at the significance level of p = 0.05. (**A**) Using DLBS dataset, extensive brain regions exhibit an age-related decrease of BOLD variability. These regions include posterior parietal cortex (pPC) and cuneus cortex. (**B**) However, the prominent regional age-related decline of BOLD variability is no longer evident at these brain regions when BOLD signals were corrected using CVR maps at each vertex; in fact, the few regions that remain significant are largely exhibiting an opposing pattern (positive relationships). These results collectively suggest that CVR maps provide fine-grained spatial features of vascular factors that largely account for the relationship between age and BOLD signal variability.

3.1.4. Discussion

In this section, I first investigated the relationship between an individual's age and their resting-state BOLD signal variability before and after strictly controlling for vascular confounds. There exists an age-associated decline in BOLD variability, consistent with prior reports (e.g., Kielar et al., 2016; Grady and Garrett, 2018; Millar et al., 2020). To carefully evaluate the contribution of distinct sources of vascular factors to BOLD variability, 3 analyses were performed. Only

controlling cardiovascular health (CVH) scores, which represent an individual-level health measure, the relationship between BOLD variability and age persists. When BOLD variability was estimated using CVR-corrected signals, the relationship between age and BOLD variability is largely absent. Finally, examining the relationship between age and CVR-corrected BOLD variability while also controlling for individual's CVH scores also reveals an absence of relationship between the measures. These results demonstrate that vascular factors may serve as a major source of variance explaining the previously reported relationships between age and resting-state BOLD signal variability.

The next segment of this section turned to my primary question, determining whether there exists a relationship between resting-state system segregation and BOLD variability. Before controlling for vascular factors, there exists a positive relationship between system segregation and BOLD variability, even after controlling for age, sex, and education. However after CVR correction, this relationship no longer exists. These results collectively suggest that vascular factors, especially cerebrovascular reactivity, play a critical role in estimates of BOLD variability and explain the age-related differences in BOLD variability. This latter observation contrasts with the relationship between age and resting-state system segregation, which was documented in Chapter 2. Further, while system segregation appears to relate to BOLD variability, this relationship is also eliminated once vascular contributions are taken into account.

There is a prior reason to believe that the relationship between age and resting-state BOLD signal variability is not straight forward. Some studies have reported that the relationship between age and BOLD variability during resting-state persists after controlling for motion and cardiovascular influences (e.g., Millar et al., 2020). However other studies have shown that large

portions of relationship can be explained by vascular measures, including both cardiovascular and cerebrovascular measures (e.g., Tsvetanov et al., 2020). Specifically, Tsvetanov and colleagues (2020) estimated voxel-wise aging-related differences of resting-state BOLD variability using multiple linear regression that included both summarized cardiovascular health (CVH) and regional cerebrovascular measure (cerebral blood flow using ASL imaging) as covariates in the model. Similar to the work presented here, combining both vascular measures revealed an absence of age-relationships with BOLD variability across all voxels on the brain. It is possible that some of the mixed findings are due to an absence of spatially specific cardiovascular information in earlier reports, which relied solely on participant-level covariates to control for vascular contributions.

Consistent with the previous idea, in the present work, together with a participant level measure of vascular health (CVH) I incorporated a spatially specific measure (CVR). CVR maps provided vertex-wise information about blood vessel's capacity in response to metabolic demands. Existing studies (e.g., Lu et al., 2011; Liu et al., 2013) and the present analysis capitalized on the spatial maps of CVR to correct for the BOLD signals, providing a stringent measure to control for vascular confounds at the regional level when estimating the relationship between age and BOLD signal variability. The absence of fine-grained regional information (e.g., Millar et al., 2020) may result in a failure to account for important variation that relates to BOLD signal variability. In addition, cardiovascular and cerebrovascular factors may have unique contributions to variability estimates. This report included both CVH and CVR-correction in the analysis and revealed diminished age-relationships with BOLD signal variability, which is in line with Tsvetanov and colleagues' findings (2020). Notably, the present work used a different

approach and measures to control for vascular factors from the work of Tsvetanov et al.; (i) using CVR maps to provide unique information on dynamic capacity of blood vessels responsive to metabolic demands, and (ii) using CVR maps to correct BOLD signals at each brain location. Tsvetanov and colleague (2020) quantified resting-state regional blood flow as a cerebrovascular measure, whereas the current worked used CVR, which is considered to be a more direct measure of vascular endothelium and smooth muscle function, reflecting dynamic vascular capacity at different brain locations (Kety and Schmidt, 1948; Kuschinsky, 1996). Another advantage of CVR is its higher signal-to-noise ratio relative to regional blood flow estimated from ASL imaging (Alsop et al., 2014; Kassner et al., 2010). As such, this work provides important and complementary evidence for vascular factors in relevance to age-accompanied difference in BOLD variability. Collectively, vascular factors serve as a major source of variance towards measures of BOLD signal variability, which necessitates stringent and comprehensive measures to minimize vascular information impacting estimates of age-relationships with this property of the BOLD signal.

Accumulating evidence has suggested that the variability of BOLD signals may summarize the moment-to-moment alterations of functional network configuration that are relevant towards reconfiguring networks for task-related processing demands. Existing studies have revealed associations of resting-state BOLD signal variability to variability of BOLD signal during tasks (Mennes et al., 2013; Grady and Garrett, 2018) and cognitive performance (e.g., fluid abilities and episodic memory [Burzynska et al., 2015]). These observations have clear parallels with those noted for resting-state system segregation, although the two bodies of work have yet to be linked. It seems possible that resting-state BOLD variability may reflect dynamic re-organization

of segregated brain networks in support of cognitive functions. To test this possibility, this chapter directly investigated whether there exists a link between measures of resting-state BOLD variability and resting-state system segregation. There exists a relationship between resting-state BOLD signal variability and system segregation. However, after a stringent procedure to control for vascular confounds, there existed no relationship between BOLD variability and system segregation. This suggests that the relationship between BOLD variability and segregation is likely confounded by vascular information. These results added another piece of evidence that vascular factors serve as a major source of variance contributing to BOLD signal properties. Individual difference of BOLD variability may best reflect alterations of blood vessels capacity in response to metabolic demands rather than an indicator of dynamic re-organization in brain networks.

3.2. Do individual differences in moments of high pairwise-covariance (i.e., highly modular 'events') help explain relationships between age and resting-state brain system segregation?

3.2.1. Introduction

An important source of time-varying information emerges from moments of strong co-fluctuating patterns of BOLD signals between sets of network nodes (Zamani Esfahlani et al., 2020). These moments (termed as events) were identified by higher root mean square (RMS) of the co-fluctuation between signals from a variety of nodes. Importantly, the modular structure of brain networks is much more prominent during events relative to non-events (**Figure 3.8**). This interesting observation suggests that neural signals may consist of heterogeneous components (moments) that exhibit different patterns of connectivity over time.

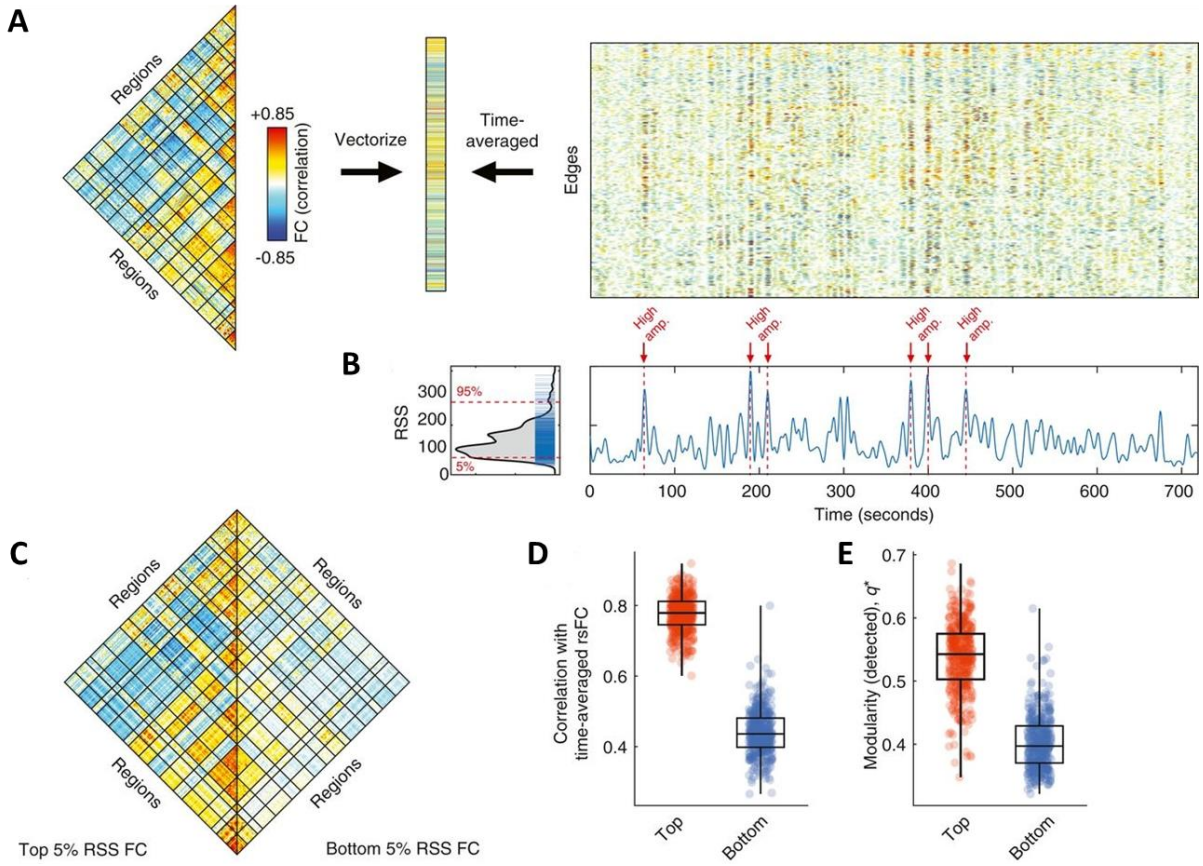

Figure 3.8. Moments with relatively greater amplitude of co-fluctuation between resting-state BOLD signals exhibit prominent modular structures of brain networks. (**A**) RSFC was estimated from Pearson correlation that could be temporally unwrapped to generate co-fluctuation timeseries for every pair of brain regions (edges). Co-fluctuation timeseries is the element-wise product of z-scored BOLD time series between node pairs. Conversely, co-fluctuation timeseries can be averaged across time, resulting in the vectorized RSFC matrix. (**B**) There are moments when co-fluctuation timeseries co-fluctuate collectively across the entire brain. These moments can be identified by estimating spatial variance across all co-fluctuation timeseries at each time point (quantified by root sum square [RSS]). The RSFC matrix from all time points (**A**) are more similar to the matrix using events' frames (top 5% of RSS) relative to the matrix from frames of non-events (bottom 5%) (**C**, **D**). (**E**) Network modularity is higher during events' frames, relative to non-event frames; also evident in the left half of (**C**). Figures adapted from Zamani Esfahlani et al. (2020).

Existing evidence of network modularly during events gives rise to a natural hypothesis that number of events in a resting-state time-series may relate to the overall magnitude of system

segregation which is typically calculated across an entire resting-state time-series. Functional brain networks exhibit much greater modular structure during events relative to non-events (Zamani Esfahlani et al., 2020; Pope et al., 2021); therefore, more frequent occurrence of events is likely to have greater contribution to modular networks over time, which can be reflected by greater system segregation within an individual. Based on this then, the first hypothesis is that participants with lower system segregation (i.e., older adult individuals) exhibit a smaller number of events.

Events can be revealed by identifying moments with greater co-fluctuation patterns across edges through computing root mean square (RMS) time series (Betzel et al., 2019; Zamani Esfahlani et al., 2020). The hypothesized relationship between events and system segregation is based on the assumption that other non-event moments with weaker RMS do not contribute to brain system. However, there exists an alternative possibility that individual difference in network organization across adult lifespan (i.e., system segregation) is not limited to high co-fluctuation moments (events), but exists across all the time points irrespective of RMS amplitude. Testing this second hypothesis requires comprehensive evaluation of relationships between age and system segregation limited to specific moments, including non-event moments with lower co-fluctuation amplitude across edges.

To test the two hypotheses, in this chapter I first investigated number of events across age and in relevance to individual differences of system segregation. The second experiment involved examining relationships between age and resting-state system segregation as a function of RMS moments, aiming to determine whether the age-system segregation relationship is limited to moments classified as events, or pervasive across the entire resting-state time-series.

3.2.2. Methods

Participants

This chapter includes 2 large separate datasets consisting of healthy participants sampled from across the adult lifespan. These two datasets were selected because of the availability of a greater amount of functional imaging data per participant, providing better estimates of events across time.

Dataset 1 was from DLBS dataset. For detailed information see Methods of previous chapters.

Dataset 2 was from the Human Connectome Lifespan Cohort (HCP Aging Release 1.0; Harms et al., 2018) with 628 healthy adults (age range: 36 – 100 years; female = 57.2%). This release has been made publicly available on Connectome Coordination Facility (http://www.humanconnectome.org/). The scanning protocol was approved by the Washington University in St. Louis's Human Research Protection Office and all participants provided written informed consent. Participants with at least 20-min high-quality resting-state data per session (see RSFC Preprocessing) were included in the final sample (n = 369).

Imaging data acquisition

HCP Aging: Participants were scanned on a Siemens 3T Prisma whole-body scanner (Siemens, Erlangen, Germany) with a Siemens 32-channel head coil at one of 4 different sites (Massachusetts General Hospital, University of California-Los Angeles, University of Minnesota and Washington University in St. Louis). Each participant completed two scanning sessions on two separate days.

Anatomical Images. Each participant has a single T1-weighted MP-RAGE structural scan (TR = 2500 ms, TE = 2.22 ms, TI = 1000 ms, resolution = 0.8 × 0.8 × 0.8 mm^3, flip angle = 8°) and a T2-weighted structural scan (TR = 3200 ms, TE = 563 ms, resolution = 0.8 × 0.8 × 0.8 mm^3).

Functional Images. Resting-state functional MRI images were acquired while the participants relaxed with eyes open using a gradient-echo EPI sequence (multiband factor = 8, TR = 800 ms, TE = 37 ms, flip angle = 52°, 104 × 90 matrix size, 72 slices, 2 mm isotropic voxels, and 488 time points (~6.5 min) per scan. There were 2 resting-state scans in each session (so a total of 4 scans across the two days), with different phase-encoding directions (RL and LR) in each scan.

Processing of anatomical MRI images, cortical surface and subcortical anatomy

HCP Aging: Anatomical MRI images were processed using the HCP structural pipelines that consist of 3 parts (PreFreeSurfer, FreeSurfer and PostFreeSurfer). These pipelines mostly overlap with the steps taken to process dataset 1, with some additional steps to specifically optimize the processing HCP dataset based on parameters of data acquisition. The PreFreeSurfer pipeline produced an undistorted native structural volume space for each participant, aligns the T1w and T2w images, performed a B1 (bias field) correction, and registers the participant's native structural volume space to MNI space. The FreeSurfer pipeline segmented the volume into predefined structures (including tissues of gray matter, white matter, and subcortical structures), reconstructed white and pial cortical surfaces, and performed FreeSurfer's standard folding-based surface registration to their surface atlas (fsaverage). PostFreeSurfer has been the final structural pipeline that produced NIFTI volumes and GIFTI surface files, along with applying the surface registration (to the Conte69 surface template; Van Essen et al., 2012), down-sampling registered surfaces, and creating the final brain mask.

Basic fMRI preprocessing

HCP Aging mainly employs the HCP fMRI Volume pipeline that largely overlaps with steps to process dataset 1 (e.g., realign the timeseries to correct for head motion and normalize the image intensity across runs to a whole brain mode value of 1000 [Miezin et al., 2000]). Due the parameters in HCP data acquisition, additional steps were taken to correct gradient-nonlinearity-induced distortion, perform EPI fMRI image distortion correction due to phase encoding directions, and combine all of the transforms for each registration and distortion correction step into a single nonlinear transformation that can be applied in a single resampling step.

RSFC preprocessing

Similar to Dataset 1 (DLBS), HCP Aging dataset has gone through additional preprocessing steps to reduce spurious variance unlikely to reflect neuronal activity in RSFC data (Power et al., 2014). (i) Demeaning and detrending. (ii) Multiple regression of the BOLD data to remove variance related to the whole brain gray matter signal (defined by each participant's own anatomy), ventricular signal, white matter signal, six detrended head realignment parameters obtained by rigid-body head motion correction, and the first-order derivative terms for all aforementioned nuisance variables. Despite of different opinions toward global signal regression in resting-state data processing, this method has been shown effective to minimize motion-related artifacts (Satterthwaite et al., 2013; Power et al., 2017), and remove global respiration-related confounds when direct estimates of respiration are unavailable (Power et al., 2018). Because older adults are more prone to head movement [Van Dijk et al., 2012; Savalia et al., 2017] that leads to altered RSFC profiles [Satterthwaite et al., 2013; Power et al., 2014], it is critical to minimize the source of bias that may contribute to erroneous estimation of RSFC. (iii)

To reduce the effect of motion artifact on RSFC, data were processed following a "scrubbing" procedure (Power et al., 2014). Motion-contaminated volumes were then identified by frame-by-frame displacement (FD) that was calculated as the sum of absolute values of the differentials of the 3 translational motion parameters and 3 rotational motion parameters (Power et al., 2014). A recent study showed that high-frequency respiratory artifact can confound estimates of FD, in particular for scans using multiband sequencies with short TRs (Fair et al., 2020). As such, the motion parameters for HCP Aging dataset were filtered to remove high-frequency components prior to the estimate of FD and a more stringent cutoff for FD was used (FD > 0.08 mm). In addition, data between two motion-contaminated frames that were less than 5 frames were also flagged. These flagged motion-contaminated frames were removed and interpolated for the subsequent processing. (iv) Band-pass filtering (0.009Hz < f < 0.08Hz). (v) Removing the interpolated frames that were used to preserve the time series during regression and bandpass filtering. Following RSFC preprocessing, 369 participants were retained with 20-min clean data for subsequent analyses.

Mapping functional data to surfaces

HCP Aging: HCP fMRI Surface pipeline was used to map functional images in volumetric space to the standard CIFTI gray ordinate space. This pipeline largely overlapped with the steps used for dataset 1, with some specific optimization for HCP dataset (e.g., 2mm FWHM kernel due to image resolution): i) used partial volume weighted ribbon-constrained algorithm to map cortical data to the cortical surface, ii) down-sampled the surface timeseries from the high-resolution native mesh to the registered 32k_fs_LR mesh, iii) smoothed the surface data with 2 mm FWHM Gaussian kernel and applied a correction for differences in the triangle areas associated with each

vertex. Subcortical timeseries were processed using a FreeSurfer parcel-constrained atlas resampling/smoothing (2 mm FWHM Gaussian kernel) process, which enables better correspondence of subcortical voxels across participants and minimizes the bias of the voxels from undesired structures. Finally, the cortical data on the surface and subcortical data in volume space were combined such that functional timeseries are now in standard CIFTI grayordinate space (91282 vertices and voxels).

Calculation of network Modularity (Newman's Q)

Newman's Q quantifies the degree to which the entire brain network could be divided into separate functional systems (Newman, 2004).

$$Q = \sum_{u \in M} \left[e_{uu} - \left(\sum_{v \in M} e_{uv} \right)^2 \right]$$

where M is a set of nonoverlapping modules in the network, and e_{uv} is the proportion of all links that connect nodes in module u with nodes in module v. A Q value was derived from a thresholded correlation matrix at each edge density from top 1% to 10% in increments of 1%.

Calculation of RMS and identification of events

Events are moments exhibiting much stronger co-fluctuation amplitude across a variety of node pairs relative to other moments across all time points. These periods have been shown to correspond to moments where there exists a highly modular structure of the brain networks (Zamani Esfahlani et al., 2020). The first step to identify events is to generate co-fluctuation timeseries for every pair of nodes (i.e., edges). The BOLD time series in each node is normalized across time, followed by calculating the element-wise products between every node pair at every time point (i.e., at each frame/volume). This co-fluctuation time series (i.e., edge time series)

reflects the degree to which the BOLD signals from two distinct nodes fluctuate together across time. This results in a n×t edge time series matrix for each participant (**Figure 3.9 A**), where n is the number of edges between node pairs and t is the number of time points (or frames/volumes of BOLD resting-state data, in the present case). Across all the edges, there are moments in time where a variety of edges collectively co-fluctuate with higher amplitude, which can be derived by calculating the root mean square (RMS) across all the edges at each time point (i.e., RMS value of each column in the matrix).

The moments with highest RMS were identified as events (red circles in **Figure 3.9 B**). Following previous reports on this topic (Zamani Esfahlani et al., 2020; Pope et al., 2021; Betzel et al., 2022), top 5% of RMS distribution was used as the threshold for detecting events in the initial analysis. This was followed up by using a more relaxed RMS threshold (top 10%). Any peaks above the threshold were identified as events, whereby peaks were defined as local maxima of the RMS time series.

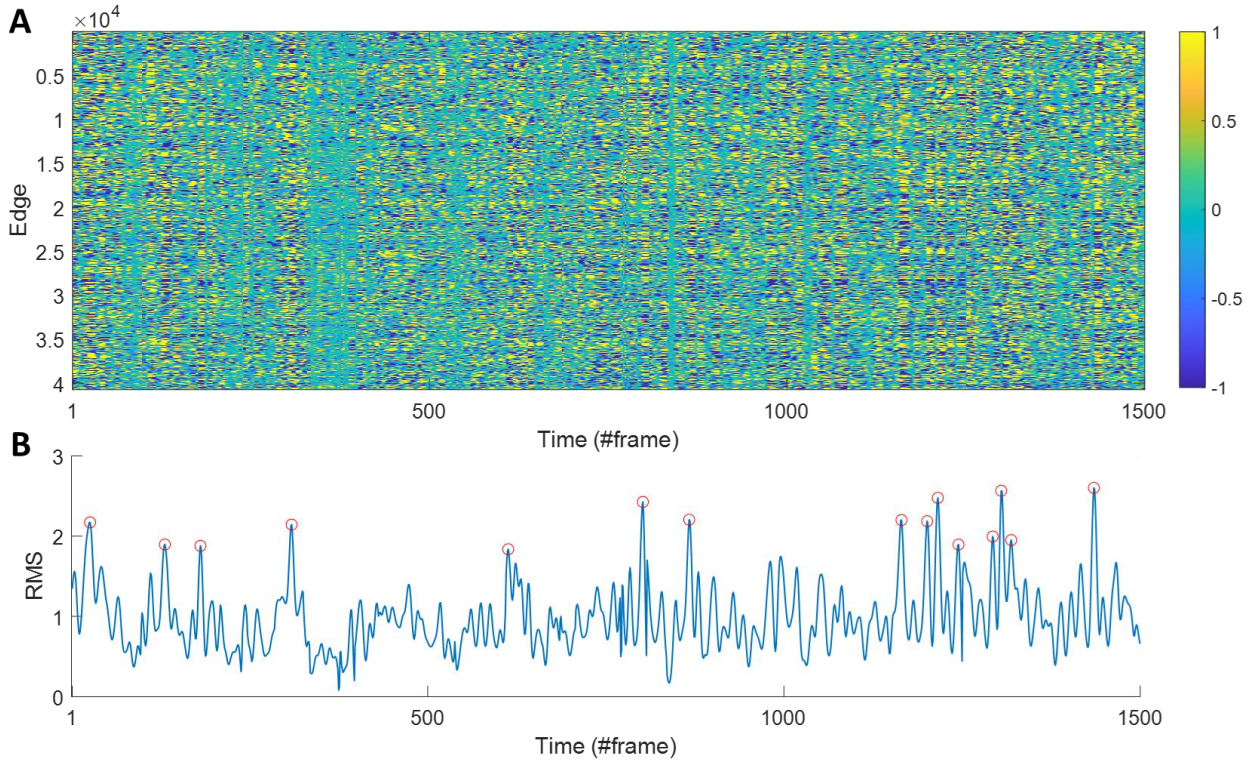

Figure 3.9. Identification of events using an exemplar participant's data. (**A**) is an edge matrix, where each row is the element-wise product between every node pair's time series. This reflects the co-fluctuation pattern between each node pair; a positive value means signals of the two nodes fluctuate in the same direction whereas a negative value denotes opposite fluctuation. (**B**) There are moments exhibiting collective co-fluctuation between edges across the entire brain. These moments can be identified by estimating spatial variability across all co-fluctuation timeseries at each time point (quantified by root mean square [RMS]). These moments are captured by identifying peaks of top RMS (e.g., top 5% [Zamani Esfahlani et al., 2020]), marked by red circles.

3.2.3. Results

3.2.3.1. Events are moments exhibiting a more modular organization and higher resting-state system segregation

Events are moments exhibiting high co-fluctuation patterns across edges, which could be captured by highest RMS values across all the edges (e.g., top 5%). Two independent datasets

were examined to evaluate the distribution of RMS. Despite of differences between the two datasets (e.g., data acquisition parameters, participants' demographics), the distributions of RMS are surprisingly consistent across the two datasets, with a comparable thresholding cutoff to identify the top 5% of RMS values (DLBS dataset: $RMS_{top5\%}$ = 1.78; HCP Aging: $RMS_{top5\%}$ = 1.85; **Figure 3.10**). For each dataset, its own cutoff value was used to identify events, which renders events comparable across participants.

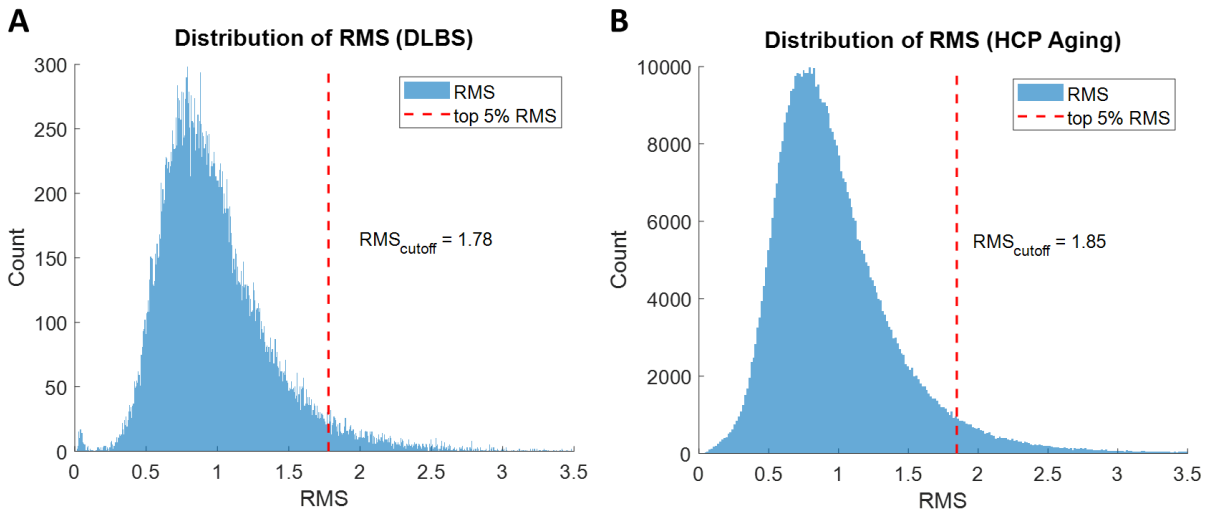

Figure 3.10. Two independent adult lifespan datasets were used in this chapter: DLBS and HCP Aging datasets. Both datasets exhibit consistent distributions of RMS values. Despite the differences across datasets (e.g., participants, data acquisition parameters), they exhibit consistent right-skewed distributions of RMS, with relatively comparable cutoff values to identify the top 5% of RMS values, which correspond to 'events' (DLBS dataset: $RMS_{top5\%}$ = 1.78; HCP Aging: $RMS_{top5\%}$ = 1.85).

It has been shown that events are accompanied by elevated modularity of functional brain networks (e.g., Zamani Esfahlani et al., 2020). Consistent with this, examining the mean correlation of events vs non-events across all participants revealed a highly modular correlation matrix (**Figure 3.11**). The upper triangle of each matrix is the node-to-node correlation matrix

using event frames (top 5% RMS), while lower triangle is from non-event frames (bottom 5% RMS). The sharp contrast of modular structures for events vs non-events is evident in both DLBS dataset (**Figure 3.11 A**) and HCP Aging (**Figure 3.11 B**). Using a different RMS cutoff to identify events (top 10% RMS) resulted in a similar contrast of patterns between the correlation matrix corresponding to event frames versus non-event frames. Consistent with these apparent patterns, Newman's Q (Newman, 2004), which quantifies the quality of the modularity partitioning revealed a significant difference between the two halves of the mean correlation matrices. A Q value was computed for each edge density from 1% to 10% at the increment of 1% for each mean correlation matrix, resulting in 10 Q values for the mean matrix from event frames and 10 Qs for the matrix from non-event frames. Using DLBS data, Q value using event frames ($M_Q = 0.659 \pm 0.08$) was consistently higher than Q from non-event frames ($M_Q = 0.617 \pm 0.12$) at each density. Using HCP Aging data revealed consistent differences between Q values from events ($M_Q = 0.672 \pm 0.08$) and Qs of non-events ($M_Q = 0.642 \pm 0.09$). These results collectively revealed more modular structure of the brain networks during events relative to non-events.

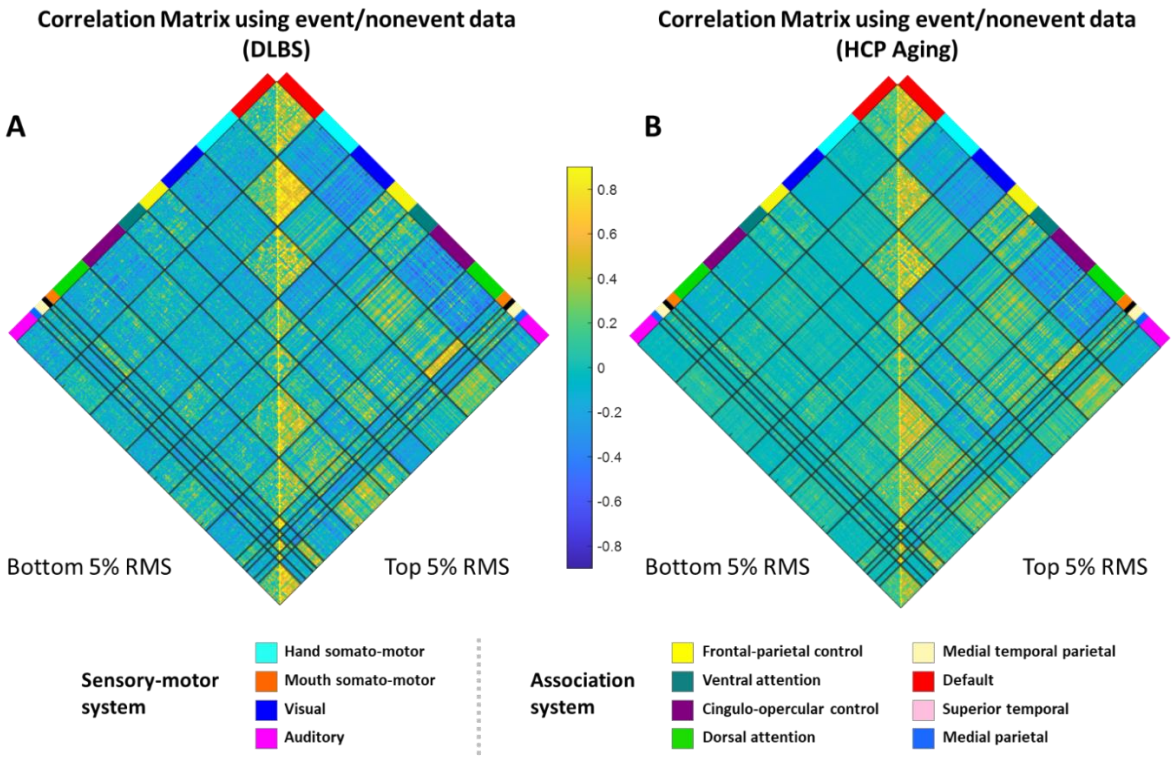

Figure 3.11. Correlation matrix from events exhibits stronger modular structure of brain networks. To compare network organization during events vs non-events frames, the node-to-node correlations were computed using frames from events (top 5% RMS) or non-events (bottom 5% RMS) in each participant. The matrices were then averaged across all participants in each dataset. In this figure, the right triangle of each correlation matrix was computed using event frames while left triangle of each matrix was from frames of non-events. The nodes of the correlation matrices are ordered and labelled according to a pre-defined atlas of brain systems (Gordon et al., 2016), to facilitate viewing of the modular pattern. Both DLBS dataset (**A**) and HCP Aging (**B**) showed sharp contrast between left and right triangles of correlation matrices, whereby a modular structure is evident in the right triangle (i.e., high within system correlations along the diagonal blocks, lower between system correlations in the off-diagonal blocks), suggesting much stronger modular structure of brain networks during events relative to non-events.

To more closely examine the apparent distinction of modular structures at different moments, system segregation using data from events (frames of top 5% RMS) was compared to system segregation of non-events (frames of bottom 5% RMS), for each participant within each dataset.

A paired-samples t-test revealed higher system segregation values during events relative to non-events in both DLBS dataset ($t(216) = 17.823$, $p < 0.001$; **Figure 3.12 A**) and HCP Aging datasets ($t(368) = 13.972$, $p < 0.001$; **Figure 3.12 B**).

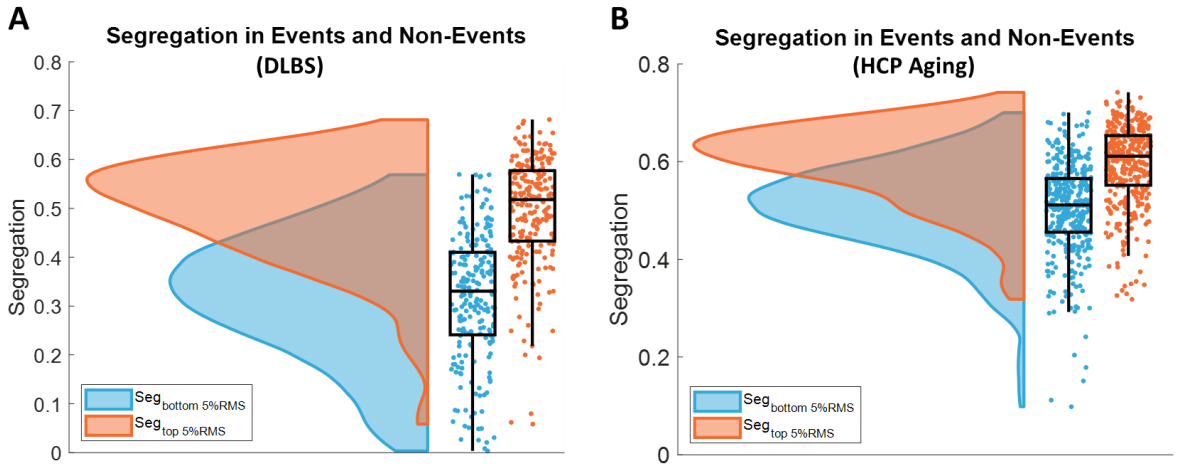

Figure 3.12. Moments with greater pairwise-covariance (i.e., events) exhibit higher system segregation relative to moments with low pairwise-covariance. Events are moments that exhibit much stronger co-fluctuation amplitude across a variety of node pairs. These moments can be identified by isolating frames with higher root mean square (RMS) across all edges (e.g., top 5% RMS). To quantify functional network organization during events, system segregation was computed using data from events (top 5% RMS), and compared to system segregation values from non-events (bottom 5% RMS). (**A**) shows greater system segregation during events relative to non-events using DLBS dataset (paired-samples t-test: $t(216) = 17.823$, $p < 0.001$) and (**B**) depicts a similar distinction using the HCP Aging dataset (paired-samples t-test: $t(368) = 13.972$, $p < 0.001$, demonstrating that resting-state functional brain networks are more segregated during event time points. In each raincloud plot, individual dots represent participants. Box and whisker plots summarize the distribution of segregation values (upper and lower bound of each box denote 25^{th} and 75^{th} percentiles). Histograms to the left depict kernel density estimate of data distribution.

To confirm that this observation was not a product of the specific RMS cutoff used to identify events, an additional analysis was done using a different threshold (top 10% RMS). This resulted in consistent findings: event system segregation is significantly higher than non-event system

segregation in both datasets (DLBS dataset: $t(230) = 21.687$, $p < 0.001$; HCP Aging: $t(368) = 12.386$, $p < 0.001$). These results demonstrate that resting-state functional brain networks are more segregated during moments at which higher pairwise-covariance between edges is present.

3.2.3.2. Mathematical proof that CVR-correction does not alter the estimation of RMS and identification of events

Events were estimated from each participant's BOLD time series. As revealed in Chapter 3.1, vascular factors can be a potential confound towards accurately estimating BOLD signals, particularly when there exist individual differences in cerebrovascular reactivity patterns. Correcting BOLD signals using CVR maps provides a stringent way to minimize vascular confounds, which potentially alters properties of BOLD signals as evidenced by the observations of BOLD signal variability across age described earlier. In this section, mathematical evidence is provided to show that estimation of events is spared from CVR-correction. Events were estimated from BOLD signals that have been normalized across all time points. Described below is the mathematical formula derivation to demonstrate that the normalized original BOLD signal is equal to the normalized CVR-corrected BOLD signal, resulting in equivalent estimation of event moments.

The normalization of the original BOLD signals for a given voxel, vertex, or node is as follows.

$$BOLD_{orig-norm} = \frac{(BOLD_{orig} - \overline{BOLD_{orig}})}{SD_{BOLD_{orig}}}$$

where $BOLD_{orig-norm}$ is the normalized original BOLD signals, $\overline{BOLD_{orig}}$ is the mean value of original signals across all time points, and $SD_{BOLD_{orig}}$ is the standard deviation of BOLD signal time-series.

Similarly, the normalization of the CVR-corrected signals can be expressed as follows.

$$BOLD_{cvr-norm} = \frac{(BOLD_{cvr} - \overline{BOLD_{cvr}})}{SD_{BOLD_{cvr}}}$$

In CVR correction, each original BOLD time-series at a given vertex was divided by the CVR value at the same vertex. This calculation is formally expressed in the following equation (Bandettini and Wong, 1997; Liu et al., 2013).

$$BOLD_{cvr} = \frac{BOLD_{orig}}{cvr}$$

And this equation can be further transformed into the following derivation.

$$BOLD_{cvr} = BOLD_{orig} \times \frac{1}{cvr}$$

This derivation was plugged-in to the equation of normalizing CVR-corrected signals.

$$BOLD_{cvr-norm} = \frac{(\frac{1}{cvr} \times BOLD_{orig} - \frac{1}{cvr} \times \overline{BOLD_{orig}})}{\frac{1}{cvr} \times SD_{BOLD_{orig}}}$$

The common factor of the numerator was extracted.

$$BOLD_{cvr-norm} = \frac{\frac{1}{cvr} \times (BOLD_{orig} - \overline{BOLD_{orig}})}{\frac{1}{cvr} \times SD_{BOLD_{orig}}}$$

Common factors of numerator and denominator were both isolated from the main expression.

$$BOLD_{cvr-norm} = \frac{\frac{1}{cvr}}{\frac{1}{cvr}} \times \frac{(BOLD_{orig} - \overline{BOLD_{orig}})}{SD_{BOLD_{orig}}}$$

Common factors were canceled by each other, resulting in 1. The expression to the right is mathematically equivalent to the normalized original BOLD signals.

$$BOLD_{cvr-norm} = 1 \times BOLD_{orig-norm}$$

As such, normalized CVR-corrected BOLD signal are equivalent to normalized original BOLD signal.

$$BOLD_{cvr-norm} = BOLD_{orig-norm}$$

3.2.3.3. The number of events declines with increasing age

Given the observed distinction in system segregation when comparing moments classified as events versus moments classified as non-events, a natural hypothesis is that events drive the relationship between an individual's age and their system segregation. Previously published results (e.g., Chan et al., 2014) and the observations in the present dissertation report have shown aging-accompanied decrease of system segregation. One hypothesis is that older individuals have a lesser number of events, and that this difference results in a decreased estimate of trait-like system segregation, which is calculated from a correlation matrix corresponding to the entire BOLD time-series. This hypothesis was directly tested by investigating the relationship between number of events, age, and system segregation.

Examining the DLBS dataset, there is no relationship between number of events and age ($r = -0.034$, $p = 0.608$; **Figure 3.13 A**). Including sex and education does not alter the non-significant

relationship ($r = -0.001$, $p = 0.986$). An additional analysis was done using a different threshold for defining events (top 10% RMS). This resulted in consistent findings: the number of events does not relate to age ($r = 0.038$, $p = 0.566$; **Figure 3.13 C**). In contrast however, using the HCP Aging dataset, the number of events is negatively correlated to age ($r = -0.289$, $p < 0.001$; **Figure 3.13 B**), even after controlling for sex ($r = -0.285$, $p < 0.001$). Due to limited availability of demographic information in the data release, education was not included in models for the remaining analysis using HCP Aging data. Using a different threshold (top 10% RMS) revealed a consistent aging-accompanied relationship ($r = -0.313$, $p < 0.001$; **Figure 3.13 D**). One possible reason leading to the mixed findings is that HCP Aging has more data per participant (20 min of cleaned data), while DLBS dataset only has 5 min data for each participant. Previous studies (e.g., Laumann et al., 2015; Gordon et al., 2017) and observations from our lab (Han et al., in preparation) have revealed that derivation of reliable estimates of brain networks necessitates significant amounts of data per participant. As such, using HCP Aging may lead to more reliable estimation of the number of event and its relationship with the participant's age.

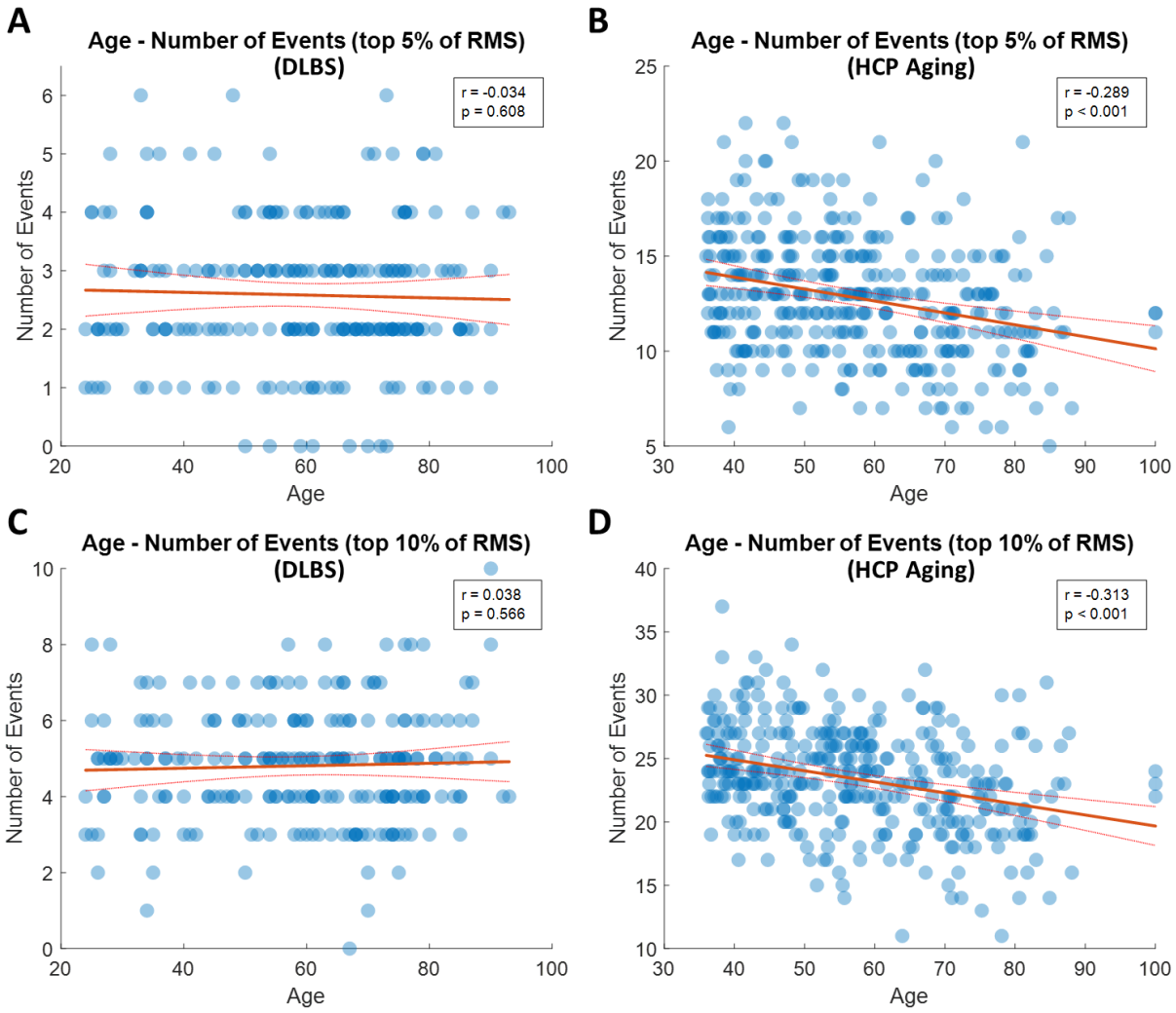

Figure 3.13. Relationship between number of events and age of participant. (**A**) In the DLBS dataset, events were identified using the top 5% RMS. The number of events is not correlated with age (r = -0.034, p = 0.608). (**C**) Using a different threshold (top 10% RMS) does not alter the non-significant result (r = 0.038, p = 0.566). (**B**) In contrast, in the HCP Aging dataset there exists a significant relationship between participant's age and the number of events identified in their resting-state time-series, both when calculated using the top 5% RMS (r = -0.289, p < 0.001), and (**D**) top 10% RMS (r = -0.313, p < 0.001).

3.2.3.4. Participants with a greater number of events in their resting-state BOLD timeseries exhibit higher system segregation

Given the potential relationship between number of events and participant's age, I next tested the hypothesis that the number of events that are evident in an individual's resting-state BOLD time-series is related to their system segregation. A Pearson correlation was calculated between number of events (top 5% RMS) and system segregation using DLBS dataset, revealing a positive relation between the two variables ($r = 0.158$, $p = 0.016$; **Figure 3.14 A**). After controlling for age, this positive relationship still holds, despite the fact that number of events was not shown to relate to participant age in this dataset ($r = 0.154$, $p = 0.018$; **Figure 3.14 B**). Controlling for additional covariates (sex and education) revealed a consistent relationship between number of events and system segregation ($r = 0.186$, $p = 0.005$).

This relationship was also evident when events were defined from the top 10% of RMS values: ($r = 0.135$, $p = 0.039$). After controlling for age, this positive relationship remained significant ($r = 0.152$, $p = 0.021$). Further controlling for variance related to sex and education did not alter the relationship ($r = 0.176$, $p = 0.008$).

A parallel analysis was performed using the HCP Aging dataset. When top 5% RMS was used to identify events, there existed a positive relationship between number of events and system segregation before ($r = 0.227$, $p < 0.001$; **Figure 3.14 C**) and after controlling for age ($r = 0.134$, $p = 0.01$; **Figure 3.14 D**). The relationships remained after further controlling for sex ($r = 0.128$, $p = 0.015$). A comparable relationship was evident when defining events using the top 10% RMS: before ($r = 0.268$, $p < 0.001$), after controlling for age ($r = 0.176$, $p < 0.001$) and additionally controlling for sex ($r = 0.166$, $p = 0.002$).

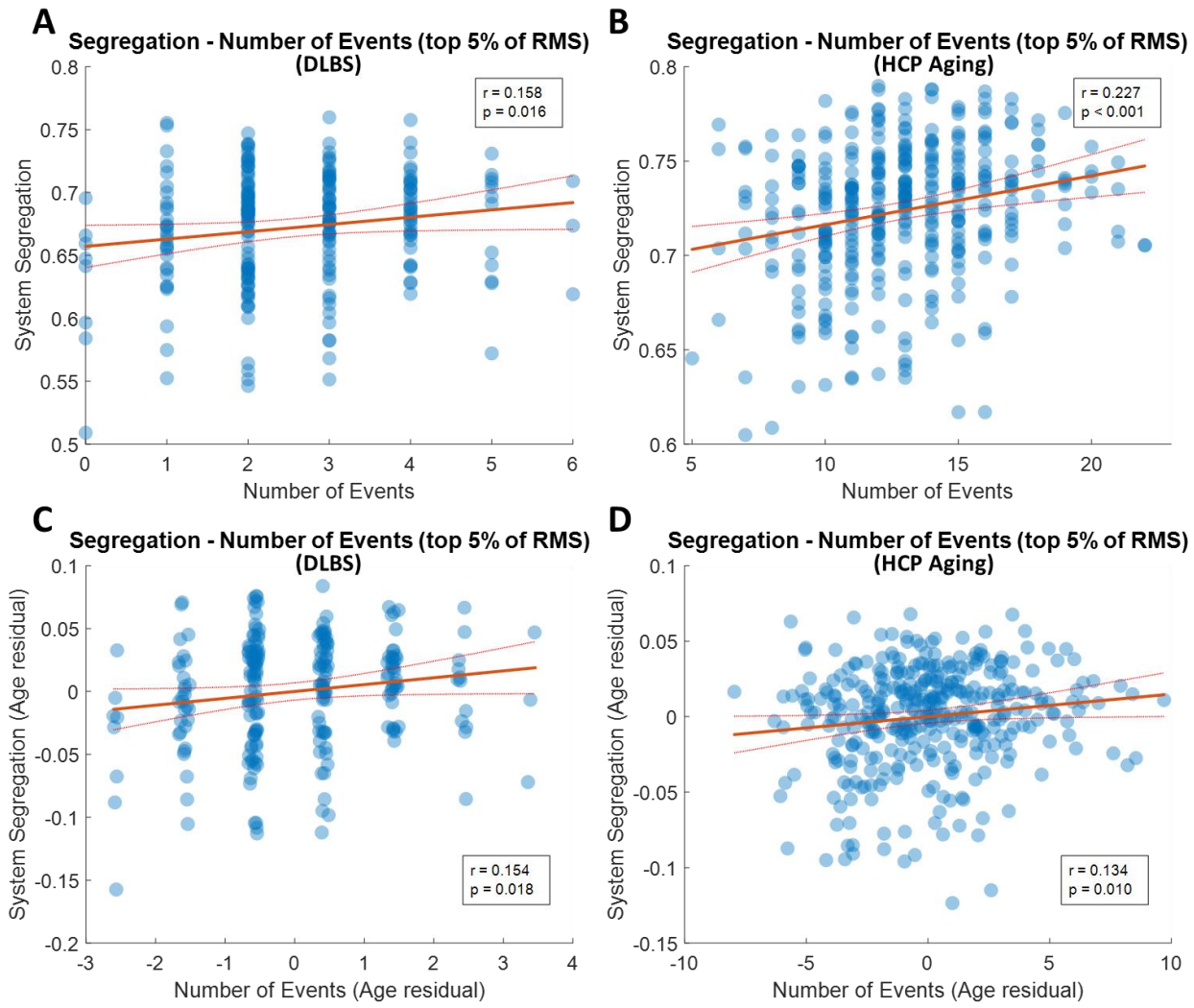

Figure 3.14. Resting-state system segregation is positively related to number of events that are evident in a participant's resting-state time-series. System segregation reflects the level of partitioning between distinct functional brain systems, calculated based on the correlation matrix from the entire BOLD time-series. This measure is correlated with number of events (top 5% of RMS; corresponding to moments exhibiting heightened modular structures of brain networks) using DLBS data (**A**). This relation persists after controlling for age (**C**). Using an independent dataset (HCP Aging), a similar relationship is evident (**B**) and remained significant after controlling age-related variance (**D**). Each in plot, dots represent individual participants.

3.2.3.5. The relationship between age and resting-state system segregation is not limited to event moments

In the previous section it was revealed that number of events is positively associated with system segregation, independent of participant age. Is an individual's system segregation entirely dictated by the presence of events? One way of evaluating this question more directly is to examine patterns of system segregation as a function of the RMS amplitude of frames. Up until this point, system segregation has been calculated form the entire time-series of all nodes (i.e., across all frames). However, if event moments define an individual's system segregation, then the relationship between age and system segregation might only be evident during higher RMS moments, corresponding to frames of higher node co-fluctuation strength. However there exists a possibility that aging-accompanied difference in network re-organization are not limited to high co-fluctuation moments (events), but exists across all the time points irrespective of RMS amplitude.

To test this hypothesis, all data frames were sampled into 10 bins based on RMS magnitude with 10% increments (i.e., 0% - 10%, 10% - 20%, …, 90% - 100%). For each RMS bin (e.g., 90% - 100%), system segregation was computed using only the frames in this particular bin for each participant, and then correlated with age across participants (**Figure 3.15**).

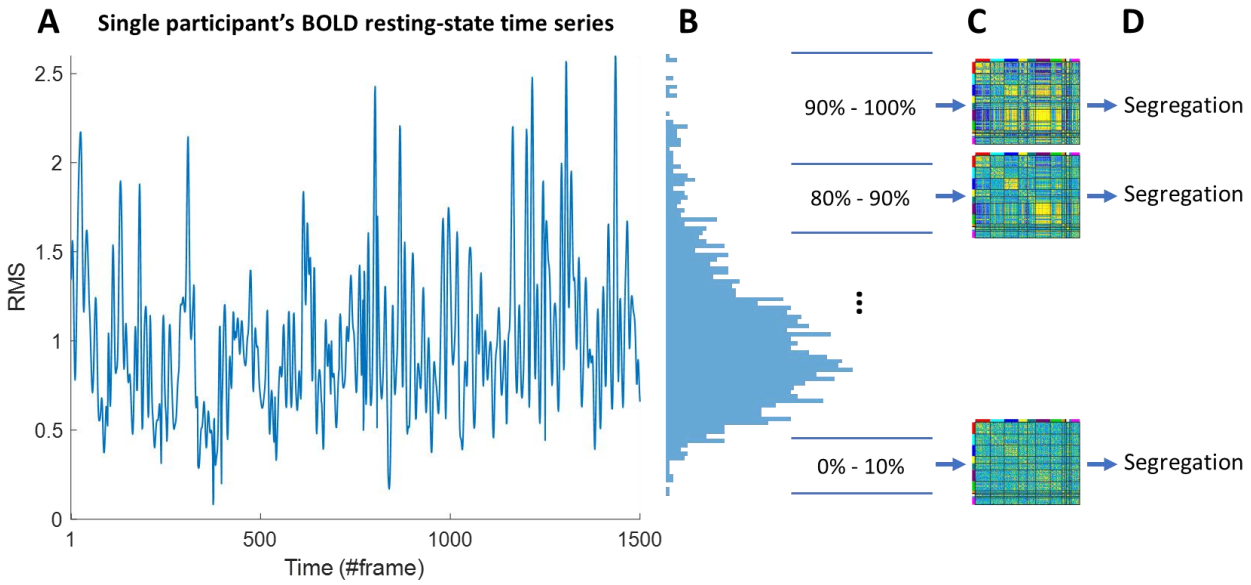

Figure 3.15. Estimating system segregation from data frames of differing RMS strength. To assess whether the relationship between a participant's age and their resting-state system segregation is limited to high co-fluctuation moments of the resting-state time-series, the following steps were taken to sample data and evaluate system segregation at distinct moments for each participant. (**A**) RMS was computed to reflect the degree to which edges collectively co-fluctuate at different moments. (**B**) The distribution of RMS was derived, based on which 10 bins were created to categorize moments of different RMS amplitude (i.e., 0% - 10%, 10% - 20%, …, 90% - 100%). (**C**) For each RMS bin (e.g., 90% - 100%), functional time series (frames) were sampled from only those moments, based on which a correlation matrix was computed for each participant. This correlation matrix reflected the participant's functional network at the corresponding moments with specific RMS strength. (**D**) The participant's resting-state system segregation was computed based on this correlation matrix for each RMS bin. As such, system segregation reflects organization of functional networks at the moments when levels of co-fluctuation across edges are similar. By comparing relationships between age and system segregation from distinct RMS bins allows testing of whether age-associated differences in brain network organization are specific to certain moments with strong RMS amplitude or across all resting-state time points irrespective of RMS strength.

As shown in **Figure 3.16 A**, system segregation calculated from higher RMS frames (top 10%) is negatively correlated with age in the DLBS2 data set ($r = -0.205$, $p = 0.002$). Surprisingly however, this relationship holds irrespective of the frames used to calculate system segregation.

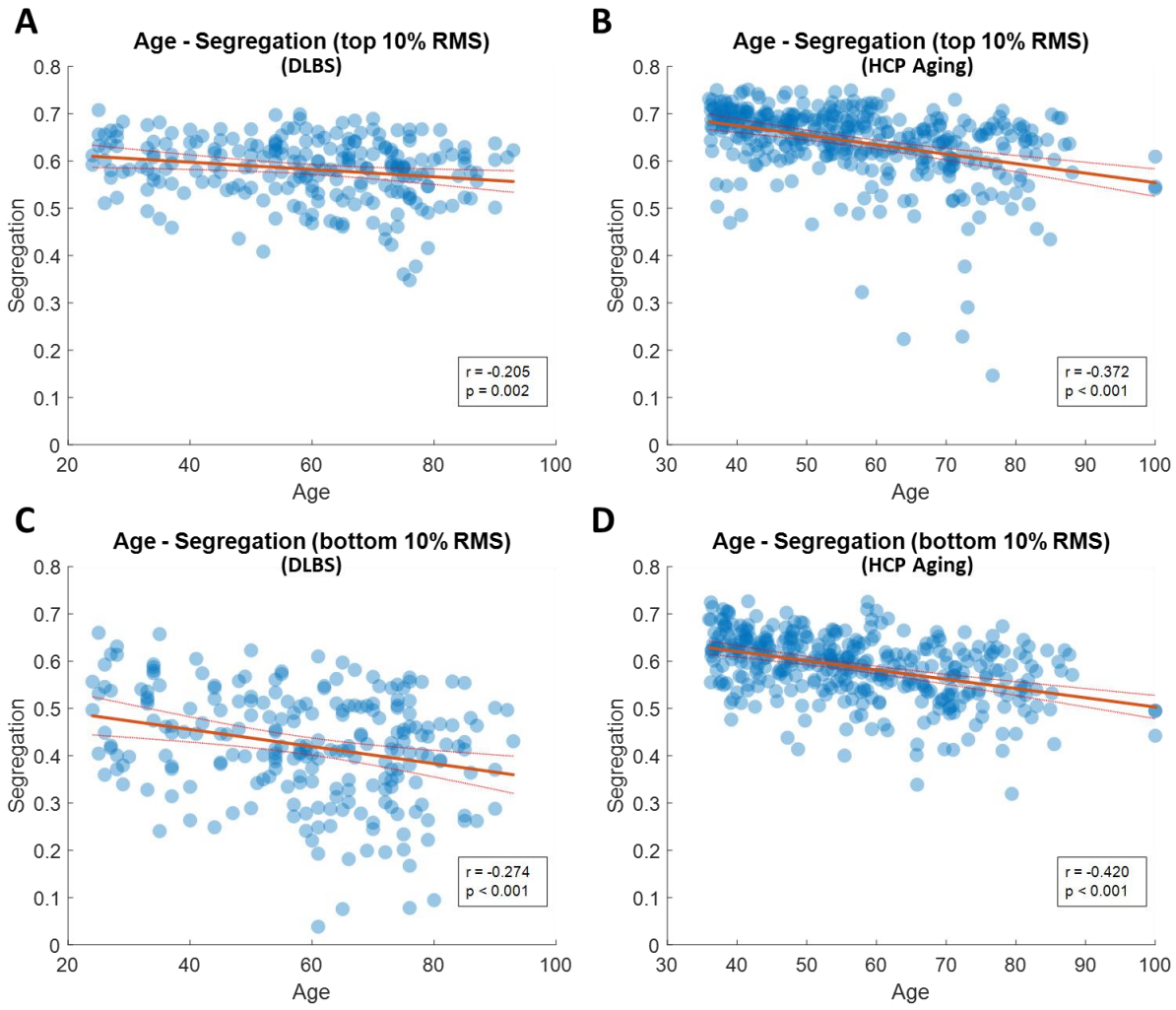

Figure 3.16. The relationship between an individual's age and the magnitude of their resting-state system segregation is evident in moments of higher RMS (e.g., events) and low RMS (non-events). Data frames were sampled into high RMS (top 10%) and low RMS (bottom 10%) bins. For each RMS bin, system segregation was computed using all frames in the corresponding bin for each participant, and then correlated with age across participants. There is an age-related decrease of system segregation using data sampled from the highest RMS frames (i.e., top 10% RMS frames) using DLBS data (**A**). However, this aging-related decrease of segregation is also evident using the lowest RMS frames (**C**). Similar relationships were revealed in an independent dataset (HCP Aging, **B** and **D**).

Even when system segregation is calculated on frames that exhibit the lowest RMS (bottom

10%), which typically exhibit lower modularity, there is a relationship with an individual's age (r

= -0.274, p < 0.001; **Figure 3.16 C**). Using an independent dataset (HCP Aging) yielded similar findings as above. First, there is a negative relationship between age and system segregation when the latter is calculated from either the highest RMS frames (top 10%; r = -0.372, p < 0.001; **Figure 3.16 B**) or lowest RMS frames (bottom 10%; r = -0.42, p < 0.01; **Figure 3.16 D**). Further, the age-related decrease of segregation exists across all bins of RMS using DLBS data, with correlation coefficients ranging from -0.151 to -0.33 (**Table 3.1 A**).

Table 3.1. The relationship between an individual's age and the magnitude of their resting-state system segregation is evident across the resting-state time-series and is not limited to moments of higher RMS (e.g., events). Data frames were sampled into 10 bins based on RMS magnitude with 10% increments (i.e., 0% - 10%, 10% - 20%, …, 90% - 100%). For each RMS bin, system segregation was computed using all frames in the corresponding bin for each participant, and then correlated with age across participants. Significant correlations between age and segregation were evident across all RMS bins using DLBS (**A**) and HCP Aging (**B**) datasets. These results demonstrate that relationship between an individual's age and their resting-state system segregation is evident across the resting-state time-series and is not limited to moments of higher RMS (e.g., events).

A **Age-relationship with Segregation from Different RMS Frames (DLBS)**

RMS bin (%)	0 – 10	10 – 20	20 - 30	30 - 40	40 - 50	50 - 60	60 - 70	70 - 80	80 - 90	90 - 100
r	-0.274	-0.267	-0.295	-0.324	-0.330	-0.209	-0.191	-0.226	-0.151	-0.205
p	<0.001	<0.001	<0.001	<0.001	<0.001	0.001	0.003	0.001	0.021	0.002

B **Age-relationship with Segregation from Different RMS Frames (HCP Aging)**

RMS bin (%)	0 – 10	10 – 20	20 - 30	30 - 40	40 - 50	50 - 60	60 - 70	70 - 80	80 - 90	90 - 100
r	-0.420	-0.484	-0.482	-0.489	-0.447	-0.428	-0.404	-0.400	-0.411	-0.372
p	<0.001	<0.001	<0.001	<0.001	<0.001	<0.001	<0.001	<0.001	<0.001	<0.001

After controlling for sex and education, all the relationships persisted with correlation coefficients ranging from -0.165 to -0.322 (all ps < 0.05). Using HCP Aging data also revealed

significant relationships between age and segregation irrespective of RMS strengths (**Table 3.1 B**). These relationships were still significant after controlling for sex, with correlation coefficients ranging from -0.37 to -0.488 (all ps < 0.001). Together, these results demonstrate that relationship between an individual's age and their resting-state system segregation is evident across the resting-state time-series and is not limited to moments of higher RMS (e.g., events).

3.2.4. Discussion

In line with previous reports (Zamani Esfahlani et al., 2020), the present chapter revealed that there exist moments (events) of greater co-fluctuation pattern across edges, in which functional brain networks exhibit a highly modular architecture relative to non-event moments. To understand events and their relationship to age-related differences of resting-state system segregation, I first investigated whether there exists a relationship between the number of events and an individual's age. The result showed that number of events decreases with increasing age (in HCP Aging dataset, but not in DLBS dataset). This finding naturally led to a hypothesis that participants with higher system segregation have more events. It was revealed that exists a positive relationship between number of events and segregation, even after controlling for participant's age and other covariates, across both datasets. These relationships were evident when different thresholds of RMS were used to categorize events.

I next investigated whether the relationship between age and system segregation is primarily evident during higher RMS moments versus moments (frames) irrespective of co-fluctuation strength. The result showed that age-accompanied decreases of system segregation are evident across all the moments of the resting-state time-series, irrespective of co-fluctuation amplitude of

edges (RMS). These findings demonstrate while events provide information related to the modular organization of brain networks, the relationship between age and system segregation is not limited to these moments of high pairwise-covariance, but rather exist across all time points of a resting-state scan.

Although the biological significance of events are not clear, recent studies have reported that events are associated with greater modular structures and attributive to greater connectivity within certain functional systems (e.g., default mode network; Zamani Esfahlani et al., 2020). Events exhibit repetitive patterns of co-fluctuation across scans, which is highly individualized and distinct from group-level patterns (Betzel et al., 2022). Interestingly, events have been revealed not only in resting-state studies but also during fMRI experiments that involve stimulus processing. For instance, events are detectable as participants watch movies in the scanner, and also during the ending scenes of a movie. Interestingly, the events that are evident at the offset of a movie exhibit distinct spatial patterns across brain networks relative to the events at other time frames during movie watching, suggesting non-equivalent network processes (Tanner et al., 2022). These observations highlight the possibility that events may provide unique information about brain networks and dominate the relationship between network organization and other variables of interest (in the present case, age). The current project revealed that number of events is associated with age and segregation. This supports our first hypothesis that a higher frequency of events results in greater degree of resting-state system segregation across time. Older adults have lesser number of events, which at least partially contributes to lower system segregation in this population.

Curiously, and in contrast to the above conclusion however, I also found that the age-associated differences in brain network organization are not limited to events, but also non-event moments. Critically, this analysis comprehensively evaluated network organization at distinct moments irrespective of co-fluctuation amplitude. The pervasive aging-related decrease of system segregation across all moments highlights the persistence of degraded brain networks in older adults, which places an important caveat on the interpretation that number of events are critical towards establishing how system segregation is established. Indeed, a recent study demonstrates that events do not exhibit discrete patterns but rather reflect continuous features of co-fluctuation associated with brain network organization. In other words, co-fluctuations and network structure are correlated in a gradually increasing way (e.g., ~ top 50% of time points show highly modular network structure) and this relationship could be explained by sampling variability (Ladwig et al., 2022). Importantly, using limited numbers of time points that are randomly sampled from the entire timeseries could largely reproduce network structures, suggesting that while events explain a large portion of variance in network structure, they may not uniquely drive the patterns of network organization (Ladwig et al., 2022).

Aging is accompanied by structural changes of the brain at multiple spatial scales, including decreases in synaptic connectivity (Barnes and McNaughton 1980; for review see Morrison and Baxter 2012), shrinkage and loss of neurons (Kril et al. 2004), loss of dendritic spines of cells (Markham and Juraska 2002; Uylings and de Brabander 2002; for review see Burke and Barnes 2006), progressive thinning of the cerebral cortex and reductions in volume and surface area (Resnick et al. 2003; Raz et al. 2005; Fjell et al. 2009; Storsve et al. 2014). Aging-related vascular differences also serve as a major source leading to changes both in brain structures and

neural activities (e.g., Lu et al., 2011; Liu et al., 2013; Tsvetanov et al., 2020). I have shown throughout this dissertation how increasing adult age is associated with decreasing resting-state system segregation, a feature of brain organization that also has relevance towards understanding cognitive ability and disease risk (Chan et al., 2021). These network changes are thought to impact human brain function across time such that the ability of functional brain networks to flexibly re-organize in adapting to environment and processing demands may be continuously compromised (Wig, 2017). This pervasive effect of aging is presumed to manifest itself at every moment as brain networks are configured dynamically to support cognition and behavior. Indeed, observations of the present chapter speak to this hypothesis and rule out the possibility of exclusive dominance of events towards establishing age-accompanied differences in system segregation.

Collectively, events with strong co-fluctuation patterns across the brain exhibit strong modular structures of brain networks. While the frequency of events shows decline across age, it may not provide unique information of aging-accompanied difference in brain network re-organization relative to other time points. Future work is needed to investigate whether these events reflect processes of biological significance or merely moments exhibiting coincidental patterns in a random manner.

CHAPTER 4

CONCLUSION

Resting-state system segregation is a feature of brain network organization that has relevance to brain function in both health and disease across adult lifespan. To investigate the genesis of resting-state system segregation requires a deeper understanding of its possible links to vascular factors and BOLD properties.

I first investigated the impact of vascular factors on the estimation of aging-relationship with segregation. After a stringent procedure to minimize cerebrovascular and cardiovascular confounds, aging-related decrease of system segregation persists, even after further controlling for other confounds including sex and education. Numerous studies have revealed aging-related difference in vascular health in cross-sectional (e.g., Liu et al., 2013) and longitudinal studies (e.g., Peng et al., 2018), and this age-accompanied relationship leads to anatomical and functional alterations in the brain (e.g., Colcombe et al., 2004; Crichton et al., 2014, Abdelkarim et al., 2019; Hutchison et al., 2013). The complexity of vascular coupling with neural activity comprises estimation of patterns brain activation using BOLD signals (for review see Zimmerman et al., 2021). The present results collectively suggest that these vascular factors do not explain age-related decreases of system segregation, and supports the hypothesis that the measure serves as a unique biomarker of functional brain organization across the adult lifespan (Wig, 2017).

Next, I tested whether dynamic properties of the BOLD signal might relate to system segregation. I showed that after carefully controlling for both CVR and CVH confounds, BOLD variability, a property of the BOLD signal which has been shown to relate to age, is not

correlated with age. Using this stringent way to rule out vascular confounds resulted in non-significant relationship between system segregation and BOLD variability. These results suggest that vascular factors, especially cerebrovascular reactivity, play a critical rule in estimating BOLD signal variability, which adds another piece of evidence that vascular factors serve as an important source of variance contributing to BOLD signal properties (e.g., Tsvetanov et al., 2020). As such, system segregation summarizes important features of brain network re-organization across age, which cannot be explained by the degree of variability in a resting-state time-series.

Further, I evaluated whether there exist moments (events) of greater co-fluctuation pattern across edges, in which functional brain networks exhibit highly modular structures relative to non-event moments. The result demonstrated that number of events decreases with increasing age. There also exists a positive relationship between number of events and system segregation, even after controlling for sex and education. However, age-related decreases of system segregation are evident across all moments, irrespective of co-fluctuation amplitude of edges. These findings demonstrate that events provide may contribute towards establishing more modular architecture of resting-state brain networks, but that the age-accompanied changes in brain network organization are not limited to these moments but rather are present across time.

System segregation summarizes brain network organization and predicts behavioral outcomes in both healthy and diseased individuals (for review see Wig, 2017). The significance of system segregation is evident its relation to aging (Chan et al., 2014; Han et al., 2018), cognitive performance (e.g., working memory capacity [Stevens et al., 2012] and visual attention [Yue et al., 2017]), and in neurological diseases (e.g., Alzheimer's disease [Brier et al., 2014]). These

observations collectively suggest that resting-state system segregation serves as a biomarker to differentiate individuals in their brain networks and behaviors. This important application naturally needs to withstand scrutiny of whether system segregation is due to any confounding effects, e.g., vascular health. Indeed, vascular differences in individuals exert profound impact on brain structure and functions (e.g., Bots et al., 1993; Longstreth et al., 1996, Marshall et al., 2017, Raz et al., 2007), and further compromise estimation of BOLD signals (for review see Tsvetanov et al., 2021; Zimmerman et al., 2021). This project addresses this question and reveals consistent aging-related differences in system segregation independent of vascular influences, which provide critical evidence exhibiting robustness of system segregation as a biomarker for network organization and behavior, and measure of functional brain network organization.

The second goal of present project was to gain a deeper understanding of driving forces of resting-state system segregation, in terms of time-varying signals, and how it is related to age. Instead of being static, brain networks re-organize in a dynamic way across time (Betzel et al., 2016), with different moments exhibiting distinct modular structures of the brain networks (Zamani Esfahlani et al., 2020; Betzel et al., 2022). Previous studies have shown that dynamic fluctuation of RSFC that may reflect transitions between distinct brain states (Allen et al., 2014; Hutchison and Morton, 2015), and these brain states bear biological significance (e.g., levels of vigilance [Barttfeld et al., 2015; Nomi et al., 2017; Shine et al., 2016]; psychiatric disorders [Damaraju et al., 2014; Rashid et al., 2014; Su et al., 2016]). On the other hand, other studies suggest that the non-stationarity of resting-state BOLD signals may be largely attributed to data sampling error, head motion and fluctuating drowsiness (Laumann et al., 2015; Laumann et al., 2017). Across dynamic time series, moments with greater co-fluctuation patterns (events) are not

special; they do not uniquely drive the patterns of network organization (Ladwig et al., 2022). This report reveals that while discrete moments may carry critical information about properties of brain networks, the impact of age on decreased segregation of large-scale functional brain networks is evident across time (within a scan session), rather than at discrete moments.

Future research directions

The goal of present project was to gain a deeper understanding of the now well documented relationships between increasing age and decreasing resting-state system segregation.

It has been shown that vascular dysfunction is associated with neural alterations at different levels, including cellular dysfunction (Fricker et al., 2018), reduced efficiency in neural processing (Hutchison et al., 2013; Toth et al., 2017), white matter lesions (Bots et al., 1993; Longstreth et al., 1996), and gray matter differences (Marshall et al., 2017, Raz et al., 2007). Accounting for these factors in addition to cardiovascular health reveals that the relationship between increasing age and an important measure of large-scale functional brain network organization remains, and is largely unaltered. The robustness of this relationship provides critical evidence of using brain system segregation as a measure of individual differences of brain function and functional brain network organization. More importantly, this finding highlights the necessity of further studies to understand the driving sources of declines in system segregation in relation to brain function and cognition across adult lifespan.

I have attempted to explore whether and how time-varying sources of resting-state relationships relate to declines in brain system segregation. While discrete moments may carry information about properties of brain networks, the impact of age on functional brain networks is evident across time (within a scan session), which likely impacts brain function at all moments.

However, this does not preclude the possibility that other measures of brain dynamics will lead to greater insights towards how brain networks are established (e.g., transition between different states and its relationship with cognition in health and disease).

In sum, this dissertation provides important support that resting-state system segregation provides measurement of age-related decline which is linked to re-organization of the brain's functionals network, and further supports the application of this approach towards measuring individual brain health across the lifespan.

REFERENCES

Allen, E.A., Damaraju, E., Plis, S.M., Erhardt, E.B., Eichele, T., and Calhoun, V.D. (2014). Tracking whole-brain connectivity dynamics in the resting state. Cerebral cortex 24, 663-676.

Barttfeld, P., Uhrig, L., Sitt, J.D., Sigman, M., Jarraya, B., and Dehaene, S. (2015). Signature of consciousness in the dynamics of resting-state brain activity. Proceedings of the National Academy of Sciences of the United States of America 112, 887-892.

Beck, J.M., Ma, W.J., Kiani, R., Hanks, T., Churchland, A.K., Roitman, J., Shadlen, M.N., Latham, P.E., and Pouget, A. (2008). Probabilistic population codes for Bayesian decision making. Neuron 60, 1142-1152.

Betzel, R.F., Cutts, S.A., Greenwell, S., Faskowitz, J. and Sporns, O. (2022). Individualized event structure drives individual differences in whole-brain functional connectivity. NeuroImage, 252, p.118993.

Betzel, R.F., Fukushima, M., He, Y., Zuo, X.N., and Sporns, O. (2016). Dynamic fluctuations coincide with periods of high and low modularity in resting-state functional brain networks. NeuroImage 127, 287-297.

Brier, M.R., Thomas, J.B., Snyder, A.Z., Wang, L., Fagan, A.M., Benzinger, T., Morris, J.C., and Ances, B.M. (2014). Unrecognized preclinical Alzheimer disease confounds rs-fcMRI studies of normal aging. Neurology 83, 1613-1619.

Bright, M.G., Bulte, D.P., Jezzard, P. and Duyn, J.H., (2009). Characterization of regional heterogeneity in cerebrovascular reactivity dynamics using novel hypocapnia task and BOLD fMRI. Neuroimage, 48(1), pp.166-175.

Burzynska, A.Z., Wong, C.N., Voss, M.W., Cooke, G.E., McAuley, E., and Kramer, A.F. (2015). White matter integrity supports BOLD signal variability and cognitive performance in the aging human brain. PLoS One 10, e0120315.

Chan, M.Y., Han, L., Carreno, C.A., Zhang, Z., Rodriguez, R.M., LaRose, M., Hassenstab, J. and Wig, G.S. (2021). Long-term prognosis and educational determinants of brain network decline in older adult individuals. Nature aging, 1(11), 1053-1067.

Chan, M.Y., Na, J., Agres, P.F., Savalia, N.K., Park, D.C., and Wig, G.S. (2018). Socioeconomic status moderates age-related differences in the brain's functional network organization and anatomy across the adult lifespan. Proceedings of the National Academy of Sciences of the United States of America 115, E5144-e5153.

Chan, M.Y., Park, D.C., Savalia, N.K., Petersen, S.E., and Wig, G.S. (2014). Decreased segregation of brain systems across the healthy adult lifespan. Proceedings of the National Academy of Sciences of the United States of America 111, E4997-5006.

Chang, C., and Glover, G.H. (2010). Time-frequency dynamics of resting-state brain connectivity measured with fMRI. NeuroImage 50, 81-98.

Dale, A.M., Fischl, B., and Sereno, M.I. (1999). Cortical surface-based analysis. I. Segmentation and surface reconstruction. NeuroImage 9, 179-194.

Damaraju, E., Allen, E.A., Belger, A., Ford, J.M., McEwen, S., Mathalon, D.H., Mueller, B.A., Pearlson, G.D., Potkin, S.G., Preda, A., et al. (2014). Dynamic functional connectivity analysis reveals transient states of dysconnectivity in schizophrenia. Neuroimage Clin 5, 298-308.

Du, Y., Pearlson, G.D., Yu, Q., He, H., Lin, D., Sui, J., Wu, L., and Calhoun, V.D. (2016). Interaction among subsystems within default mode network diminished in schizophrenia patients: A dynamic connectivity approach. Schizophrenia research 170, 55-65.

Fair, D.A., Miranda-Dominguez, O., Snyder, A.Z., Perrone, A., Earl, E.A., Van, A.N., Koller, J.M., Feczko, E., Tisdall, M.D., van der Kouwe, A., et al. (2020). Correction of respiratory artifacts in MRI head motion estimates. NeuroImage 208, 116400.

Fischl, B., Sereno, M.I., and Dale, A.M. (1999). Cortical surface-based analysis. II: Inflation, flattening, and a surface-based coordinate system. NeuroImage 9, 195-207.

Fox, N.C., and Schott, J.M. (2004). Imaging cerebral atrophy: normal ageing to Alzheimer's disease. Lancet 363, 392-394.

Garrett, D.D., Kovacevic, N., McIntosh, A.R., and Grady, C.L. (2010). Blood oxygen level-dependent signal variability is more than just noise. The Journal of neuroscience : the official journal of the Society for Neuroscience 30, 4914-4921.

Garrett, D.D., Kovacevic, N., McIntosh, A.R., and Grady, C.L. (2011). The importance of being variable. The Journal of neuroscience : the official journal of the Society for Neuroscience 31, 4496-4503.

Garrett, D.D., Kovacevic, N., McIntosh, A.R., and Grady, C.L. (2013a). The modulation of BOLD variability between cognitive states varies by age and processing speed. Cerebral cortex 23, 684-693.

Garrett, D.D., Samanez-Larkin, G.R., MacDonald, S.W., Lindenberger, U., McIntosh, A.R., and Grady, C.L. (2013b). Moment-to-moment brain signal variability: a next frontier in human brain mapping? Neuroscience and biobehavioral reviews 37, 610-624.

Glasser, M.F., Sotiropoulos, S.N., Wilson, J.A., Coalson, T.S., Fischl, B., Andersson, J.L., Xu, J.Q., Jbabdi, S., Webster, M., Polimeni, J.R., et al. (2013). The minimal preprocessing pipelines for the Human Connectome Project. NeuroImage 80, 105-124.

Good, C.D., Johnsrude, I.S., Ashburner, J., Henson, R.N., Friston, K.J., and Frackowiak, R.S. (2001). A voxel-based morphometric study of ageing in 465 normal adult human brains. NeuroImage 14, 21-36.

Gordon, E.M., Laumann, T.O., Adeyemo, B., Huckins, J.F., Kelley, W.M., and Petersen, S.E. (2016). Generation and Evaluation of a Cortical Area Parcellation from Resting-State Correlations. Cerebral cortex 26, 288-303.

Grady, C.L., and Garrett, D.D. (2014). Understanding variability in the BOLD signal and why it matters for aging. Brain Imaging Behav 8, 274-283.

Grady, C.L., and Garrett, D.D. (2018). Brain signal variability is modulated as a function of internal and external demand in younger and older adults. NeuroImage 169, 510-523.

Han, L., Savalia, N.K., Chan, M.Y., Agres, P.F., Nair, A.S., and Wig, G.S. (2018). Functional Parcellation of the Cerebral Cortex Across the Human Adult Lifespan. Cerebral cortex 28, 4403-4423.

Harms, M.P., Somerville, L.H., Ances, B.M., Andersson, J., Barch, D.M., Bastiani, M., Bookheimer, S.Y., Brown, T.B., Buckner, R.L., Burgess, G.C., et al. (2018). Extending the Human Connectome Project across ages: Imaging protocols for the Lifespan Development and Aging projects. NeuroImage 183, 972-984.

Hutchison, R.M., and Morton, J.B. (2015). Tracking the Brain's Functional Coupling Dynamics over Development. The Journal of neuroscience: the official journal of the Society for Neuroscience 35, 6849-6859.

Kastrup, A., Krüger, G., Glover, G.H., Neumann-Haefelin, T. and Moseley, M.E., (1999). Regional variability of cerebral blood oxygenation response to hypercapnia. Neuroimage, 10(6), pp.675-681.

Kelso, J.A.S. (2008). Haken-kelso-bunz model. Scholarpedia 3, 1612.

Kelso, J.A.S., Del Colle, J.D., and Schöner, G. (1990). Action-perception as a pattern formation process. In Attention and performance 13: Motor representation and control (Hillsdale, NJ, US: Lawrence Erlbaum Associates, Inc), pp. 139-169.

Kelso, J.A.S., and Haken, H. (1995). New laws to be expected in the organism: synergetics of brain and behaviour. In What is Life? The Next Fifty Years: Speculations on the Future of Biology, L.A.J. O'Neill, and M.P. Murphy, eds. (Cambridge: Cambridge University Press), pp. 137-160.

Kelso, J.A.S., and Tognoli, E. (2007). Toward a Complementary Neuroscience: Metastable Coordination Dynamics of the Brain. In Neurodynamics of Cognition and Consciousness, L.I. Perlovsky, and R. Kozma, eds. (Berlin, Heidelberg: Springer Berlin Heidelberg), pp. 39-59.

Kielar, A., Deschamps, T., Chu, R.K., Jokel, R., Khatamian, Y.B., Chen, J.J., and Meltzer, J.A. (2016). Identifying Dysfunctional Cortex: Dissociable Effects of Stroke and Aging on Resting State Dynamics in MEG and fMRI. Front Aging Neurosci 8, 40.

Kong, T.S., Gratton, C., Low, K.A., Tan, C.H., Chiarelli, A.M., Fletcher, M.A., Zimmerman, B., Maclin, E.L., Sutton, B.P., Gratton, G. and Fabiani, M., (2020). Age-related differences in functional brain network segregation are consistent with a cascade of cerebrovascular, structural, and cognitive effects. Network Neuroscience, 4(1), 89-114.

Knill, D.C., and Pouget, A. (2004). The Bayesian brain: the role of uncertainty in neural coding and computation. Trends Neurosci 27, 712-719.

Ladwig, Z., Seitzman, B.A., Dworetsky, A., Yu, Y., Adeyemo, B., Smith, D.M., Petersen, S.E. and Gratton, C. (2022). BOLD cofluctuation 'events' are predicted from static functional connectivity. bioRxiv.

Lancaster, J.L., Glass, T.G., Lankipalli, B.R., Downs, H., Mayberg, H., and Fox, P.T. (1995). A Modality-Independent Approach to Spatial Normalization of Tomographic Images of the Human Brain. Human brain mapping 3, 209-223.

Laumann, T.O., Gordon, E.M., Adeyemo, B., Snyder, A.Z., Joo, S.J.u., Chen, M.Y., Gilmore, A.W., McDermott, K.B., Nelson, S.M., Dosenbach, N.U.F., et al. (2015). Functional System and Areal Organization of a Highly Sampled Individual Human Brain. Neuron 87, 657-670.

Laumann, T.O., Snyder, A.Z., Mitra, A., Gordon, E.M., Gratton, C., Adeyemo, B., Gilmore, A.W., Nelson, S.M., Berg, J.J., Greene, D.J., et al. (2017). On the Stability of BOLD fMRI Correlations. Cerebral cortex 27, 4719-4732.

Liu, P., Hebrank, A.C., Rodrigue, K.M., Kennedy, K.M., Section, J., Park, D.C. and Lu, H., (2013). Age-related differences in memory-encoding fMRI responses after accounting for decline in vascular reactivity. Neuroimage, 78, 415-425.

Lu, H., Xu, F., Rodrigue, K.M., Kennedy, K.M., Cheng, Y., Flicker, B., Hebrank, A.C., Uh, J. and Park, D.C., (2011). Alterations in cerebral metabolic rate and blood supply across the adult lifespan. Cerebral cortex, 21(6), 1426-1434.

Ma, W.J., Beck, J.M., Latham, P.E., and Pouget, A. (2006). Bayesian inference with probabilistic population codes. Nature neuroscience 9, 1432-1438.

Mennes, M., Kelly, C., Colcombe, S., Castellanos, F.X., and Milham, M.P. (2013). The extrinsic and intrinsic functional architectures of the human brain are not equivalent. Cerebral cortex 23, 223-229.

Mennes, M., Zuo, X.N., Kelly, C., Di Martino, A., Zang, Y.F., Biswal, B., Castellanos, F.X., and Milham, M.P. (2011). Linking inter-individual differences in neural activation and behavior to intrinsic brain dynamics. NeuroImage 54, 2950-2959.

Mesulam, M.M. (1990). Large-scale neurocognitive networks and distributed processing for attention, language, and memory. Annals of neurology 28, 597-613.

Miezin, F.M., Maccotta, L., Ollinger, J.M., Petersen, S.E., and Buckner, R.L. (2000). Characterizing the hemodynamic response: Effects of presentation rate, sampling procedure, and the possibility of ordering brain activity based on relative timing. NeuroImage 11, 735-759.

Millar, P.R., Petersen, S.E., Ances, B.M., Gordon, B.A., Benzinger, T.L.S., Morris, J.C., and Balota, D.A. (2020). Evaluating the Sensitivity of Resting-State BOLD Variability to Age and Cognition after Controlling for Motion and Cardiovascular Influences: A Network-Based Approach. Cerebral cortex 30, 5686-5701.

Nomi, J.S., Bolt, T.S., Ezie, C.E.C., Uddin, L.Q., and Heller, A.S. (2017). Moment-to-Moment BOLD Signal Variability Reflects Regional Changes in Neural Flexibility across the Lifespan. The Journal of neuroscience : the official journal of the Society for Neuroscience 37, 5539-5548.

Peng, S.L., Chen, X., Li, Y., Rodrigue, K.M., Park, D.C. and Lu, H. (2018). Age-related changes in cerebrovascular reactivity and their relationship to cognition: a four-year longitudinal study. Neuroimage, 174, 257-262.

Pfefferbaum, A., Mathalon, D.H., Sullivan, E.V., Rawles, J.M., Zipursky, R.B., and Lim, K.O. (1994). A Quantitative Magnetic-Resonance-Imaging Study of Changes in Brain Morphology from Infancy to Late Adulthood. Arch Neurol-Chicago 51, 874-887.

Power, J.D., Mitra, A., Laumann, T.O., Snyder, A.Z., Schlaggar, B.L., and Petersen, S.E. (2014). Methods to detect, characterize, and remove motion artifact in resting state fMRI. NeuroImage 84, 320-341.

Power, J.D., Plitt, M., Laumann, T.O., and Martin, A. (2017). Sources and implications of whole-brain fMRI signals in humans. NeuroImage 146, 609-625.

Rashid, B., Damaraju, E., Pearlson, G.D., and Calhoun, V.D. (2014). Dynamic connectivity states estimated from resting fMRI Identify differences among Schizophrenia, bipolar disorder, and healthy control subjects. Frontiers in human neuroscience 8, 897.

Raz, N., Lindenberger, U., Rodrigue, K.M., Kennedy, K.M., Head, D., Williamson, A., Dahle, C., Gerstorf, D., and Acker, J.D. (2005). Regional brain changes in aging healthy adults: general trends, individual differences and modifiers. Cerebral cortex 15, 1676-1689.

Satterthwaite, T.D., Wolf, D.H., Ruparel, K., Erus, G., Elliott, M.A., Eickhoff, S.B., Gennatas, E.D., Jackson, C., Prabhakaran, K., Smith, A., et al. (2013). Heterogeneous impact of motion on fundamental patterns of developmental changes in functional connectivity during youth. NeuroImage 83, 45-57.

Savalia, N.K., Agres, P.F., Chan, M.Y., Feczko, E.J., Kennedy, K.M., and Wig, G.S. (2017). Motion-related artifacts in structural brain images revealed with independent estimates of in-scanner head motion. Human brain mapping 38, 472-492.

Schölvinck, M.L., Maier, A., Ye, F.Q., Duyn, J.H., and Leopold, D.A. (2010). Neural basis of global resting-state fMRI activity. Proceedings of the National Academy of Sciences of the United States of America 107, 10238-10243.

Ségonne, F., Grimson, E., and Fischl, B. (2005). A genetic algorithm for the topology correction of cortical surfaces. Inf Process Med Imaging 19, 393-405.

Shine, J.M., Bissett, P.G., Bell, P.T., Koyejo, O., Balsters, J.H., Gorgolewski, K.J., Moodie, C.A., and Poldrack, R.A. (2016). The Dynamics of Functional Brain Networks: Integrated Network States during Cognitive Task Performance. Neuron 92, 544-554.

Snyder, A.Z. (1996). Difference image vs. ratio image error function forms in PET-PET realignment. In Quantification of Brain Function Using PET, R. Myer, V.J. Cunningham, D.L. Bailey, and T. Jones, eds. (San Diego, CA: Academic Press), pp. 131-137.

Stevens, A.A., Tappon, S.C., Garg, A., and Fair, D.A. (2012). Functional brain network modularity captures inter- and intra-individual variation in working memory capacity. PLoS One 7, e30468.

Su, J., Shen, H., Zeng, L.L., Qin, J., Liu, Z., and Hu, D. (2016). Heredity characteristics of schizophrenia shown by dynamic functional connectivity analysis of resting-state functional MRI scans of unaffected siblings. Neuroreport 27, 843-848.

Tanner, J.C., Faskowitz, J., Byrge, L., Kennedy, D., Sporns, O. and Betzel, R. (2022). Synchronous high-amplitude co-fluctuations of functional brain networks during movie-watching. bioRxiv.

Tognoli, E., and Kelso, J.A. (2014). The metastable brain. Neuron 81, 35-48.

Tsvetanov, K.A., Henson, R.N.A., Jones, P.S., Mutsaerts, H., Fuhrmann, D., Tyler, L.K., Cam, C.A.N., and Rowe, J.B. (2020). The effects of age on resting-state BOLD signal variability is explained by cardiovascular and cerebrovascular factors. Psychophysiology, e13714.

Tsvetanov, K.A., Henson, R.N. and Rowe, J.B., (2021). Separating vascular and neuronal effects of age on fMRI BOLD signals. Philosophical Transactions of the Royal Society B, 376(1815), 20190631.

Van Dijk, K.R., Sabuncu, M.R., and Buckner, R.L. (2012). The influence of head motion on intrinsic functional connectivity MRI. NeuroImage 59, 431-438.

Van Essen, D.C., Glasser, M.F., Dierker, D.L., Harwell, J., and Coalson, T. (2012). Parcellations and Hemispheric Asymmetries of Human Cerebral Cortex Analyzed on Surface-Based Atlases. Cerebral cortex 22, 2241-2262.

Wang, C., Ong, J.L., Patanaik, A., Zhou, J., and Chee, M.W. (2016). Spontaneous eyelid closures link vigilance fluctuation with fMRI dynamic connectivity states. Proceedings of the National Academy of Sciences of the United States of America 113, 9653-9658.

Wig, G.S. (2017). Segregated Systems of Human Brain Networks. Trends in cognitive sciences 21, 981-996.

Yang, G.J., Murray, J.D., Wang, X.J., Glahn, D.C., Pearlson, G.D., Repovs, G., Krystal, J.H., and Anticevic, A. (2016). Functional hierarchy underlies preferential connectivity disturbances in schizophrenia. Proceedings of the National Academy of Sciences of the United States of America 113, E219-228.

Yue, Q., Martin, R.C., Fischer-Baum, S., Ramos-Nunez, A.I., Ye, F., and Deem, M.W. (2017). Brain Modularity Mediates the Relation between Task Complexity and Performance. Journal of cognitive neuroscience 29, 1532-1546.

Zamani Esfahlani, F., Jo, Y., Faskowitz, J., Byrge, L., Kennedy, D.P., Sporns, O., and Betzel, R.F. (2020). High-amplitude cofluctuations in cortical activity drive functional connectivity. Proceedings of the National Academy of Sciences 117, 28393.

Zimmerman, B., Rypma, B., Gratton, G. and Fabiani, M., 2021. Age-related changes in cerebrovascular health and their effects on neural function and cognition: A comprehensive review. Psychophysiology.

BIOGRAPHICAL SKETCH

Liang Han was born in China. In August 2015, he joined Wig Neuroimaging Lab as a PhD student in the Cognition and Neuroscience program at UT Dallas. He earned his bachelor's degree in English and master's degree in Psychology from Qufu Normal University. His research interests are centered on understanding how the organization of functional brain networks vary across the adult lifespan in both health and disease. In pursuit of this, Liang has done research in area parcellation and assessment of brain network reliability within individuals. Liang is also interested in better understanding time-varying sources and properties of age-accompanied functional brain network reorganization. In his spare time, he enjoys spending time with his family and cooking Shandong cuisine.

CURRICULUM VITAE

Liang Han

University of Texas at Dallas | Center for Vital Longevity

E-mail: liang.han@utdallas.edu

EDUCATION

2015 – current	PhD student
	School of Behavioral and Brain Sciences, The University of Texas at Dallas, USA
	Advisor: Gagan Wig, Ph.D.
2002 – 2005	MA, Psychology
	Qufu Normal University, China
	Advisor: Guangwen Song, Ph.D.
1998 – 2002	BA, English Linguistics
	Qufu Normal University, China

ACADEMIC APPOINTMENT

2005 – 2015	Teacher, Shanghai University of Engineering Science, China

AWARDS, SCHOLARSHIPS AND HONORS

2016	Travel award from the BBS at The University of Texas at Dallas for presenting at Society for Neuroscience
2001	The First Prize of National Challenging Cup Championship in Shandong District, China

PEER-REVIEWED PUBLICATIONS

1. Chan, M.Y., **Han, L.**, Carreno, C.A., Zhang, Z., Rodriguez, R.M., LaRose, M., Hassenstab, J., Wig, G.S. (2021). Long-term prognosis and educational determinants of brain network decline in older adult individuals. *Nature Aging*. 1(11):1053-1067.

2. **Han, L.**, Savalia, N.K., Chan, M.Y., Agres, P.F., Nair, A.S., Wig, G.S. (2018). Functional parcellation of the cerebral cortex across the human adult lifespan. *Cerebral Cortex*. 28(12):4403-4423.

CONFERENCE TALKS

2018 Dallas-Austin Area Memory Meeting, Waco, TX

2017 Dallas-Austin Area Memory Meeting, Austin, TX

CONFERENCE ABSTRACTS/POSTERS

1. Zhang, Z., Chan, M.Y., **Han, L.**, Carreno, C.A., Winter-Nelson, E., Wig, G.S., Alzheimer's Disease Neuroimaging Initiative (ADNI). (2021). Independent effects of Alzheimer's disease and aging on functional brain network organization at rest. Dallas aging and cognition conference, Dallas, TX.

2. Chan, M.Y., **Han, L.**, Carreno, C., Zhang, ZW., Rodriguez, R., LaRose, M., Hassenstab, J., Wig, G.S. (2020). Educational attainment relates to longitudinal brain network decline in older age adult individuals. Dallas-Austin Area Memory Meeting, Austin, TX.

3. Yu, JC., Chan, M.Y., **Han, L.**, Abdi, H. (2019). A multivariate resting-state fMRI technique for subject-specific parcels and sub-networks. Semantic processing and semantic knowledge (Co-sponsored by the Center for Cognitive Neuroscience and the Neukom Institute for Computational Science), Hanover, NH.

4. **Han, L.**, Chan, M.Y., Agres, P.F., Wig, G.S. (2019). Assessment of resting-state brain network reliability over multiple measurements: implications for longitudinal observations. Dallas aging and cognition conference, Dallas, TX.

5. Agres, P.F., Chan, M.Y., **Han, L.**, Savalia, N.K., Wig, G.S. (2018). Organized patterns of cortical thinning observed across the healthy adult lifespan. Cognitive Neuroscience Society Annual Meeting, Boston, MA.

6. **Han, L.**, Savalia, N.K., Chan, M.Y., Agres, P.F., Wig, G.S. (2017). Functional parcellation of the cerebral cortex across the healthy adult lifespan using resting-state functional connectivity. Dallas aging and cognition conference, Dallas, TX.

7. Cooper, C.M., Savalia, N.K., Agres, P.F., Chan, M.Y., **Han, L.**, Fava, M., Kurian, B., McGrath, P., Parsey, R., Weissman, M., Wig, G.S. Trivedi, M.H. (2016). Identifying clinically relevant subgroups in major depressive disorder using resting-state functional connectivity: results from the EMBARC study. American college of neuropsychopharmacology annual conference, Hollywood, FL.

8. Savalia, N.K., Cooper, C.M., Agres, P.F., Chan, M.Y., **Han, L.**, Fava, M., Kurian, B., McGrath, P., Parsey, R., Weissman, M., Trivedi, M.H., Wig, G.S. (2016). Resting-state functional connectivity classifies patients with Major Depressive Disorder into clinically distinct sub-groups. Society for Neuroscience 46th annual Meeting, San Diego, CA.

9. **Han, L.**, Savalia, N.K., Chan, M.Y Agres, P.F., Wig, G.S. (2016). Functional parcellation of the cerebral cortex across the healthy adult lifespan using resting-state functional connectivity. Society for Neuroscience 46th annual Meeting, San Diego, CA.

TEACHING EXPERIENCE

The University of Texas at Dallas

2019	TA: Cognitive Psychology
	TA: Experimental Projects in Psychology
2018	TA: Cognitive Development
	TA: Introduction to Psychology
2017	TA: Cognitive Psychology
	TA: Cognitive Development
2016	TA: Cognitive Psychology
	TA: Experimental Projects in Psychology
2015	TA: Cognitive Psychology

Shanghai University of Engineering Science

2007 – 2015	Instructor: Introduction to Psychology and Mental Health

CERTIFICATE/LICENSE

2009 – present	National Certificate of Psychological Consultant (Level II, China)
2007 – 2015	Certificate of School Psychological Consultant (Shanghai, China)

PROFESSIONAL SERVICE

2007 – 2015	Psychotherapist, Shanghai University of Engineering Science

PROFESSIONAL MEMBERSHIP

2017 – present	Cognitive Neuroscience Society
2016 – present	Society for Neuroscience

PROFESSIONAL SKILLS

- Programming language: MATLAB, Python, R, Bash
- Neuroimaging software: SPM, FSL, FreeSurfer, HCP Workbench
- Data processing environment: High Performance Computing (HPC)